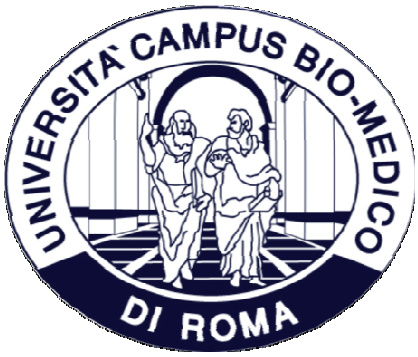

UNIVERSITÀ CAMPUS BIO-MEDICO DI ROMA

FACOLTÀ DI INGEGNERIA

DOTTORATO DI RICERCA IN INGEGNERIA BIOMEDICA
XXVI CICLO

Substrate engineering to control cell behaviour

Supervisor
Prof. Marcella Trombetta

Candidate
Abbruzzese Franca

Co-supervisor
Alberto Rainer, PhD

Summary

Abstract 4
CHAPTER 1: Introduction 5
1.1 Basics of Soft Lithography 5
1.1.1 Photolithographyand Electron Beam Lithography 7
1.1.2 Fabrication of the elastomeric stamp 9
1.1.3 Microcontactprinting 10
1.1.4 Embossing of structures in a polymer 11
1.2 Soft lithography in tissue engineering 12
1.2.1 Microfluidic Strategies for Design and Assembly of Microfibers and Nanofibers 13
1.2.2 Organ-on-chip 15
1.2.3 Nano/Micropatterned substrates to engineer cell behavior 18
1.2.3.1 Physical cues to guide stem cell differentiation 20
1.2.3.2 Biochemical cues to guide cell growth and differentiation 23
1.2.3.3 Biologicalcues 23
CHAPTER 2: Surface pattern drives the biological response of tendon-derived cells. 24
Introduction 24
2.1 Materials and Methods 26
2.1.1 Fabrication of microstructured master 26
2.1.2 PDMS replica molding 26
2.1.3 PDMS washing protocol 27
2.1.4 PDMS substrates characterization 27
2.1.5 Cells study 27
2.1.5.1 Tendon stem cells seeding 28
2.1.5.2 Tenocytes seeding 30
2.1.6 Statistical analysis 32
2.2 Results and discussion 33
2.2.1 PDMS FE-SEM analysis 33
2.2.2 TSC cell culture 34
FE-SEM analysis 34
Immunofluorescence analysis 35
2.2.3 Tenocytes culture 40

Cell culture analysis 40
Immunofluorescence analysis 41
2.3 Conclusion 50
CHAPTER 3: Microcontact printing on hard substrates 51
Introduction 51
3.1 Materials and Methods 52
3.1.1 Fabrication of microstructured master 52
3.1.1.1 Replica molding and washing of PDMS 53
3.1.2 Fluorescently labeling procedure 54
3.1.3 Microcontact printing procedure 54
3.1.3.1 Immunofluorescence images 56
3.1.4 Cells seeding 56
3.1.4.1 TSCs seeding 56
3.1.4.2 hMSC seeding 58
3.1.5 Statistical analysis 58
3.2 Results and discussion 59
3.2.1 PDMS FE-SEM analysis 59
3.2.2 Immunofluorescence images 62
3.2.3 TSCs culture 64
Cell culture analysis 64
Focal adhesion analysis 66
Stem cell preservation 67
3.3 hMSCs culture 70
hMSC morphology and focal adhesion analysis 70
3.3.1 Conclusions 72
CHAPTER 4:µCP on soft substrates 73
Introduction 73
4.1 Materials and Methods 74
4.1.1 Stamp fabrication 74
4.1.1.1 SU-8 Master molds fabrication 74
4.1.1.2 Replica molding and washing of PDMS 74
4.1.2 Scaffold fabrication 74
4.1.3 Soft substrates fabrication 75
4.1.4 Microcontact printing procedure 75
4.1.5 Cell culture experiments 77

4.1.5.1 Cell morphology analysis on soft substrates 77
4.1.6 Statistical analysis 77
4.2 RESULTS AND DISCUSSION 78
4.2.1 FE-SEM analysis and optimization of protein transfer 78
4.2.2 Effects of protein patterns on cell organization 81
4.3 Conclusions 83
CHAPTER 5: 84
Conclusion 84
Future outlook 85
5.1 Biomimetic micro-fibrous PLLA substrates for tendon regeneration: a preliminary in vitro study 85
5.2 Chemical grafting of protein islands on biomimetic micro-fibrous PCL scaffolds 87
References 91

Abstract

The topographic study of nano and micro-surfaces assumes considerable importance in Tissue Engineering. It allows, in fact, to obtain information on the interaction of cells with substrates that mimic the micro-architectural features of the extracellular matrix (ECM) of the native tissue of interest. In this way it is possible to develop biomaterials having biophysical (topography, mechanical properties) and biochemical (oxygen tension, surfacecoating) characteristics, which is able to replace *in vitro* complex biological systems.

The aim of this PhD thesis is to study the influence of differently engineered substrates obtained through two well-established soft-lithographic techniques (ReplicaMolding (REM) and Micro-Contact Printing (μCP)) on the behaviour of several cell types (tenocytes, tendon-derived stem cells and bone marrow stromal cells).

The REM technique was used for the fabrication of polydimethylsiloxane (PDMS) substrates with different stiffness obtained modifying the ratio between pre-polymer and curing agent (5:1 and 10:1 w/w). Cell culture has allowed to study the role of the different topographical features on cell morphology, proliferation, migration and production of collagen (type I and type III).

The second technique (μCP) was used to obtain protein (type I collagen and poly-L-lysine) patterns both on polypropylene substrates and on polycaprolactone (PCL) 3D scaffolds obtained by electrospinning. PDMS molds with different relief structures were fabricated by REM technique and used to print the protein islands. The influence of substrate topography on cell morphology, proliferation, and preservation of cell stemness was analyzed.

CHAPTER 1: Introduction

Micro- and nano engineering of materials offer novel technologies and represent a good interface between material sciences and biomedical nanotechnology. In particular, recent advances in microfabrication technologies paved the way to refined scaffold generation and systems to better reproduce physiological cell environment, in order to faithfully predict their functions and behavior *in vitro*.

Microfabrication methods commonly adopted in tissue regeneration include photolithography, electron beam lithography (EBL), nano imprint lithography (NIL), and soft lithography (SL). Among all, soft lithography has found application in a huge number of fields such as cell biology, microfluidics, lab-on-a-chip, microelectromechanical systems and flexible electronics/photonics [1]. Among main advantages, soft lithography generates well-defined and controllable surface chemistries, and is generally compatible with biological applications. Furthermore, this method is inexpensive and straightforward once the mold is fabricated: the replication procedure requires neither expertise nor sophisticated equipment [1-2]. In fact, procedures involving relatively large features (such as those used in microfluidic devices) can be conducted in an ordinary chemical laboratory and are thus particularly useful to those who do not have routine access to clean room facilities or for applications where the fabrication cost is a serious concern. However, soft lithography still relies on the use of photolithography to generate the master.

1.1 Basics of Soft Lithography

The term soft lithography includes a family of techniques involving a soft polymeric mold such as a polydimethylsiloxane (PDMS) replica from an original hard master [3-5]. Mold masters are typically fabricated by photolithography in order to define the desired stamp pattern. The core set of soft lithographic techniques, organized as proposed by Gates *et al*. are based on printing, molding and embossing with an elastomeric stamp [1, 6]. Apart from "replica molding", a well-known technique for generating a polymer channel replicated from an original silicon master, soft lithography provides many simple yet robust routes toward the fabrication of micro/nanostructures onto a surface [4, 7-8]. Indeed, a large number of techniques—microcontact printing (μCP) [9], replica molding (REM) [10], microtransfer molding [11], micromolding in capillary [12], solvent-assisted micromolding (SAMIM) [13], phase-shifting edge lithograph [14], nanotransfer printing [15]—can be numbered among soft lithography [1].

Figure 1 outlines the four major steps of the procedure generally used for soft lithography:

(i) pattern design,

(ii) fabrication of the mask and then the master,

(iii) fabrication of the PDMS stamp and,

(iv) fabrication of micro- and nanostructures with the stamp by printing, molding and embossing.

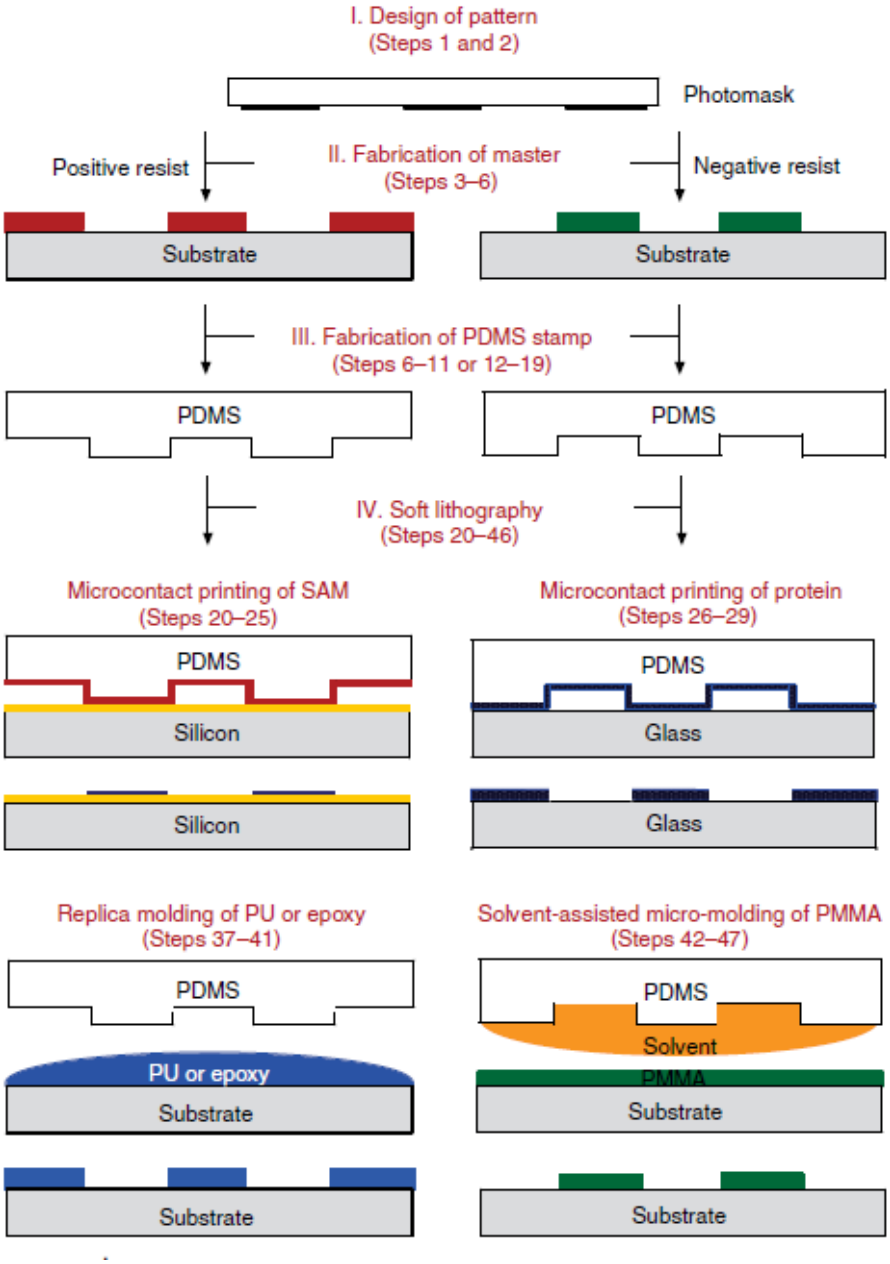

Figure1: major steps of the procedure generally used in soft lithography[1].

Usually the first step in soft lithography is the master fabrication and it needs the use of conventional lithography. A silicon wafer with polymeric structures patterned on its surface is

typically referred to as the master copy, or simply the master, and is used as the negative for replication. Photolithography and e-beam lithography (EBL) are the primary two techniques for fabricating a 'master' that contains patterned relief structures on the surface[16]. In particular, conventional photolithography is a classic technique for patterning structures larger than 1 μm, while EBL is preferred in case of features below 1 μm[1].

1.1.1 Photolithographyand Electron Beam Lithography

Photolithographic process consists of a number of steps in which a desired pattern is generated on the surface of a substrate through the selective exposure of regions of a material sensitive to ultraviolet (UV) light. The process involves the exposure of the photoresist to the UV light to modify its solubility (with respect to changes in its molecular structure), followed by developing in a proper developer solution. After immersion in this solvent, the exposed or unexposed photoresist regions get dissolved, providing access to the substrate surface [1].

Resist materials are usually organic polymers consisting of long molecular chains. When resist is exposed to a radiation source of a specific wavelength, the chemical resistance of the resist to developer solution changes. Depending on the prevalence of chain scission or chain bonding the resist is termed a "positive" or a "negative" resist. For positive resists, material will become more soluble in exposed regions, while a negative photoresist will become less soluble in exposed regions during development.

Exposure systems typically produce an image on the wafer using a photomask which is a square glass plate with a patterned emulsion of metal film on one side. The light shines through the photomask, which blocks it in some areas and lets it pass in others. Figure 2A shows the schematics of photolithographic method [17].

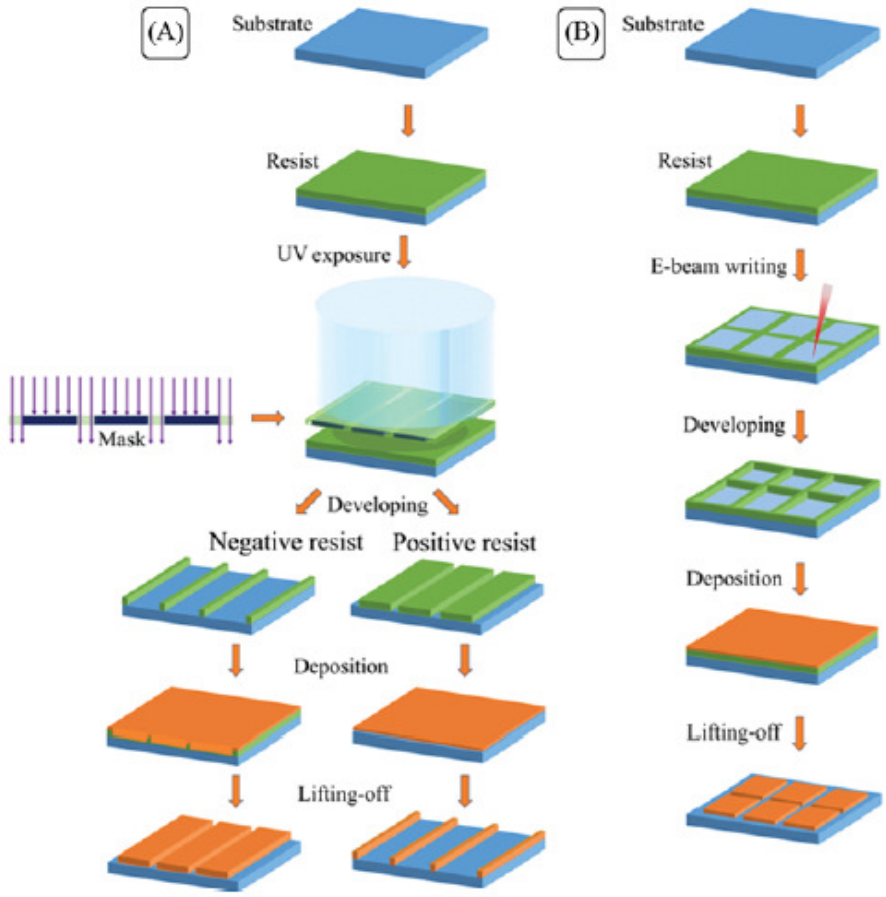

Figure 2:schematics of photolithography (A) and electron beam lithography (B) processes[17].

In the EBL a beam of electrons are exposed to the surface of an electron sensitive resist-coated material. Compared with other lithographic processes, the use of electron guns to scan a material and form the desired pattern is the core characteristic of the electron beam lithography technique. Due to the interaction of electron beam with the resist, changes in its solubility occurs and the electrons cause chain scission that makes the polymer soluble in a developer, just as photographic film changes its properties when irradiated with light. The resolution obtained through this type of lithography is greatly influenced by the beam spot size. Specimen position and beam characteristics are electronically controlled to achieve the desired resolution. Figure 2B demonstrates the schematics of EBL [18].

Advantages quoted are especially related to its popularity in research labs, since it is efficient and accurate in producing structures (20–30 nm in lateral dimensions) much smaller than those available through photolithography (1–2 μm), which is mainly limited by optical diffraction. Its precision and nano lithographic capabilities generally make it the tool of choice for making masks for other kinds of lithographic procedures and hence EBL is frequently coupled with microcontact

printing to obtain high resolution surface features that are smaller than the size of a cell. However, it is generally much slower than photolithography since the pattern has to be exposed 1 pixel at a time. Furthermore, EBL is a process that requires expensive equipment, an experienced operator and hence it is subject to much longer waits for access to the facility.

1.1.2 Fabrication of the elastomeric stamp

The key element of soft lithography is an elastomeric stamp with relief structures on its surface. The stamp is typically fabricated by casting a liquid precursor against a master whose surface was patterned with the complementary structures. The mechanical properties of the elastomeric stamp are critical to its ability to transfer a pattern with high fidelity. Although in principle, any elastomer can be used to cast the stamp, most works were focused on the silicone-based rubber or cross-linked PDMS [19].

PDMS has several unique properties that make it a perfect choice for fabrication of microdevices for cell culture [20]. First, PDMS has a high gas permeability that ensures sufficient oxygen supply to cells in microchannels, eliminating the need for separate oxygenators that are commonly required in silicon, glass, and plastic devices. This is a particular advantage for culture and maintenance of differentiated function of primary cells with high metabolic demands, such as liver epithelial cells, which are critical for toxicology studies [21]. Furthermore, PDMS microfluidic systems enabled the formation of viable and functional human tissues comprised of kidney epithelial cells [22], epidermal keratinocytes [23], osteoblasts [24-25], and chondrocytes [26] for drug screening and mechanotransduction studies [27].

Another advantage of PDMS is its optical transparency, which allows real-time, high-resolution optical imaging of cellular responses. This property was leveraged, for example, to carry out real-time microfluorimetric measurements of nitric oxide production and measure changes in pulmonary vascular resistance in a microfluidic model [28]. Optical monitoring of cell morphology and motility in PDMS microdevices also has proven useful for the analysis of tissue repair and reorganization [29], as well as embryonic development[30-31]. In addition, the high flexibility of PDMS makes it possible to microfabricate tissue models with precise automated control of fluid flow. Among various types of commercial PDMS, Sylgard 184 from Dow Corning was most commonly used for fabrication of stamps with feature sizes larger than 500 nm. Composite stamps consisting of two layers—a stiffer layer (30- to 40-μm thick h-PDMS) supported by a flexible layer (3- to 5-mm thick Sylgard 184 PDMS)—can extend the capability of soft lithography down to the

50–100 nm regime. Figure 3outlines a procedure for fabricating PDMS stamps from masters with different relief structures.

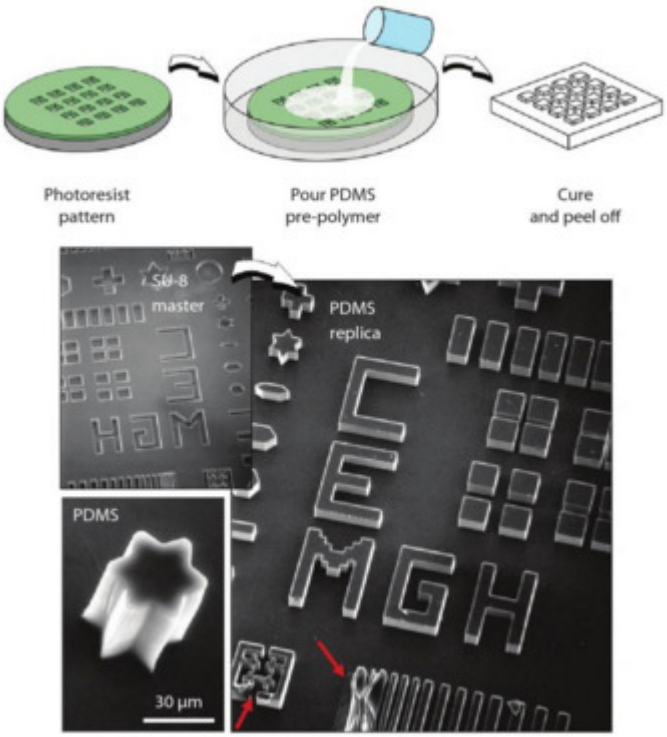

Figure 3: procedure for fabricating PDMS stamps from masters with different relief structures.[32]

1.1.3 Microcontactprinting

Microcontact printing (µCP) is a soft lithography technique used to transfer chemical and biological molecules onto a surface using a topographically patterned elastomeric stamp, which is typically fabricated in PDMS (see figure 1). In microcontact printing, the PDMS stamp is inked with protein solution, dried, and brought in contact with a surface for a period ranging from 30s to several minutes. Upon removal of the stamp, a pattern is generated on the surface that is defined by the raised bas-relief structure of the stamp, and hence precisely recreates the microscale pattern of the original master. The µCP process is attractive because of the ease and low cost of generating the stamp with commercially available precursors.

One of the first major contributions made by applying soft-lithography-based microcontact printing to cell culture was the demonstration that ECM molecules presented in a 2D configuration can induce similar levels of tissue-specific differentiation to 3D ECM gel cultures, if presented on small, planar, microfabricated adhesive islands that restrict cell spreading to mimic the rounded and retracted shapes that cells exhibit when cultured on 3D ECM matrices. Under 2D conditions that partially restrict cell spreading, primary rat hepatocytes secrete higher levels of albumin and

fibrinogen [33], capillary cells form hollow tubular networks [34], and vascular smooth muscle cells exhibit optimal response to vasoconstrictors [35].

Micropatterning techniques were also used to culture cardiomyocytes on thin elastomeric films micropatterned with ECM proteins to generate functional 2D heart tissues that generate stresses comparable to those measured *in vivo* [36]. Moreover, when the polymer is moved to a rigid planar substrate, the heart tissue spontaneously contracts rhythmically and pulls the tissue into a 3D form, which is governed by the microcontact printed pattern of ECM [37].

1.1.4 Embossing of structures in a polymer

REM consists of three steps (see figure 1): (i) creating a topographically patterned master; (ii) transferring the pattern on the master into PDMS by REM; and (iii) transferring the pattern on the PDMS back into a replica of the original master by solidifying a liquid prepolymer such as UV-curable polyurethane (PU), or thermally curable epoxy, against the PDMS mold. The master mold can be reused several times to replicate devices. Thus, this method is especially desirable due to its low cost, flexibility, and rapid prototyping [1].

REM offers a number of advantages over traditional fabrication process at the nanoscale such as EBL: (i) REM can produce many copies (> 50) of molds, replicas and patterned surfaces from each master with a possible resolution at the atomic level; (ii) REM can work with a wide range of polymers other than e-beam-sensitive materials; (iii) REM allows patterning over large areas rapidly, not limited to a serial process defined by EBL; and (iv) REM can be applied to transfer patterns to non-planar surfaces[38-39].

Alternatively, REM provides a new method for fabricating microfluidic devices using PDMS, and this method has proved to be particularly suitable for various biomedical applications. Microfluidic devices are typically created by inverting the PDMS mold and conformally sealing it to a flat smooth substrate, such as glass, to create open cavities in the form of small, linear, hollow chambers, or 'microfluidic channels,' with openings at both ends of the polymer block for perfusion of fluids [40].

1.2 Soft lithography in tissue engineering

Soft lithography has provided a low-expertise route toward micro/nanofabrication and is playing a leading role in microfluidics, ranging from simple channel fabrication to the creation of micropatterned substrates [2]. Indeed, soft lithography was first used to pattern microscale adhesive islands made of ECM molecules as a way to specify the shape, position and function of cells cultured on silicon chips, and later on conventional culture substrates. Subsequently, this approach was modified by inverting the PDMS mold and sealing it to a smooth glass substrate, to create multipurpose microfluidic devices. Due to their small size, fluid flow in microfluidic systems is entirely laminar, and virtually no mixing occur between neighboring streams that flow beside each other within the same hollow channel. This novel property was leveraged to generate step gradients on the micrometer scale to deliver gradients of chemicals across the diameter of a single cell [41], and to sustain chemical gradients with complex shapes over many hours to days to study cell motility in response to chemotactic stimuli [42-43]. Furthermore, miniaturized perfusion bioreactors for culturing cells were made by coating the surface of the central channel with ECM molecules, flowing cells into the channel so that they adhere to the ECM substrate, and then perfusing the channel continuously with culture medium.

The development of these microengineering approaches has altered the way to study and manipulate living cells in both 2D and 3D systems and has opened entirely new possibilities to create in vitro models that reconstitute more complex, 3D organ-level structures, and to integrate critical dynamic mechanical cues as well as chemical signals. To this aim, more complex microfluidic devices were created to develop controlled microenvironments for manipulation and long-term differentiation of various types of cells.

As examples of this revolution introduced by soft lithography in tissue engineering, three of the most common applications were reported. In particular: (i) microfluidic strategies for design and assembly of micro/nano-fibers, (ii) microfluidic devices for 3D culture systems and organs-on-a-chips and, (iii).nano/micropatterned substrates to engineer cell behaviour, will be presented.

1.2.1 Microfluidic Strategies for Design and Assembly of Microfibers and Nanofibers

Microfluidic technologies were recently shown to hold significant potential as novel tools for the synthesis of polymeric fibers at the micro and nanoscale for a variety of applications in tissue engineering and cell biology. These microfluidic systems provide fine control over fiber shape, size, chemical anisotropy, and biological activity without the use of complicated devices or facilities, and the produced structures can be used as bottom-up scaffolds. Furthermore, their flexibility enables the safe loading of biological materials and drugs, including compounds, proteins, enzymes, genes, and cells [44].

An overview of various microfluidic spinning methods used for fiber fabrication was reported in figure 4.

In particular, microfluidic platforms, such as PDMS-based chips obtained through soft-lithography, were recently developed and used to replace conventional fiber generation platform such as micropipette-based spinning chips. These systems have broken several barriers to conventional fiber generation systems, including: (1) the preparation of fibers with complex morphologies and tunable compositions; (2) the development of low-cost facile devices; and (3) the combination of various microfluidic chip designs for fiber generation [45-48].

Non-cylindrical microfiber shapes were prepared using PDMS microfluidic chips, including flat fibers, grooved fibers, and belts, through the use of devices having rectangular channels. Depending on the shape of the channel cross-section, a variety of patterns may be engraved onto the surfaces of the fibers along the longitudinal direction. Longitudinal grooves on the inner surfaces of cylindrical channels can enable the spinning of microfibers bearing grooved surfaces.

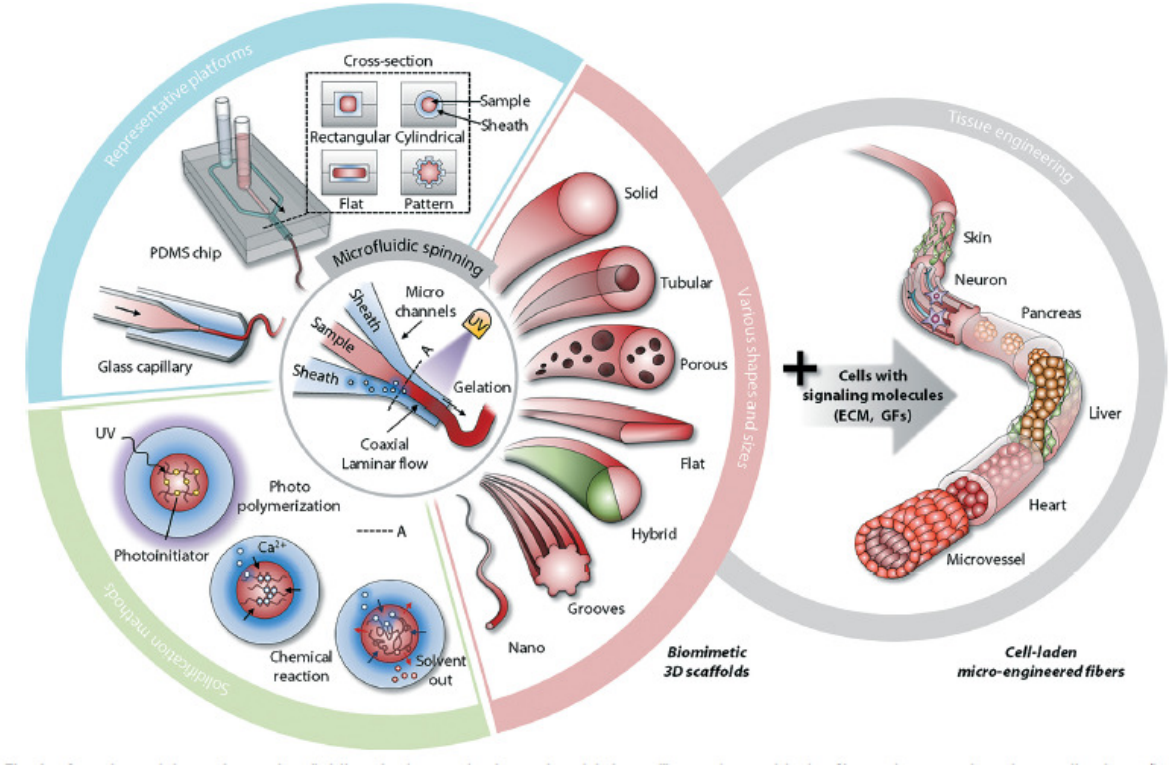

Figure 4: overview of various microfluidic spinning methods used to fabricate fibers, along with the fibers' tissue engineering applications[44].

The fibers can be created either by photopolymerizing a sample fluid or through chemical reactions between the sample and the sheath fluids undergoing coaxial laminar flow in a microchannel. The most popular central fluid materials for ECM or biomedical applications are alginate, PLGA, and chitosan. For the microfluidic spinning of alginate fibers, a sodium alginate solution is introduced into a sample channel and a $CaCl_2$ solution is introduced into a sheath channel. At the interface between the twofluids, sodium alginate is cross-linked due to the diffusion of Ca^{2+} ions into the alginate solution. Depending on the platform and the materials, fibers with a variety of shapes and sizes may be produced [44].

Other thrilling results have demonstrated facile production of cell-laden constructs that mimic natural tissue and organ function. Cell-laden fibers can be implanted into the body and can play a pivotal role in supporting and regenerating failed organs. Fibers can protect encapsulated cells from both mechanical stress and the host's immune system, and they allow excellent bidirectional transport of nutrients, oxygen, and wastes. Nonetheless, the manipulation of cell-laden fibers to form large tissue or organ constructs is currently limited by the mechanical properties of the synthetic matrices, and continued attempts to incorporate physically and chemically robust materials into the microfluidic fiber fabrication process should be a goal for all researchers in the field [44].

1.2.2 Organ-on-chip

An organ-on-a-chip is a microfluidic cell culture device created with microchip manufacturing methods that contains continuously perfused chambers inhabited by living cells arranged to simulate tissue- and organ-level physiology. Thanks to the possibility to recapitulate the physicochemical microenvironments and vascular perfusion of the body, these devices produce levels of tissue/organ functionality not possible with conventional 2D or 3D culture systems. They also enable high-resolution, real-time imaging and in vitro analysis of biochemical, genetic and metabolic activities of living cells in a functional tissue and organ context [49].

The simplest system is a single, perfused microfluidic chamber containing one kind of cultured cell (e.g., hepatocytes or kidney tubular epithelial cells) that exhibits functions of one tissue type (figure 5A). Similar microsystems were used to develop disease models. For example, a microfluidic co-culture platform was developed that allows for communication between different tissue types through 3D ECM gels to examine capillary cell invasion and sprouting in response to malignant breast and brain tumors (figure 5B) [27, 50]. In more complex designs, two or more microchannels are connected by porous membranes, lined on opposite sides by different cell types, to recreate interfaces between different tissues (e.g., lung alveolar-capillary interface or blood-brain barrier).The ability to integrate porous substrates to separate two parallel microchannelshas enabled analysis of tissue barrier functions and trans cellular transport, absorption and secretion (figure 4C) [44]. By culturing two different cell types on opposite sides of the substrate, one can create tissue-tissue interfaces that mimic the interactions of vascular endothelium and parenchymal tissues that define nearly all organs. These systems can incorporate physical forces, including physiologically relevant levels of fluid shear stress, cyclic strain and mechanical compression. Cyclic mechanical strain can be produced using flexible side chambers and applying cyclic suction that rhythmically stretches the lateral wall and the attached central membrane. Thus, cells adhered to the membrane can be exposed simultaneously to cyclic mechanical deformation and fluid shear stresses, similar to what most cells experience in living organs during processes such as breathing and peristalsis. Fluid shear stresses can be simply controlled by altering flow rates or channel dimensions, and by separating cells from the flow path using a nanoporous membrane or microengineered posts that restrict cell passage. Electrical fields can also be applied to pace contractile cells and to stimulate wound healing on chips.

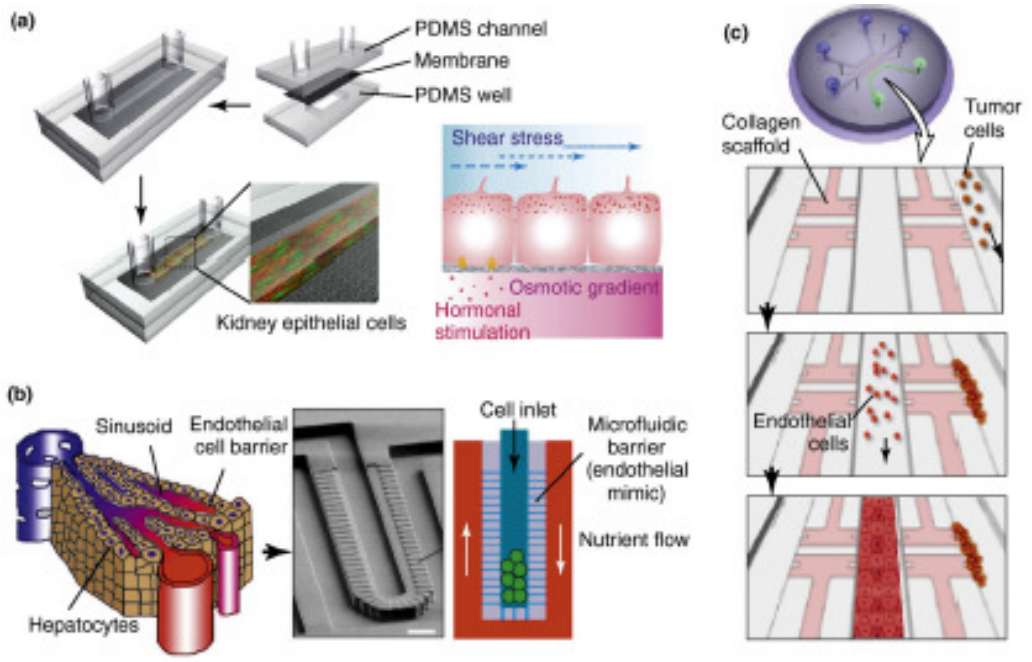

Figure 5: examples of microfluidic cell culture devices for organ-on-a-chip[27].

Control of fluid flow has also proved enormously useful in chips *in vitro* studies. For example, because viscous forces dominate over inertial one sat small length scales, the flow is laminar if the diameter of the microfluidic channel is less than about one millimeter. This allows the generation of physical and chemical gradients, which were exploited for non-invasive study of directional cell migration, cardiac tissue formation, nerve axon outgrowth, and graded metabolic responses.

These systems can permit analysis of organ-specific responses, including recruitment of circulating immune cells in reaction to drugs, toxins or other environmental perturbations as well as disease models [27].

Despite the considerable advances in the creation of in vitro engineered tissue and organ models, much remains to be accomplished in the development of complex 3D models that reconstitute whole organ metabolism and physiology because virtually all organs are functionally integrated in the human body. Indeed, several research groups are developing integrated 'human-on-a-chip' models that consist of interconnected compartments, each containing a cell type representing a different organ, linked through a microfluidic circulatory system [51]. Liver and lung cells were cultured in different microchambers interconnected by microfluidic channels contained in a microfabricated bioreactor able to develop physiologically relevant pharmacokinetic models [52].

This study reveals that toxic effect of metabolite product from liver compartment, as naphthalene, leads the depletion of glutathione in the lung epithelial cell compartment [53].This microfluidic system was further modified by incorporating 2D and 3D cultures of adipocytes, cancer cells, and bone marrow stem cells to study drug accumulation, distribution, metabolism and toxicity [54-56]. Similar approaches were used to develop microfluidic models of multi-organ interactions useful for studying intestinal absorption, hepatic metabolism and activity of breast cancer drugs [57].

Researchers' studies aimed to link more complex, mechanically active, organ-on-chip models via microfluidics to meet similar results, while providing more complete physiological biomimicry. This ability to integrate functional organ mimetics, such as gut-, liver-, lung- and skin-on-chips within a 'human-on-a-chip' (figure 6), could provide improved methods to explore different routes of drug delivery, as well as their effects on efficacy or toxicity of different drug formulations [27].

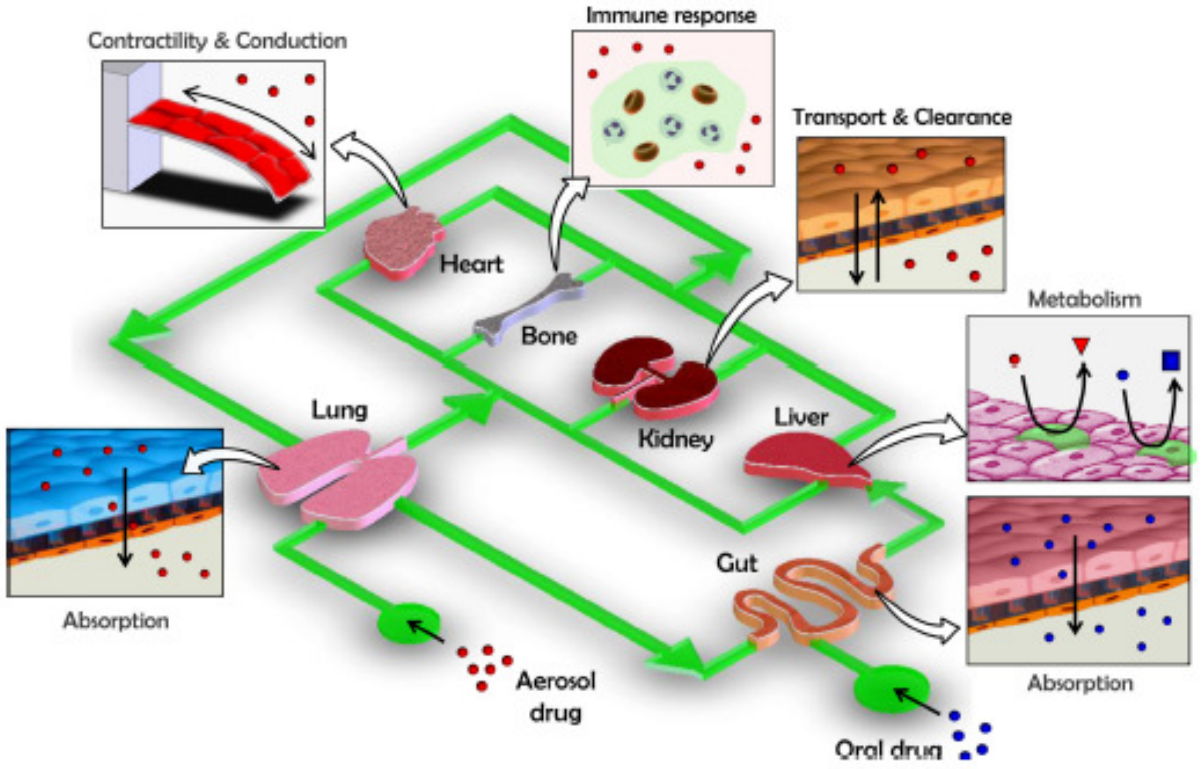

Figure 6: the human-on-a-chip concept[27].

1.2.3 Nano/Micropatterned substrates to engineer cell behavior

Cellular *in vivo* microenvironment is characterized by a complex combination of biophysical, biochemical, and biological signals, which define cells own phenotype and behavior. The cellular niche is defined as the three dimensional instructive microenvironment that involves a dynamic interplay between stimuli provided by the ECM, cell-cell interactions and soluble factors [58]. The ECM is a network composed of various proteins (e.g. collagen and elastin), proteoglycans, and glycosaminoglycans, which provides to the surrounding cells a structural topographic support [59], besides allowing the sensing and transduction of mechanical (stiffness, shear stress, and mechanical loading) and biochemical cues (oxygen tension, protein adsorption, and scaffold functionalization) (figure 7). In conventional *in vitro* cultures, cells are normally grown on smooth and stiff tissue culture plastic, in dilute culture conditions, under hyperoxic tension and without mechanical stimulation [60].

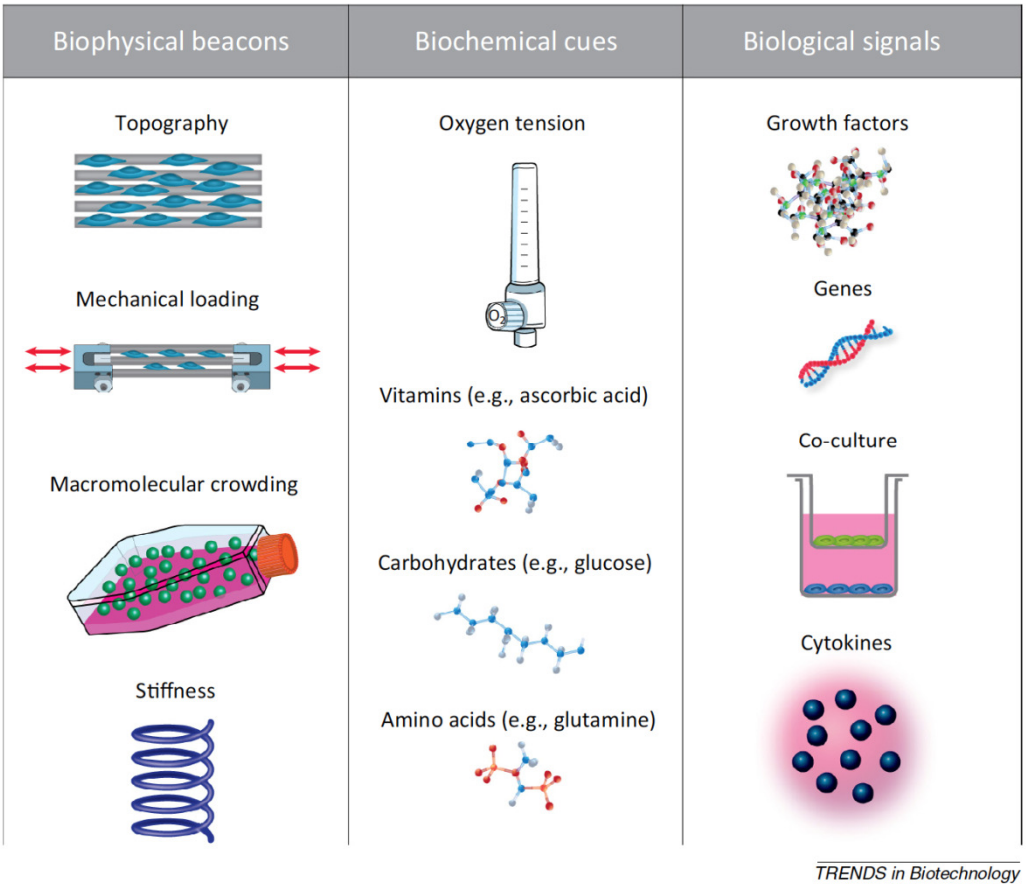

Figure 7: overview of the principal modulators of cell phenotype and behavior[60]

Several microfabrication techniques might be employed to recreate nanotopographies found within cellular environments (dimensions less than 100 nm). The principal requirements to be respected are that the features have to be repeated across a large surface area, they need to be reproducible and accessible by current fabrication technologies. Wood*et al.* separated nanopatterning into three main categories: primary pattern definition or writing, pattern transfer and mechanical transfer techniques (figure 8).

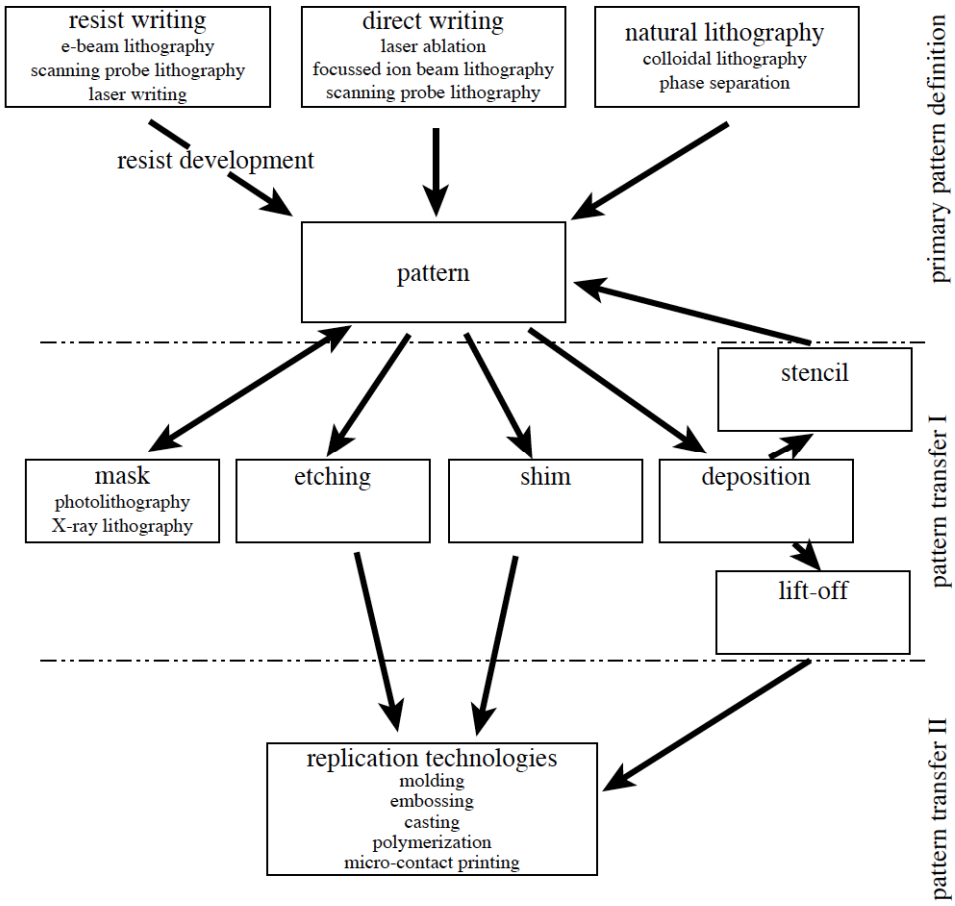

Figure 8: overview of nanolihographic techniques and processes[61]

The first one includes techniques ranging from e-beam lithography, to laser ablation, and focused ion beam lithography. It is the first stage of the pattering process, enabling high-resolution details despite being very expensive. The second step exploits photolithographic, etching, and deposition techniques to produce a master die. Finally, several softlithographic replication technologies, such as molding, embossing, and μCP, mechanically transfer an inverse representation of the original

pattern to a deformable polymer [61].It allows the production of a great number of samples in a low-cost fashion, although care must be taken in case volatile solvents are used, in order to avoid polymer shrinking, and the distortion or damaging of the pattern to be transferred. Advanced fabrication techniques also transferred conventional 2D cultures studies, performed on rigid substrates, on deformable 3D matrices, better mimicking cellular microenvironment and allowing detailed analysis of live cells [62]. Therefore, it is possible to precisely control the alignment of the latters.

Cell alignment refers to a oriented organization of cells and is crucial in several fields, ranging from biomechanics to cell biology, and from tissue engineering to regenerative medicine. In fact, it affects ECM remodeling, cytoskeleton reorganization, membrane protein relocation, and nucleus gene expression [63]. Generally speaking, it involves cell differentiation, tissue maturation and functions. To engineer cell alignment *in vitro*, different techniques can be used, such as topographical patterning [64], chemical treatment [65], and a combination of them.

1.2.3.1 Physical cues to guide stem cell differentiation

Surface topography and mechanical properties are key modulators of permanently differentiated cells and stem cells. In fact, focal adhesion distribution and intracellular signaling, which are functions of the topographic structure, act on cell growth, morphology, differentiation and motility.

The reason of this property relies on the fact that cells *in vivo* are surrounded by their ECMs, which contain 3D topographical cues themselves. In fact, the characteristic dimensions to induce cell alignment are comparable to the physiological ones [63]. The migratory, polarizarion, and alignment mechanisms are guided by substrate contact interaction [66].

Previous studies already [60] demonstrated how different patterns are active reprogramming mediators, able to up- and down- regulate specific markers, even in the absence of growth factors. Chen *et al*. [67] showed how patterning of nanoroughness on glass surfaces influenced human embryonic stem cells (hESC) adhesion, spreading and self-renewal. In general, cell movement can be guided by topography density gradients, thus obtaining a directional migration towards them.

Exploiting nanofabrication technologies, different topographical patterns can be obtained to engineer cell alignment. Grooved features (figure 9 A) are characterized by repeated patterns with equal ridge width and set groove depth. They are used to culture fibroblasts, epithelial cells, and endothelial cells, which align and migrate along the direction of the major axis of the groove [62].

Micro- and nano- grooved pattern differ on the mechanism of alignment. Hence, in the first one the ridge width is comparable with cell dimensions, while in the latter the features are similar to ECM

architectures, thus mimicking the membrane receptor signaling [63]. Furthermore, smaller and deeper grooves seem to enhance cell alignment and orientation.

For different types of cells, such as mesenchymal cells and neurons, the pillar topographical feature (figure 9 B) was used. The alignment depends on their spacing, height, and aspect ratio. Nano-pits (figure 9 C) instead, with appropriate size and spacing, well reproduce ECM nanopores, fundamentals in the regulation of cell behavior. A slightly different approach is based on wrinkled surfaces; rapid and inexpensive, it gives substrates multiscale topographical cues (Figure 9 D). It was used for various types of cells including fibroblasts, smooth muscle cells and embryonic stem cells. Khademhosseini*et al*. [68] cultured hESC within polymeric microwells in order to control cluster size and number, since it has been shown to favor proliferation, thus preventing heterogeneous differentiation. Even more similar to ECM architecture *in vivo* are fibrous scaffolds (figure 9 E), composed by nano-fibers and nano-pores, whose shape and dimension is responsible of cell seeding and alignment. Examples of fabrication bottom-up technologies to produce substrates for aligned fibers (e.g. for tendon regeneration) are electrochemically aligned fibers, extruded fibers, or electrospun polymeric fibers. It was previously demonstrated how cell actin filaments and nuclei preferentially align to the direction of the scaffold fiber. In conclusion it is clear how ECM architecture influences patho-physiological events, and several pathological conditions, such as cancer invasion, are thus accompanied by ECM remodeling [59].

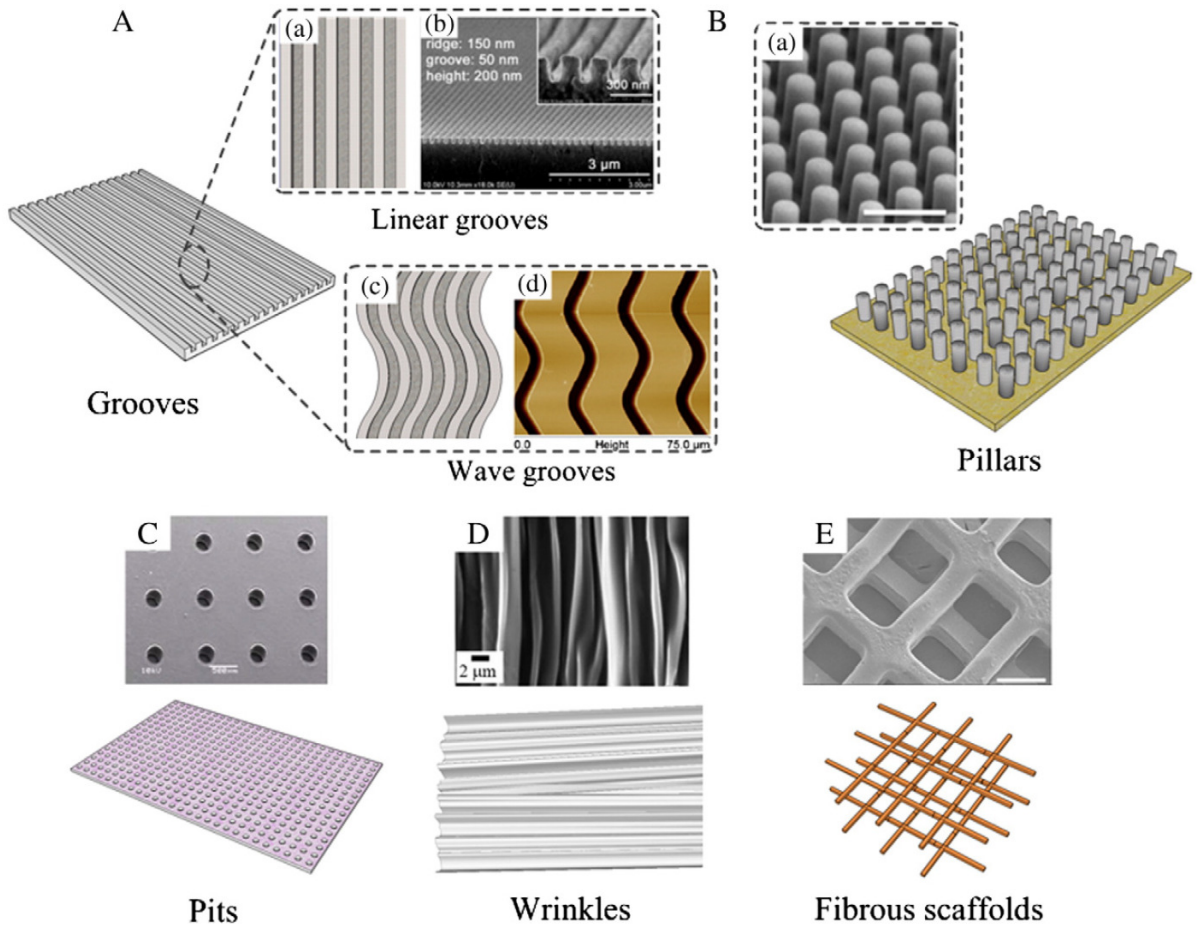

Figure 9: different topographical patterns[63]

On the other side, the molecular mechanism by which extracellular forces are translated into intracellular events, such as paracrine regulation, and the subsequent regulation of the cell secretome, is called mechano transduction. Integrins play the role of mechanoreceptors, while focal adhesions the one of nanoscale mechanosensory organelles; finally mechanical signals can be quickly transmitted through cytoskeleton [69]. Focal adhesions and matrix rigidity interaction control cells enlogation and polarization through a mechanosensing process [70]. Engineered substrates with controlled stiffness can be used to address stem cells differentiation and behavior, thus mimicking physiological ECM [71-72]. In a previous work [73], soft hydrogel substrates contributed to the regeneration of muscle, thanks to the mimicking of the elasticity proper of the tissue itself.A part from substrate rigidity, other mechanical forces influence cell organization (e.g. shear stress and tension). For example, vascular tissues are subject to long-term stimulation provided by pulsatile blood flow.

1.2.3.2 Biochemical cues to guide cell growth and differentiation

As it was largely demonstrated by traditional cell cultures, biochemical supplements, such as vitamins, glucose, essential amino acids, and the oxygen tension itself, strongly influence cell proliferation, differentiation and migration [60]. The method consists in providing chemical cues through biomolecules (e.g., proteins) adsorption or chemical functionalization of patterns with specifically designed shape, size and periodicity, thus alternating cell adhesive and repulsive zones [63]. The principal technique to produce biochemical patterns for engineering cell alignment is microcontact printing. Initially developed for self-assembled monolayers (SAMs) patterning of alkanethiolates, it is now used for various biomolecules such as poly-L-lysine, peptides, fibronectin, laminin, and bovin serum albumin to induce cell alignment [63, 74].

Finally, in some cases, especially for neuronal alignment, it is possible to combine μCP with the integration of multi electrode arrays, to add the electrical stimulation [63].

Surface chemical treatments can also be useful for different aims; one of these is to limit bacterial growth on specific area, achieved through microprinting of antimicrobial compounds [74].

1.2.3.3 Biologicalcues

Several studies demonstrate that behavior of different cell types can be influenced by various biological stimuli such as growth factors, cytokines, hormones, small chemicals, and extracellular matrix [60, 75-77]. In particular growth factor supplementation is the most studied biological cue. In fact, i*n vitro*, even the supplementation with a single growth factor controls stem cell differentiation [78-80] or cell specific fate [81]. Although, in several study the addition of multiple growth factors to tissue-specific cells [62,63] led to optimal results, an accurate combination of concentration and number of growth factor types is often difficult to determine. However such approaches have produced only promising preliminary data that cannot be translated directly to the clinical practice mainly due to lack of standardization procedures [82].

CHAPTER 2: Surface pattern drives the biological response of tendon-derived cells.

Introduction

Nano and micro-patterned surfaces assume considerable importance in the tissue engineering field [61, 83-85], as they allow the study of cell-substrate interactions by mimicking the micro-architectural featuresof the extracellular matrix(ECM) of native tissues [62]. In this way, it is possible to develop biomaterials with biophysical (topography, mechanical properties, etc.) and biochemical (oxygen tension, surface coating, etc.) characteristics suitable to replace *in vitro* complex biological systems [60]. Several literature studies reported the influence of substrate topography on the behaviour of different cell types: cardiac cells, neuronal, muscles, mesenchymal stem cells, fibroblasts, epithelial cells [86-94]. In particular, the behaviour of tendon-derived cells cultured on different topographical cues was studied to promote tendon repair [83]. To date, surgical procedure has been used to stimulate vascular ingrowth and tissue repair, but this approach does not restore native tendon function. Tissue engineering is an alternative way to surgical treatments. In fact, several studies demonstrated that the engineering of biomaterials surfaces able to mimic the ECM is the goal of tendon tissue engineering [95-97]. The ECM of tendon is mainly composed of hierarchical aligned collagen type I fibrils and other less-abundant collagen types such as III, V, VI, XII, XIV in which tenoblasts, tenocytes and tendon stem cells (TSCs) are engrafted [83, 98-100]. The ECM owns topographical features ranging from nanometersto micrometers (figure 1) which have a great effect on cell elongation, cell function and enhancement of cell migration [101-105].

In this study, tendon-derived cellsresponse to microstructured PDMS surfaces with different topographical features was analyzed. In order to mimic ECM topographical features, PDMS replica molding was used to produce substrates for TSCs and tenocytes culture with a characteristic dimension in the physiological range (1-20 micron).

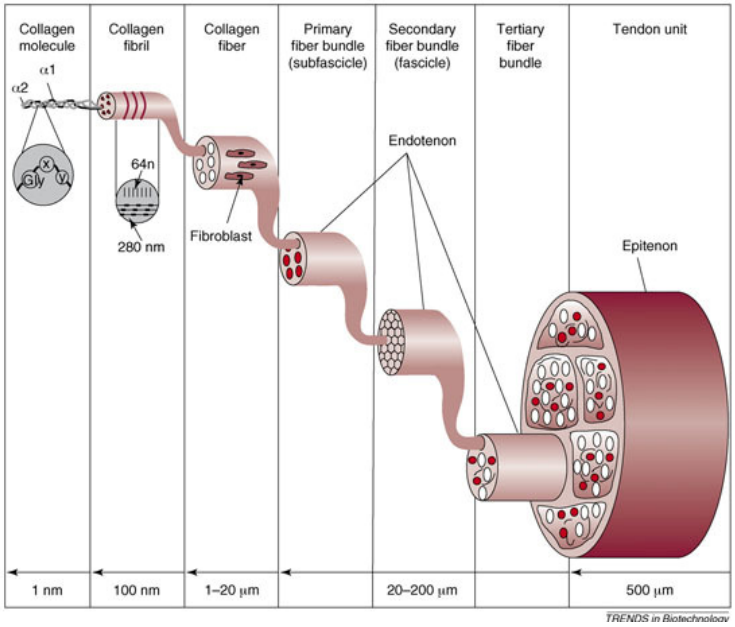

Figure 10: hierarchical structure of collagen fibers of the tendon unit [106].

2.1 Materials and Methods

2.1.1 Fabrication of microstructured master

Silicon masters were fabricated to replica-mold substrates on PDMS (Sylgard 184, Dow Corning) with line-grating and pillar-shaped geometries. Patterns features were 700nm in depth with half pitches of 1, 3, 10 μm, respectively.

Patterns were designed with Layout Editor software and converted by CATS software into machine files for EBL lithography. The fabrication process started with the patterning of PMMA positive resist (spin rate: 4000 rpm 1 min, pre-bake: 5 min @ 170°C) on Si wafers by 100keV electron-beam lithography Master features were exposed with a dose of 700 $\mu C/cm^2$. PMMA-coated wafers were developed in MIBK: IPA 1:1 for 30s and rinsed in isopropanol. A 20nm chromium film was evaporated by electron gun followed by lift-off process in acetone at 50 °C and sonication. Samples were then etched by RIE (reactive ion etching) using CHF_3, O_2, SF_6 and Ar gas mixtures.

After cleaning in Piranha solution (H_2SO_4/H_2O_2 3:1), microstructured Si wafers were silanized with 10% trimethylchlorosilane (TMCS) in toluene in N_2 environment to generate a low-energy surface and facilitate the subsequent mold/PDMS separation.

2.1.2 PDMS replica molding

Silicon master templates were replicated by ReM on PDMS molds. Sylgard 184 (Sylgard184 kit, Dow Corning) is a thermal curable elastomer which consist of two components: the prepolymer and the curing agent which can be added in different ratio in order to obtain PDMS substrates with controlled stiffness for cell seeding.

In this study PDMS substrates with 5:1 w/w ratio prepolymer/curing agent were prepared.

Microstructured substrates with higher stiffness (Young's modulus: 3.59 ± 0.11 MPa, [107]) were prepared starting from two PDMS layers of different ratio (prepolymer/curing agent). In the first layer, prepolymer and curing agent were mixed in 5:1 w/w ratio and the mixture was diluted with hexane in 1:20 w/v ratio to lower the polymer viscosity [108-109]. The PDMS mixture was evaporated under hood for 2h at room temperature and then cured at 95°C for 30 min. The second layer was comprised by a PDMS mixture with a 10:1 w/w ratio. The bubbles generated after mixing were removed by placing the PDMS mixture in a dessicator connected to the vacuum system for 30 minutes. When the mixture was completely degassed, PDMS mixture was poured on first layer and cured at 70°C for 2h and. After cooling down, they were carefully peeled off from the master and heated at 100°C for 1h.

PDMS replicas obtained had two types of patternwith different dimensions: linesandsquared pillars, both with half-pitch of 1, 3 and 10 µm (L1, L3, L10 and P1, P3, P10, respectively).

PDMS control substrates (CTRL) were prepared in a similar manner, pouring the PDMS mixture in a petri dish and curing as previously described.

To standardize cell seeding area, PDMS replicas were cut in a cylindrical shape with a biopsy punch (Ø 6mm).

2.1.3 PDMS washing protocol

An accurate cleaning process [110] was adopted to remove contamination of the PDMS surface deriving from the low-molecular-weight siloxane fragments. Patterned and unpatterned PDMS substrates were washed using the protocol described by Graham *et al*. [110-111] that consists of three steps: (i) drowning in hexane overnight; (ii) drying samples in a vacuum chamber; (iii) sonication in a 2:1v/v ethanol/water solution. All steps were repeated for three times. After drying all samples were placed in 96 multiwell plates, cleaned with O_2 plasma cleaner system (FEMTO plasma cleaner, Diener Electronic, Ebhausen, Germany, 10 W, 1.0 mbar, 36 sec) and then sterilized under UV for 10 minutes before to use.

2.1.4 PDMS substrates characterization

Field emission scanning electron microscopy (FE-SEM, Supra1535, LEO Electron Microscopy, Oberkochen, Germany) was used to characterize the geometry of the fabricated PDMS microstructures. Patterned and non-patterned PDMS replica were sputter-coated with gold alloy and viewed at 8 mm working distance (WD) and at an accelerating voltage of 5 kV using the SE (secondary electron) detector.

2.1.5 Cells study

In order to study the effect of pattern topography on cell behavior, the response of two different tendon cell types was analyzed. Tendon stem cells (TSCs) and tenocytes were obtained from tendons of adult non-tendinopathic individual l (age 30 years, male).Cell seeding on PDMS surfaces was performed carefully to avoid clusters and to ensure uniform cell distribution on the substrates.

Cell culture media and all their supplements were provided by Life Techonologies (Life Techonologies, Milano, IT).

2.1.5.1 Tendon stem cells seeding

Tendon stem cells (TSCs) were obtained from hamstring tendons of adult non-tendinopathic individual. The tendon samples were cleaned in Phosphate Buffer Solution (PBS, Sigma), cut into small pieces and digested with 3 mg/mL collagenase type I and 4 mg/mL dispase in PBS for 1 h at 37 °C as previously described [2]. The resulting cell suspension was centrifuged and cultured in growth medium consisting of alpha modified Eagle's medium (αMEM) supplemented with 20% (v/v) Fetal Bovine Serum (FBS), 1% (v/v) penicillin and streptomycin (pen-strep) and, 100 mM 2-mercaptoethanol (Sigma). After 8–10 days of culture, the TSC were screened for CD44 positivity with Mini MACS separation system (Miltenyi Biotec Bergisch Gladbach, Germany). Briefly, cells were harvested by trypsinization and then incubated with mouse anti-human CD44-labelled magnetic beads, recognizing a tendon stem cell–specific surface antigen. The cell suspension was then passed over a magnetic separation (MS) column housed within a magnetic field. CD44+ cells were retained on the column, while CD44- cells passed through it. The retained cell fraction was eluted from the MS column and cultured in αMEM supplemented with 10% (v/v) FBS, 1% (v/v) pen-strep and 1% glutamine. TSCs were isolated and characterized to evaluate stem cell properties such as clonogenicity, surface cell markers expression and multi-potency [112]. TSCs passage 1 were seeded on the PDMS patterned substrates (L1, L3, L10, P1, P3 and P10) and PDMS non-patterned (CTRL) substrates at $2 \cdot 10^4$ cells per cm^2 and cultured for one week in culture media supplemented as previously described, under humidified atmosphere with 5% CO_2 at 37°C. Medium was changed twice a week. Each micropatterned PDMS substrate and CTRL was seeded on 20 replicates for morphometric and immunofluorescence analysis.

2.1.5.1.1 FE-SEM analysis

The morphology of TSCs cultured on patterned and control PDMS substrates for one week was analyzed by FE-SEM. Samples were fixed in 3% v/v glutaraldehyde solution (Sigma) in PBS 0.1 M for 10 minutes at room temperature, rinsed three times with PBS and post-fixed in 1% v/v of osmium tetroxide (Sigma) solution in PBS 0.1 M for 4 minutes at room temperature. After washing with PBS, samples were dehydrated in graded ethanol solution in water (30, 50, 80, 90, 96 and 100% v/v, 10 minutes each) and dried with critical point drying (CPD, Emitech K850) in order to replace alcohol phase with liquid CO_2 first and then gaseous CO_2. Specimens were mounted on

aluminium stubs with adhesive carbon tape and gold-sputtered (Emitech K550), prior to SEM observation.

2.1.5.1.2 Immunofluorescence staining

TSCs cultured onto PDMS substrates were immune stained for actin-FITC conjugate (FITC-Phalloidin, green, Thermo Fisher Scientific, Monza, IT). Briefly, samples were fixed in 4% w/v PFA (Paraformaldehyde, Sigma-Aldrich, Milano, IT) solution for 3 minutes, washed in PBS and permeabilized with 0,1% v/v of Triton-X 100(Sigma-Aldrich, Milano, IT) solution in water for 10 minutes at room temperature. After washing actin cell cytoskeleton was stained with FITC-Phalloidin (diluted in PBS 1:40).DAPI (4′,6-Diamidino-2-phenylindole dihydrochloride, Sigma-Aldrich, Milano, IT) was used as a nuclear counterstain (blue) at 2 µg/mL for 10 minutes. Samples were then washed in PBS, mounted with ProLong Diamond Antifade Mountant (Thermo Fisher Scientific, Monza, IT) and examined under a phase contrast inverted microscope (Eclipse Ti-E, Nikon, Japan).

2.1.5.1.3 Cell image analysis

Cell orientation was determined from actin images obtained as described in §2.1.5.1.2 using FIJI Directionality tool. This plugin returns a directionality histogram by exploiting image fast-fourier transform (FFT) algorithms: isotropic images generate a flat histogram; whereas oriented images are expected to give a histogram peaked at the orientation angle. These histograms are finally fitted by Gaussian curves. Two fitting parameters were considered for evaluate cell alignment: dispersion (σ) and directionality (α) which report the standard deviation and the center of the Gaussian curve, respectively. The major axis of tenocytes was taken as the main direction of orientation, measured by the Fiji angle tool and used as reference angles. For non-patterned surface, random directions were chosen.

Approximately 70 cells for each experiment were analyzed. Data analysis was performed using Origin ver. 9.1 software (OriginLab, Northampton, MA).

Cellular orientation was also evaluated measuring the elongation of cellular nuclei and cytoskeleton [63]. Nuclear elongation is defined as the ratio of the major axis to minor axis of the immunostained nuclei (DAPI, blue). Fluorescence images (d5) were manually adjusted in order to eliminate cells overlapped or aggregated, divided into 9 ROIs (250 · 250µm) and then analyzed by NIS Elements AR software (Nikon, Tokyo, Japan). Approximately, 100cells per experiments were assessed.

2.1.5.2 Tenocytes seeding

Tenocytes from intact tendon were isolated from gracilis and semitendinosus tendons during arthroscopic surgery for anterior cruciate ligament repair. The tendon tissues were cut into 1 cm^2 pieces, washed in PBS and then cultured in Dulbecco's modified Eagle's medium (DMEM) with 10% of FBS, 1% of L-glutamine (200mM)and 1% of penicillin-streptomiycin (10k/10k)under humidified atmosphere with 5% CO_2 at 37°C.The cells were obtained by outgrowth and medium was changed twice a week. At passage 3, tenocytes were seeded at a density of $7 \cdot 10^4$ cells/cm^2 and cultured to different end points: 24, 72 and 120 h (d1, d3 and d5). At each time point, cells were analyzed for viability, proliferation and expression of collagen type I and III. All experiments were conducted in triplicate.

2.1.5.2.1 Cell viability

Cell viability was evaluated by Vybrant® Cytotoxicity Assay Kit (Thermo Fisher Scientific, Monza, IT) according to [Ref].Briefly, the release of the cytosolic enzyme glucose 6-phosphate dehydrogenase (G6PD) poured in the culture media from damaged cells was quantified every 24 hours until the end of the experiment (d5). 50 µL of supernatant from each well were incubated for 10 min with 50 µL of resazurin/reaction mixture at 37 °C in 5% CO_2, and the fluorescent metabolite of resazurin (resorufin) was detected at a fluorescence emission wavelength of 590 nm (λ excitation 530-560 nm, λ emission 580-600 nm) on a Tecan Infinite M200-Pro multiplate reader (Tecan, Männedorf, Switzerland). The fluorescence signal was proportional to the G6PD released into culture media and hence to the number of deadcells. Each experiment was performed in triplicate. No-cell and fully lysed controls were used to express cell viability as a percentage.

2.1.5.2.2 Cell proliferation

Cell proliferation was evaluated by MTT assay (3-(4,5-Dimethyl-2-thiazolyl)-2,5-diphenyl-2H-tetrazolium bromide, Sigma-Aldrich, Milano, IT), which is based on the reduction of MTT reagent to formazan salts by mitochondrial dehydrogenases of living cells. A solution of MTT 0,5 mg/mL in complete DMEM was added to each well at selected time points (d1, d3 and d5). The solution was incubated for 3 h at 37 °C and then removed in order to solubilize the formazan salts in DMSO (Dimethylsulfoxide, Sigma-Aldrich, Milano, IT). Absorbance was measured at 590 nm with microplate reader Tecan Infinite M200.

2.1.5.2.3 Immunofluorescence staining

After 5 days of culture, samples were fixed in 4% w/v PFA solution for 3 minutes, washed in PBS three times and permeabilized with 0.1% v/v Triton-X 100solution for 10 minutes at room temperature. After washing, Bovine Serum Albumine solution (BSA, Sigma-Aldrich, Milano, IT)at 2% w/v in PBS was added for blocking non-specific sites and left to react for 45 minutes. Actin cell cytoskeleton was stained in all samples with TRITC (red) or FITC (green) conjugated Phalloidin (Thermo Fisher Scientific, Monza, IT). DAPI was used as a nuclear counterstain at a concentration of 2 µg/mL.

The expression of collagen type I and III was alternatively investigated by immunofluorescence using specific mouse anti-human antibodies (Sigma-Aldrich, Milano, IT) against the two collagen isoforms and a secondary goat anti-mouse AlexaFluor 488 (green) or AlexaFluor 555 (red, Thermo Fisher Scientific, Monza, IT) for collagen type I and type III, respectively.

The samples were then incubated for 1 h at 37 °C with primary antibodies (1:1000) and subsequently for 45 minutes with the specific secondary antibodies as previously described (1:500).

The fluorescence intensity of the acquired images was calculated by NIS Elements AR software and used to quantify the amount of two collagen isoform produced by the cell during the culture period. Each image was divided into 9 ROIs and for each the background was subtracted to the light intensity to avoid overestimation of the measurements.

2.1.5.2.4 Cell image analysis

Cell orientation was evaluated on fluorescence microscopy images after 5 days of culture using FFT analysis (FIJI Directionality tool) as previously described in § 2.1.5.1.3 for TSCs.

Cellular elongation was evaluated measuring orientation of cellular nuclei [63] starting from fluorescence images (d5) and analyzed as previously described in § 2.1.5.1.3.

Cell migration was analyzed onto patterned and non-patterned PDMS substrates using time lapse microscopy. The multi-well culture plate was introduced in the inverted microscope equipped with an incubation chamber with controlled levels of temperature (37 °C), humidity (95%) and CO_2 concentration (5%). The images of tenocytes cultured onto PDMS substrates (n=3) were acquired at 10X magnification every 50 minutes, starting from 3 hours after seeding until the end of the experiment (15 h). Cell migration was evaluated using NIS Elements AR software and IBIDI Chemotaxis and Migration Tool (n=12).

2.1.6 Statistical analysis

Experimental data were analyzed using GraphPad Prism® 5 (GraphPad Software, USA). Conditions of normality were checked with Shapiro–Wilk test. Normally distributed data were analyzed for significance by ANOVA (one- or two-way), followed by Tukey's multiple comparison post hoc test (Tukey). Statistical significance was accepted at $p < 0.05$. Data are presented as mean value ± standard deviation.

2.2 Results and discussion

2.2.1 PDMS FE-SEM analysis

PDMS substrates obtained by replica molding were analyzed by FE-SEM microscopy. The micrographs reported in figure 2 show the micro-lines and micro-squared pillars of the PDMS substrates.

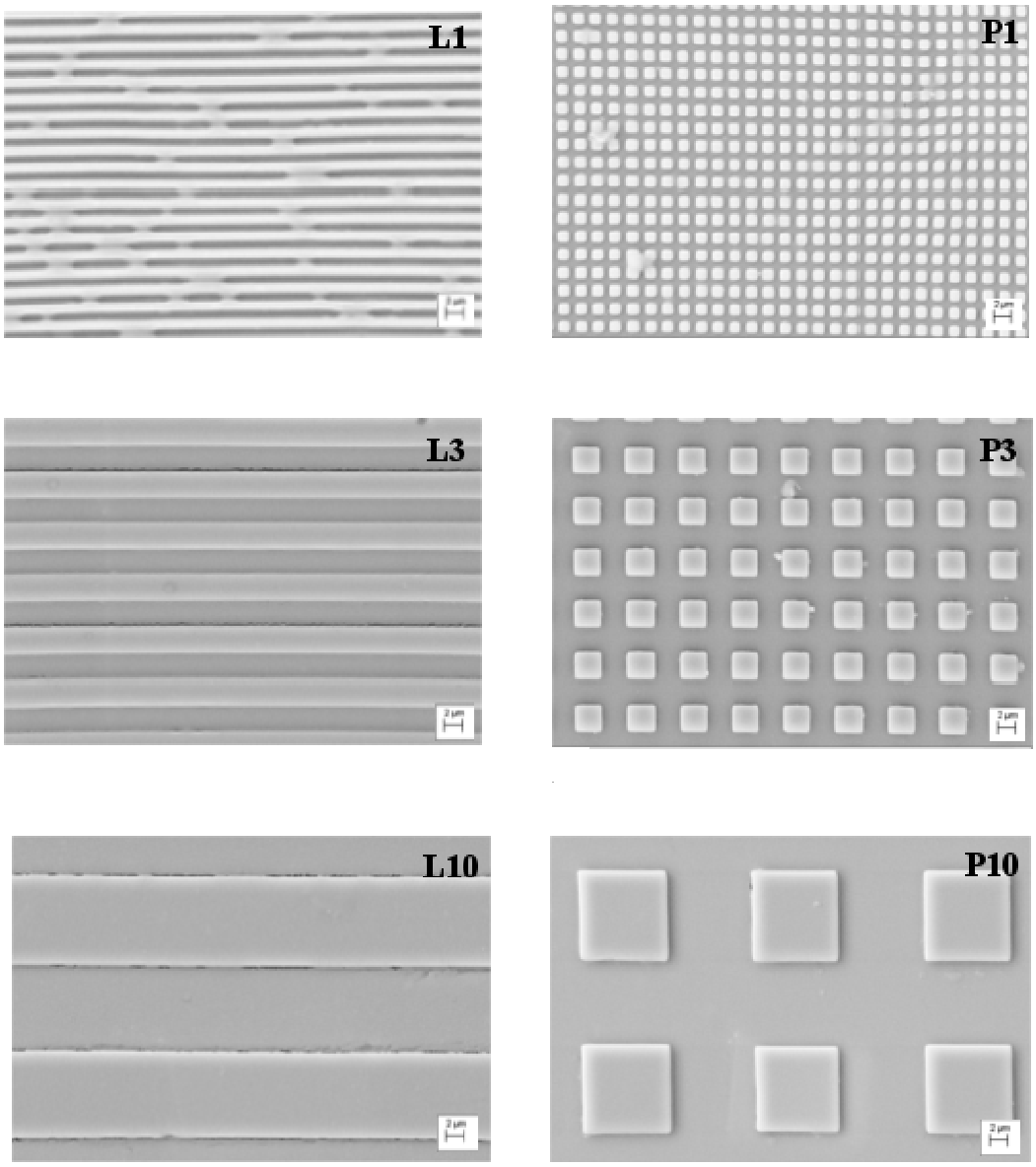

Figure 11: PDMS replica of microstructured Si masters: FE-SEM micrographs of the different substrates. Scale bar 2µm.

As shown in figure 2, high conformity between PDMS replica and Si master in terms of features characteristic dimensions (half pith, square and line width and depth) was obtained.

2.2.2 TSC cell culture

FE-SEM analysis

FE-SEM micrographs of TSCs cultured on micropatterned substrates are reported in figure 3.A significant difference in terms of morphology between cells cultured onto linear and squared pillar patterned surfaces could be observed. In particular, the representative images highlighted an elongated morphology in the linear pattern substrates and a more star-shaped morphology in the pillar pattern substrates.

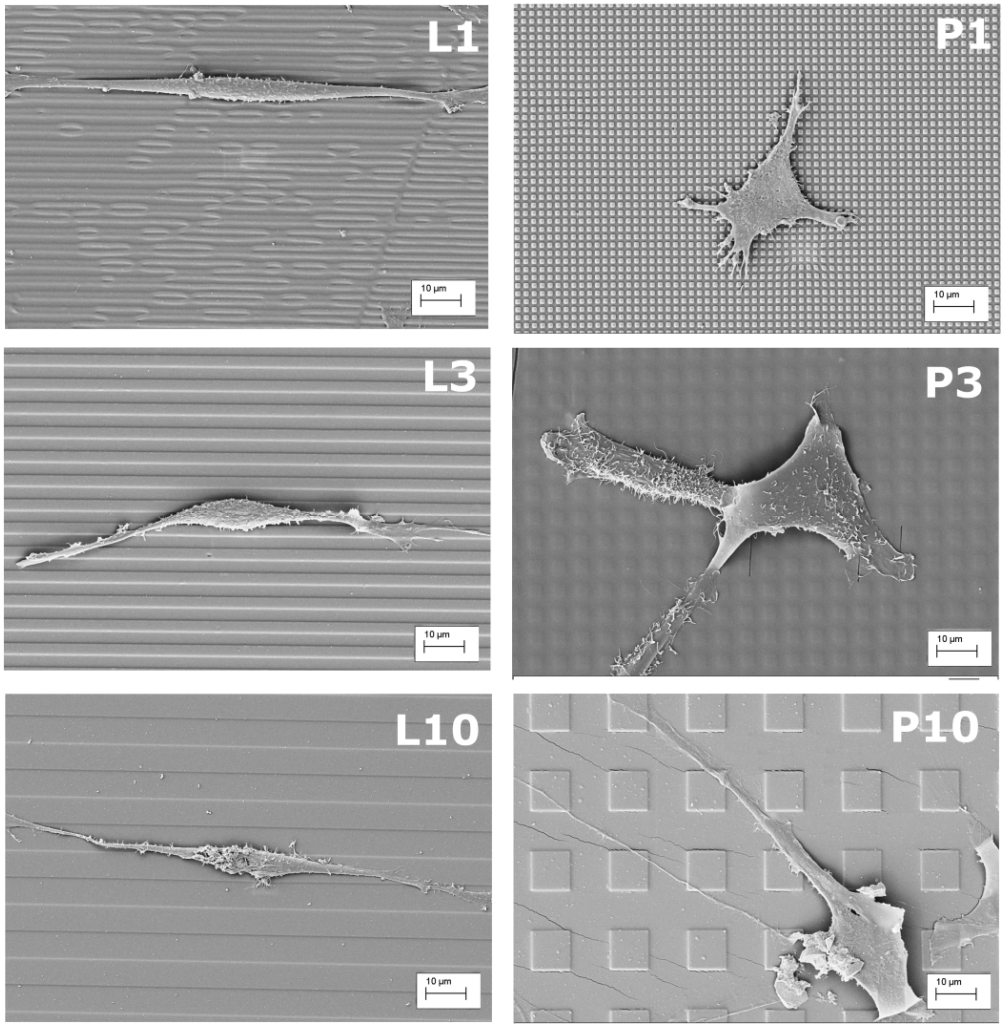

Figure 12: FE-SEM micrographs of TSCs cultured on different micropatterned substrates at 1.00 KX magnification. Scale bar 2µm.

Immunofluorescence analysis

Fluorescence microscopy images (figure 4) confirmed the topography-induced modulation of cell behavior revealed by FE-SEM. Actin cytoskeleton and nuclei were stained after 1 day of culture on micropatterned PDMS surfaces. As evidenced from the images, cells cultured onto linear pattern showed an elongated cellular morphology with a degree of alignment that decrease with the increase of the half-pitch of the substrate features. On the other side, cells cultured on squared pillars showed well spread star-shaped morphology with an orientation that roughly followed the perpendicular topography of the substrates.

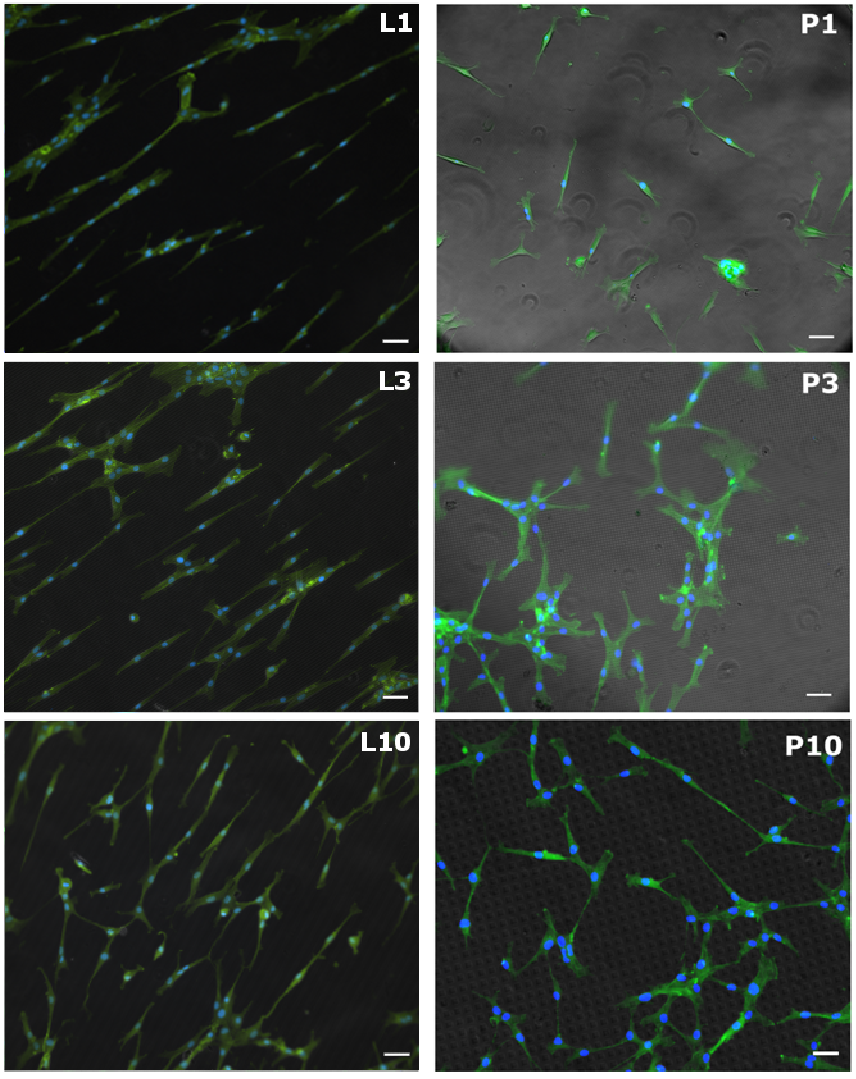

Figure 13:microscope images of TSCs grown on linear (L1, L3, L10) and pillar (P1, P3, P10) micro-patterns after 1 day of culture. Actin cytoskeleton stained with FITC-conjugate phalloidin (green); nuclear counterstain with DAPI (blue). Scale bar:50 μm.

Cell directionality

The average directionality was assessed by fluorescent images of actin immunostaining as previously described (§ 2.1.5.1.3.). Polar plots (figure 5) reveal the overall directionality of TSCs cultured on micropatterned PDMS surfaces after 5 days. Results demonstrated that cell orientation was sensibly affected by the different substrate topography. In fact, cells grown on line patterns showed preferential alignment, while cells grown on the pillar patterns revealed a random directionality that summarily followed the topographic features of the substrates in agreement with morphologic analysis.

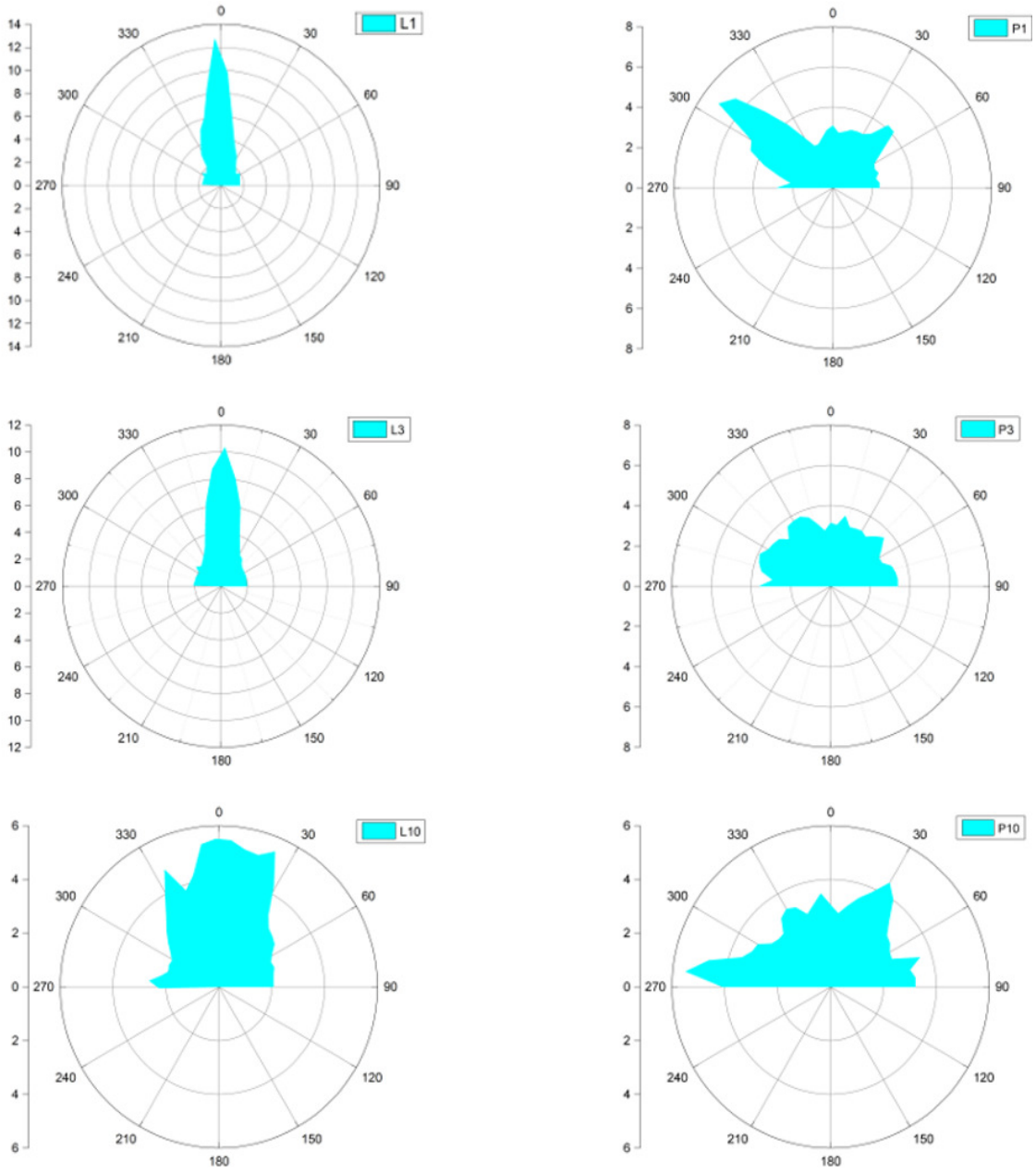

Figure 14: polar plots of TSCs orientation as function of the microfeatured topographic surfaces after 5 days of culture.

In order to quantitatively assess cell spatial organization, directionality histograms were fitted with Gaussian curves and dispersion (w) and directionality (xc) were quantified. Figure 6 summarizes the results of this analysis. Overall, w and xc were significantly affected by the presence of topographic features on the PDMS surface. In particular, while line patterns gave well fitted (Rsquare> 0.918) and very sharp Gaussian profiles, pillar histograms couldn't successfully be fitted with a single peak distribution (Rsquare< 0.806). Furthermore, differences in TSCs directionality were found on the base of the line pitch. As demonstrated by the increased value of Gaussian dispersion, contact guidance was more efficient in the case of smaller features than larger ones (22.387, 22.383 and 51.661 for L1, L3 e L10, respectively). Taken together, these data demonstrate that surface topography led to an evident change in TSCs polarization, and this effect was even sensitive to the different features spacing.

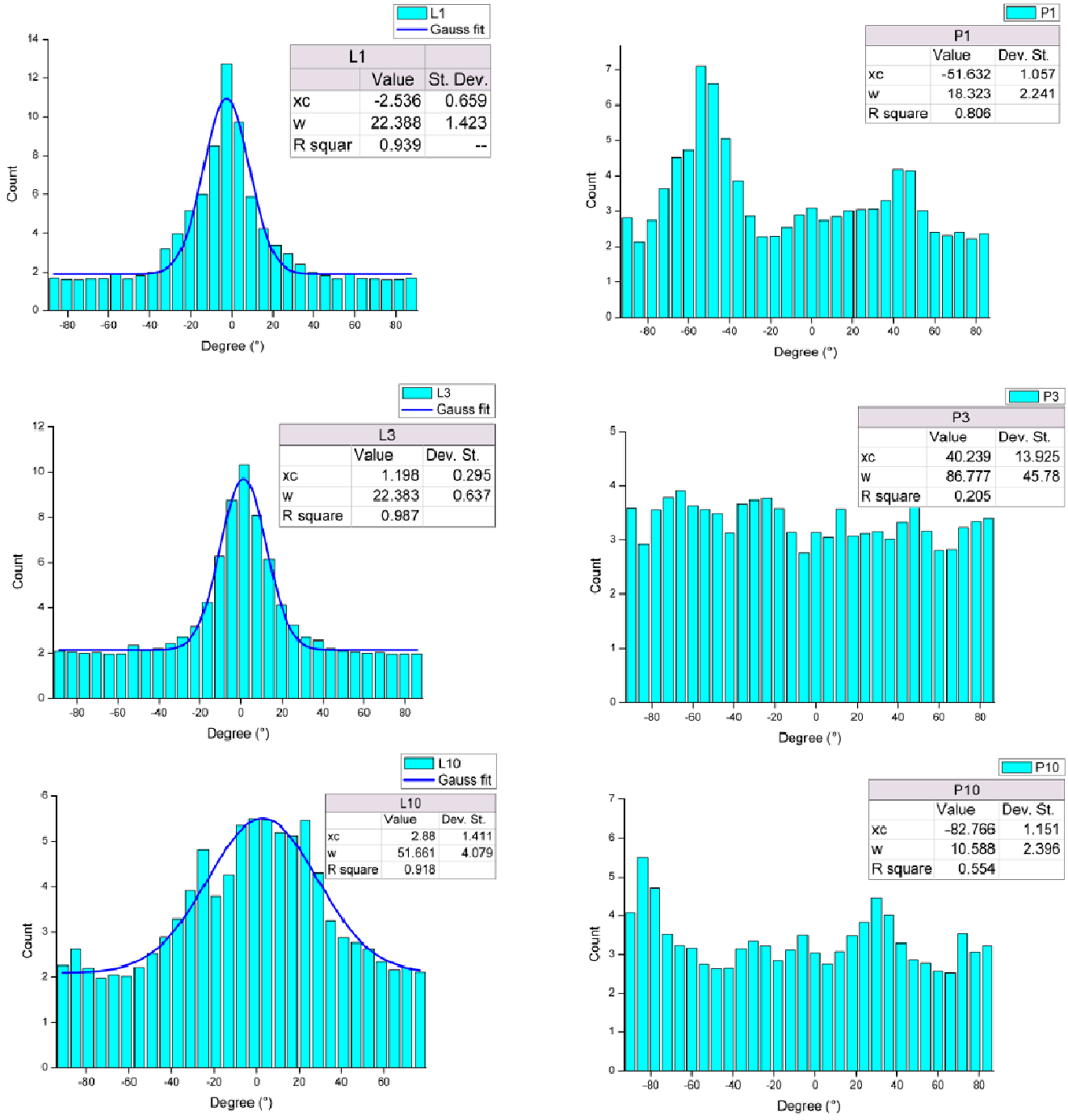

Figure 15: orientation histograms of TSCs cultured onto line and pillar patterned surfaces.

Cell elongation

Fluorescence micrographs (actin and nuclear counterstain) after 5 days of culture on PDMS were used to quantify cytoskeletal and nuclear elongation, respectively.

Quantitative analysis of cytoskeletal elongation was measured by the cellular aspect ratio as previously described in §2.1.5.1.3.The statistical analysis of the cytoskeletal elongation of TSCs cultured on PDMS substrates is reported in figure7 A. In particular, linear patterns with 3 µm half-pitch revealed a significantly higher ($p < 0.05$) aspect ratio compared to all other patterned substrates and CTRL. The statistical analysis also confirmed that cells cultured onto pillar patterned substrates did not show any difference in elongation behavior independently from half-pitch spacing.

This evidence was further confirmed by the analysis of nuclear elongation (figure 7 B). In fact, significantly enhanced elongation behavior was reported for TSCs cultured on the lower half-pitch in linear patterned PDMS. More in general, the nuclear aspect ratio of all linear surfaces was significantly higher than that of squared pillar surfaces as demonstrated by two-way ANOVA between linear (L1, L3, L10) and pillar (P1, P3, P10) groups.

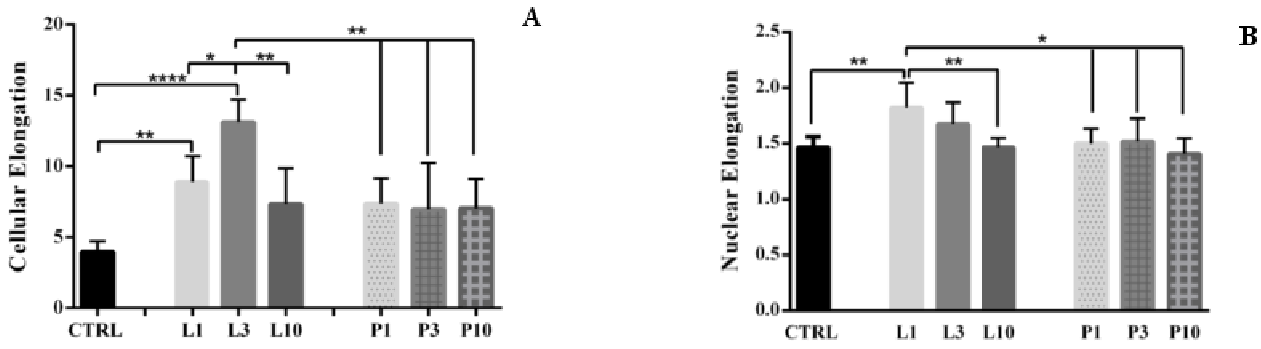

Figure 16: cellular (A) and nuclear (B) elongation (aspect ratio) of TSCs on PDMS substrates.

2.2.3 Tenocytes culture

Cell culture analysis

Cell viability and proliferation of TSCs cultured onto PDMS substrates were analyzed.

G6PD enzyme released every day in culture medium from apoptotic cells was evaluated to assess cell viability. Results showed a similar trend in all typologies of samples with viability percentage greater than 60% (figure 8 A).

Cell proliferation was evaluated by MTT assay as previously described. Figure 8 B shows a similar trend of cell proliferation in all types of PDMS substrates. Seeding efficacy was also evaluated after 1 day of culture and calculated as the ratio between the optical density (O.D.) of each sample and the O.D. of the same amount of cells seeded on plastic support. No difference in terms of seeding efficacy could be highlighted (table 1).

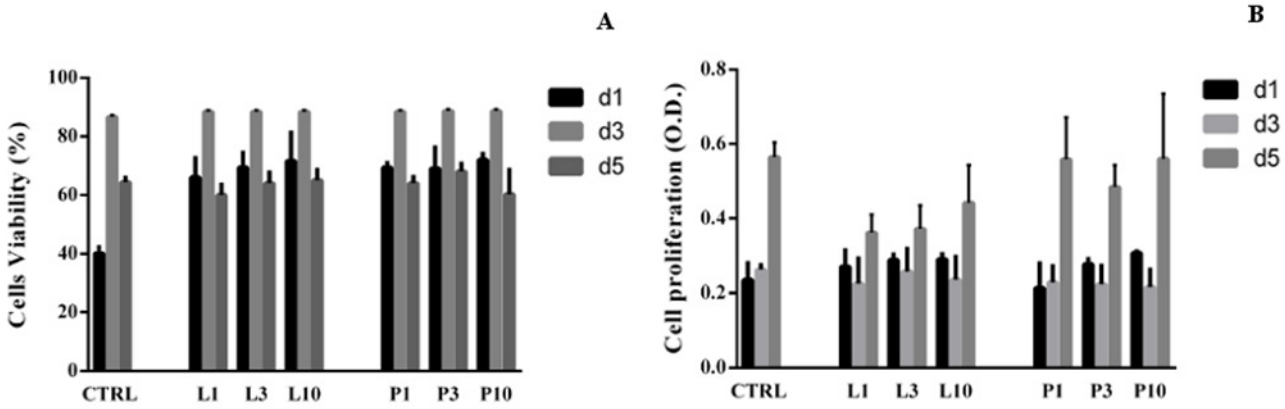

Figure 17: viability of tenocytes cultured on PDMS substrates (A);proliferation of tenocytes cultured on patterned andunpatterned PDMS substrates evaluated with MTT assay (B).

%	L1	L3	L10		P1	P3	P10		CTRL
PDMS	65 ± 4.4	66 ± 4.5	70 ± 1.4		51 ± 6.6	67 ± 1.3	74 ± 0.5		57 ± 18.9

Table 1: seeding efficacy of tenocytes cultured on patterned and unpatterned PDMS substrates after 1 day of culture.

Immunofluorescence analysis

In order to analyze the morphology of tenocytes grown on patterned and control PDMS substrates, samples were stained for actin cytoskeleton and nuclei after 1 day of culture (figure 9). Although immunofluorescent images showed good spread morphology on all types of substrates, cell shape was sensibly affected by the topographic features of the surfaces. In fact, cells cultured on linear features showed an elongated cellular cytoplasm, while tenocytes cultured on squared pillar showed a more spread morphology.

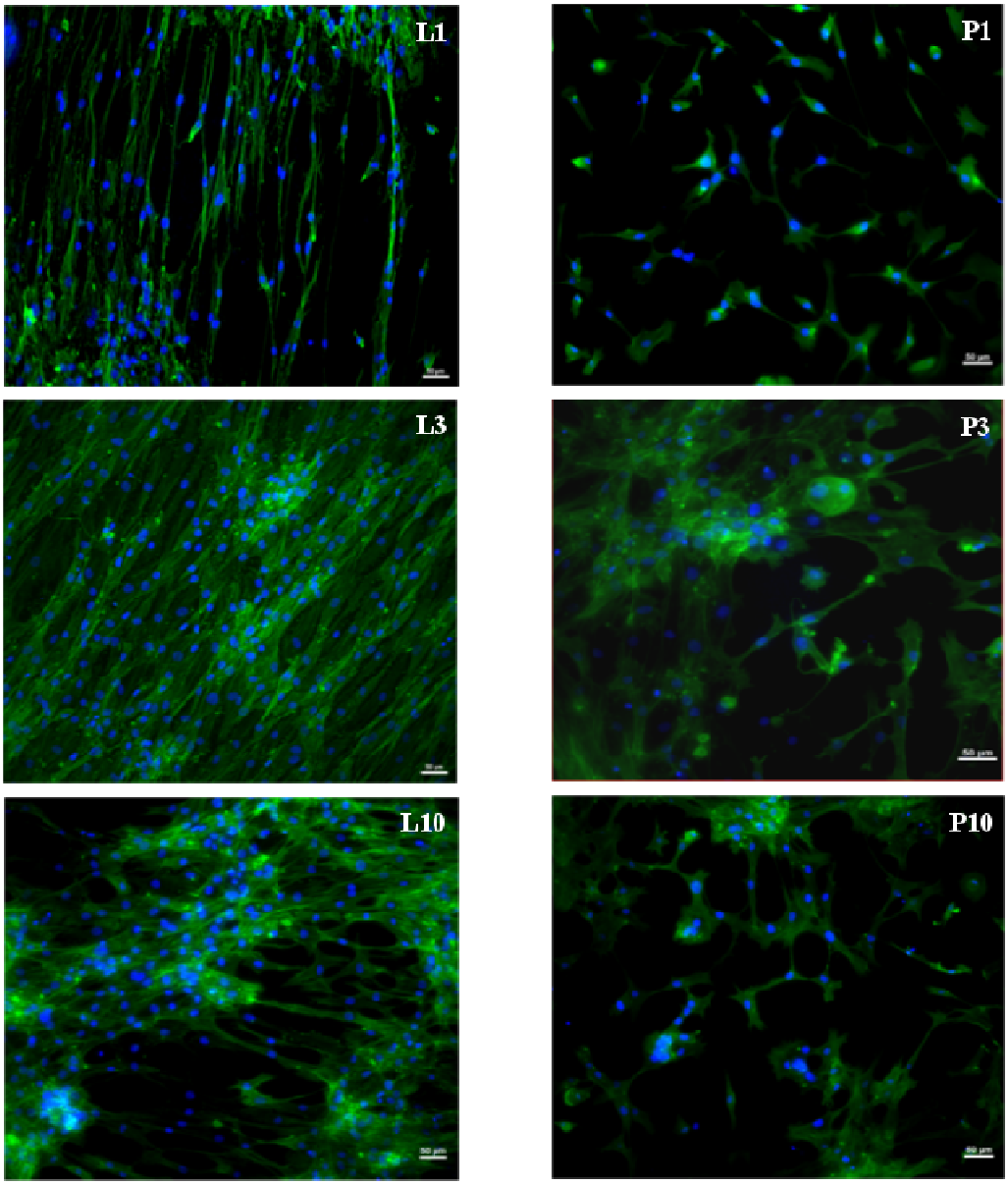

Figure 18: microscope images of tenocytes grown on linear (L1, L3, L10) and pillar (P1, P3, P10) micro-patterns after 1 day of culture. Actin cytoskeleton stained with FITC-conjugate phalloidin (green); nuclear counterstain with DAPI (blue). Scale bar: 50 µm.

ECM deposition

Immunofluorescence micrographs for collagen I and III were analyzed in terms of mean fluorescence intensity with NIS Elements AR software and results normalized with respect to CTRL, were reported in figure 10. As demonstrated by the bar chart in figure, while linear patterns mainly promoted the deposition of type I collagen, an increased yield of production of type III collagen was registered in square patterns. Since in healthy tendon ECM was mainly composed by collagen type I (80-95 %) [60, 113], linear features could represent the best candidate substrate to mimic a healthy native ECM.

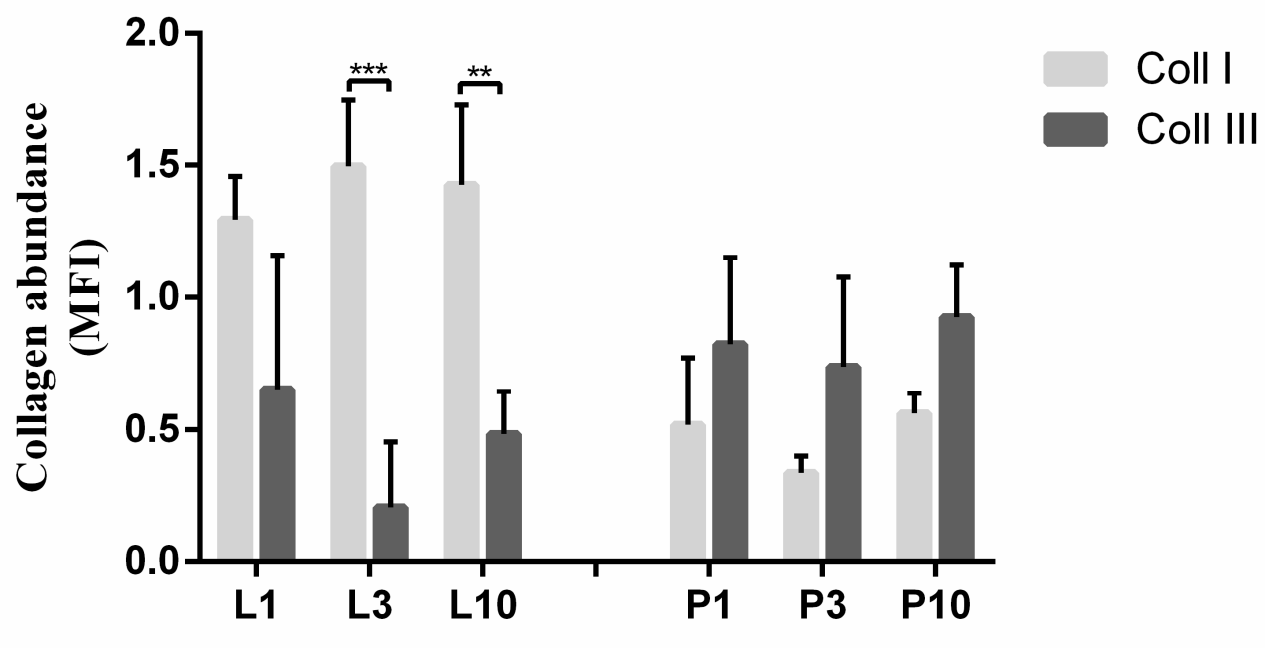

Figure 19: fluorescence intensity of type I and type III collagen deposited from tenocytes after 5 days of culture onto PDMS substrates**.**

Cell directionality

Cell directionality was assessed as previously described for TSCs (§ 2.3.2.2.1). Figure 11 shows the polar plot of tenocytes cultured for 5 days onto line and pillar patterned surfaces. As demonstrated for TSCs directionality, a higher alignment was evidenced for linear pattern, particularly for 1 and 3 µm half-pitch. On the other hand, tenocytes grown on pillar patterns were only slightly influenced by the substrate topography, showing only rough orientation along the main direction of the pattern surfaces.

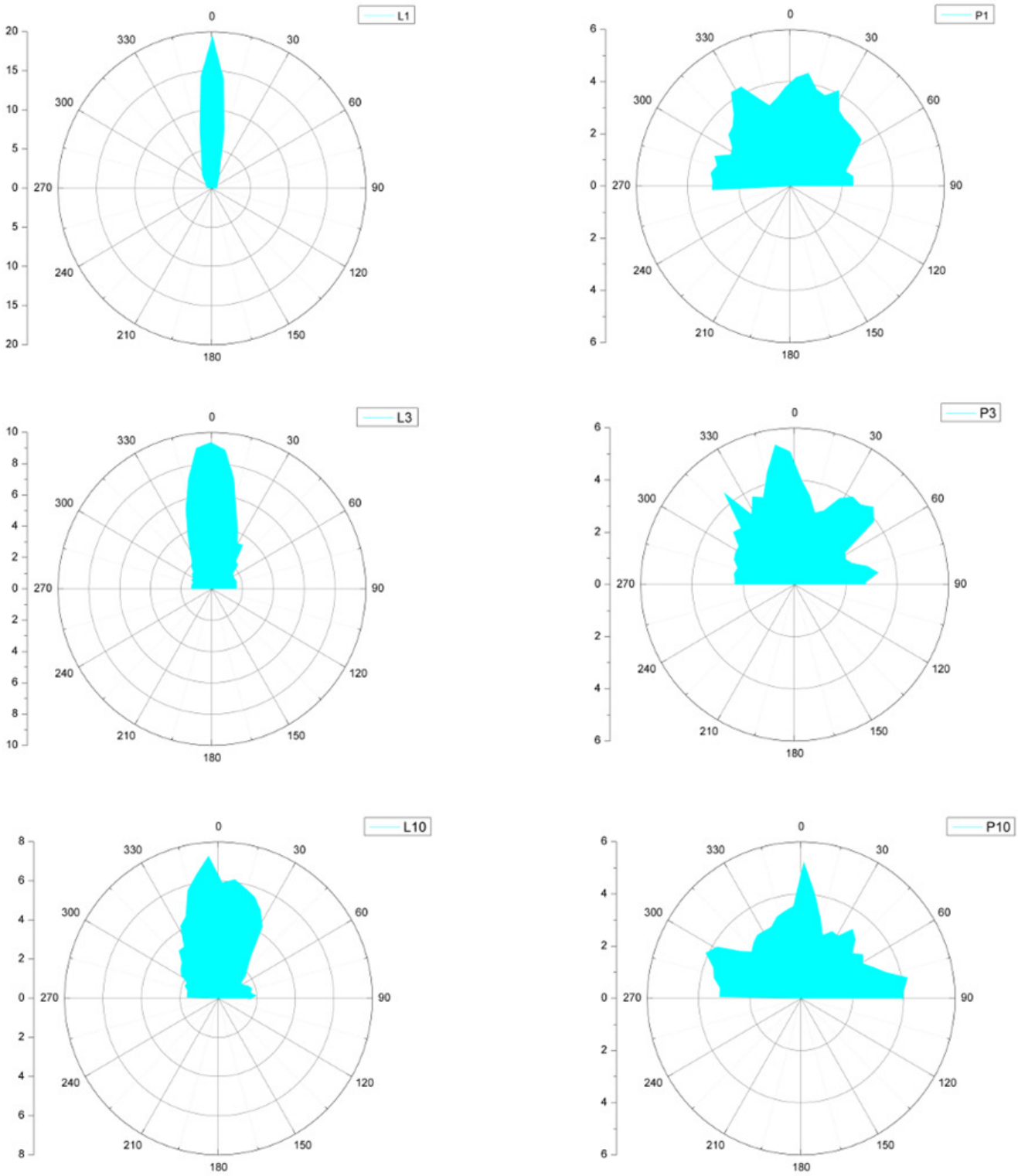

Figure 20: polar plots of tenocytes orientation as function of the microfeatured topographic surfaces after 5 days of culture

As previously described for TSCs directionality analysis, tenocytes spatial organization were quantified fitting with Gaussian curves fluorescence dispersion (w) and directionality (xc) results in order to obtain directionality histograms. Even in this case, w and xc were significantly affected by the presence of topographic features on the PDMS surface (figure 12). In particular, while line patterns returned well fitted (Rsquare> 0.960) and very sharp Gaussian profiles, pillar histograms couldn't successfully be fitted with a single peak distribution (Rsquare< 0.371). Furthermore, differences in tenocytes directionality were found on the base of the line pitch. As demonstrated by the increased value of Gaussian dispersion, contact guidance was more efficient in case of small pitch than on larger one (18.034, 32.130 and 48.403 for L1, L3 e L10 respectively). Taken together, these data demonstrate that surface topography led to an evident change in tenocytes polarization, and this effect was even sensitive to the different features spacing.

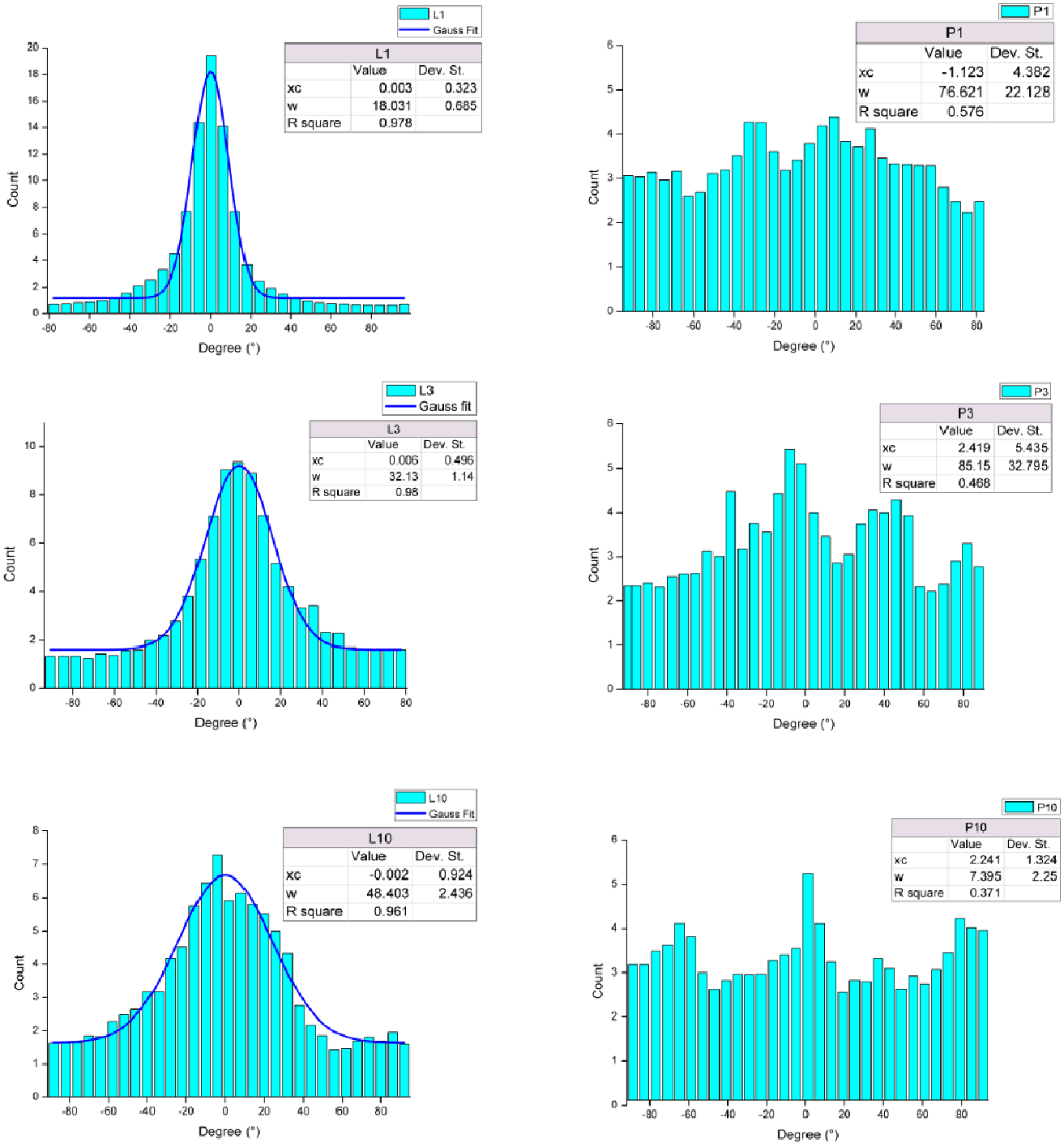

Figure 21: orientation histograms of tenocytes cultured onto line and pillar patterned surfaces.

Cell elongation

Fluorescence micrographs (actin and nuclear counterstain) after 5 days of culture on PDMS substrates was used to quantify cytoskeletal and nuclear elongation, respectively. The statistical analysis of the cytoskeletal elongation of tenocytes cultured on PDMS substrates is reported in figure 13 A. As already demonstrated for TSCs, linear patterns with low half-pitch (1 and 3 µm) revealed a significant higher ($p < 0.05$) aspect ratio with respect to all other patterned substrates and CTRL. The statistical analysis also confirmed that cells cultured onto pillar patterned substrates did not show any difference in elongation behavior independently from half-pitch spacing.

Nuclear elongation is reported in figure 13 B. The results did not show statistical differences between cells plated on patterned and non-patterned surfaces independently from the considered half-pith. These data are in agreement with extracellular matrix (collagen type I or III) produced by tenocytes cultured onto all types of PDMS substrates as previously described in § 2.3.3.2.1.

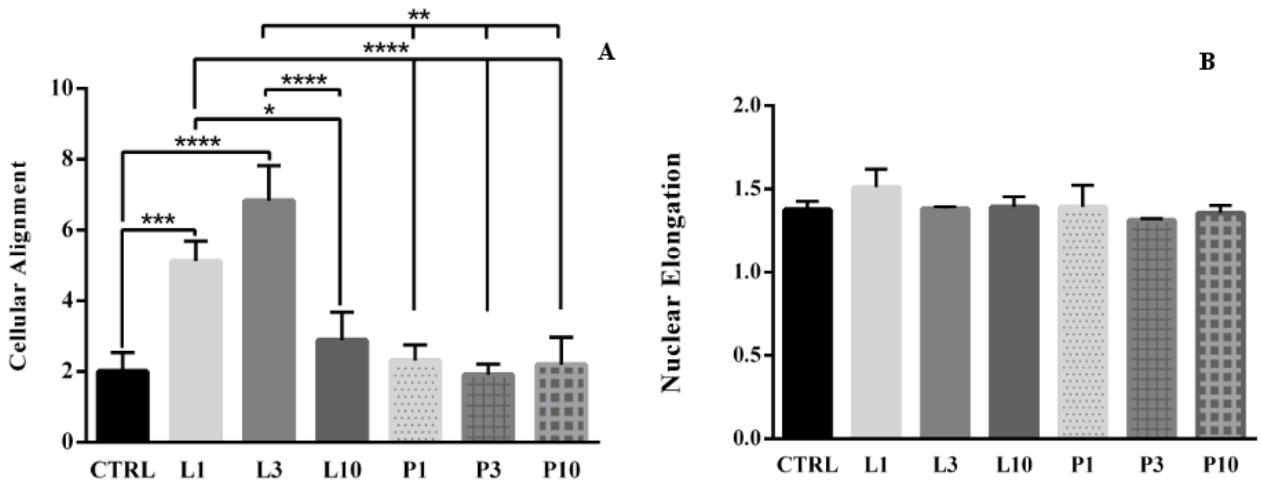

Figure 22: cellular (A) and nuclear (B) elongation (aspect ratio) of tenocytes on PDMS substrates

Cell migration

As known cell migration is influenced by topographical features [62]. In particular it is involved in physiological and pathological processes like embryogenesis, tissue organization, tissue repair, immuno-response, vascular disease and methastasis [114-117]. Figure 14 shows 2D trajectory plots obtained from the tracking of 12 single cells cultured on each type of substrate for 15 h. Each plot shows a cross symbol named center of mass (COM) that represents the spatial averaged point of all cell endpoints.

$$COM = \frac{1}{n}\sum_{i=1}^{n}(x_{i,end}, y_{i,end})$$

This value reveals the preferential direction of the migration of all cells analyzed. In the linear features, COM is particularly close to y-axis, proving the preferential migration of cells along linear topography. Conversely, COM of cells cultured on pillar substrates is farther than y-axis positioned approximately 45°. This result proves a significant effect of substrate topography on the overall direction of cell migration not only for linear features, but also for pillar patterned surfaces.

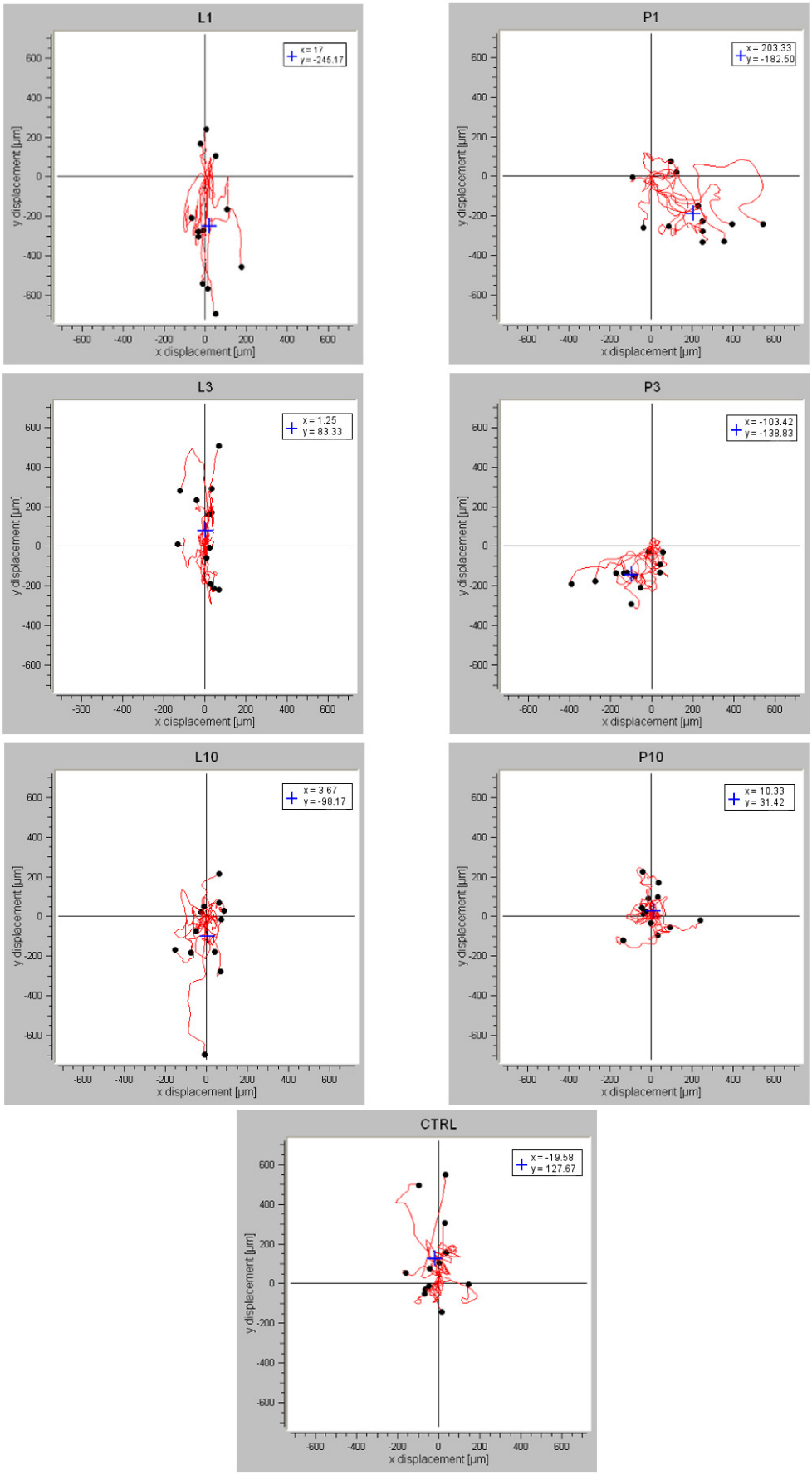

Figure 23: 2D trajectory plots of tenocytes migration for 15 h of culture.

Figure 15 shows the trend of Line Length value, which is defined as the distance travelled by the cell in each frame respect to its starting point. The plots were obtained from the average of line lengths of 12 cells for each substrate. Although the results show a similar trend for all the samples, a greater distancing from the starting point is evidenced for L1 and P1 substrates probably due to the small topographical features. However, velocity of cell migration is substantially independent from the typology of substrate (around 46.8 ± 14.4 µm/h for all PDMS surfaces).

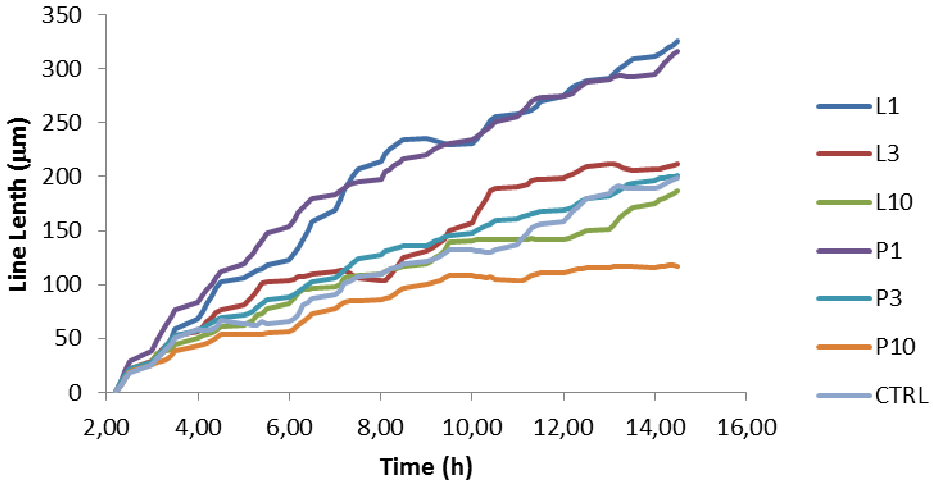

Figure 24: plot of line length for 15 h in culture conditions (n = 12).

2.3 Conclusion

Several literature studies demonstrated the capability to control cell response after culture on patterned 2D surfaces [118-123]. In this work, micropatterned PDMS were fabricated with different topographical features (lines and squared pillars) and different half-pitch values (1, 3 and 10 μm) in order to mimic tendon ECM conditions. These substrates were used for TSCs and tenocytes culture without any additional physical or mechanical external stimuli. Results demonstrate the strongly influence of surface features whit regard to spreading, morphology and cell orientation. In fact, TSCs and tenocytes follow the topographical features of the surfaces both on the linear and pillar pattern in agreement with their cytoskeleton and nuclear elongation and cell directionality. Extensive studies on the tenocytes ECM deposition and migration were addressed. In particular, the lack of significant differences in nuclear elongation of tenocytes cultured on lines and pillar pattern, are in keeping with deposition of collagen type I and III respectively. These results demonstrate that, independently of the type of features, an ECM deposition is present although the lower lines half-pitch are able to produce type I collagen like native tendon ECM.

Regarding tenocytes migration, results demonstrate that there are preferential directions of the migration of all cells cultured on the linear features although there aren't differences in terms of velocity. Only lower topographical features (L1 and P1) highlight a greater motility from their starting point probably due to their small features.

Overall this work suggests a potential 2D substrates for cell *in vitro* studies for synthesis of biomaterials for tissue engineering applications.

CHAPTER 3: Microcontact printing on hard substrates

Introduction

Targeting surface patterning, self-assembled monolayer [124], dip-pen nanolithography [125-126], ink-jet printing [127-128], and microcontact printing(μCP) [1] are among the most widely used techniques for spatially controlled deposition of biomolecules. In less than two decades, μCP has emerged as one of the most straightforward methods for the preparation of microstructured and nanostructured surfaces due to its simplicity and wide range of possible applications. μCP relies on a polymeric stamp with a relief pattern obtained as a replica from a photolithographically structured master. The stamp is 'inked' with biomolecules and placed in contact with the substrate. Because of its surface relief structure, the stamp only contacts the substrate in predefined areas, where the structure protrudes from the stamp. Well-defined protein patterns with precisely controlled size, shape, and spacing have been successfully obtained by μCP and used to study cell adhesion, migration, proliferation, and apoptosis, as well as to perform high-throughput drug screening and disease diagnosis [128-130].

Aim of this study is to analyze the response of tendon-derived cells and mesenchimal stromal cells cultured on patterns obtained through μCP. *In vitro* performance of the patterned substrates has been evaluated in order to study the influence of substrate topography on cell morphology, proliferation, and preservation of cell stemness.

3.1 Materials and Methods

3.1.1 Fabrication of microstructured master

Silicon masters were fabricated in order to obtain PDMS replicas consisting in an array of circular pillars, with different dimensions and spacing.

Master molds were fabricated on a silicon wafer with SU-8 negative photoresist (SU8-2010, Microchem, Newton, MA) following a standard photolithographic process according to the manufacturer's instructions.

To obtain maximum process reliability, substrates were first cleaned using a O_2 plasma in a reactive ion etching (RIE, Diener Electronic, Ebhausen, Germany, 10 W, 1.0 mbar, 36 sec) system to improve the adhesion of SU-8 films. Then, the photoresist was spin-coated on the silicon wafer and exposed to ultraviolet light through a patterned photomask. Finally, the master was developed in propylene-glycol-methyl-ether-acetate (PGMEA, Sigma-Aldrich, Milano, IT), rinsed with isopropanol (Sigma-Aldrich, Milano, IT) and thermally cured at 150 °C for 1h. Optimized process parameters are summarized in table 1. Final thickness and uniformity of SU-8 microstructures were measured by a profilometer.

Prior to casting the elastomer in the silicon master, the mold was silanized with trimethylchlorosilane (TMCS, Sigma-Aldrich, Milano, IT) vapor in a closed desiccator for 2 hour. At the end of the process, a silanization layer coats the SU-8 mold and facilitates detachment of cured PDMS elastomer.

Spin rate	Pre-bake	Exposure	Post-bake	Develop
1500 rpm 30 s	65°C 1min. 95°C 2 min.	16 s	95°C 45 s	3.50 min.

Table 2: process parameters for the fabrication of SU-8 patterned master.

3.1.1.1 Replica molding and washing of PDMS

PDMS stamps were obtained by a replica molding technique starting from silicon masters with the desired negative patterns. Once fabricated, masters can be repeatedly used to cast PDMS stamps, and the stamps themselves can be routinely cleaned and reused several times. PDMS and its curing agent were mixed thoroughly at the weight ratio of 10:1, poured over the photolithographically patterned master and cured as previously described in § 2.2.2. Pattern features are reported in table 2.

All PDMS replicas were cut in a cylindrical shape with a biopsy punch (Ø 8 mm) in order to standardize μCP area.

To avoid the transfer of low molecular weight non-crosslinked PDMS oligomers, the washing protocol developed by Graham *et al* was adopted [110-111].

PDMS Prepol./curing ag.	Ø (μm)	Pitches (μm)	Depth (μm)	Cells
10:1 w/w	25, 50, 75, 100	200	20	TSCs
	25	50		MSCs

Table 1: Pattern features of PDMS replicas

3.1.1.1.1 PDMS substrates characterization

Field emission scanning electron microscopy (FE-SEM, Supra1535, LEO Electron Microscopy, Oberkochen, Germany) was used to characterize the geometry of the fabricated PDMS microstructures. Patterned PDMS replicas were sputter-coated with a conductive layer of gold (EmitechK550 sputter coater, Quorum Technologies Ltd) and viewed at 8 mm working distance (WD) and at an accelerating voltage of 5 kV with SE detector.

3.1.2 Fluorescently labeling procedure

Two types of proteins were utilized and labeled with Rhodamine B isothiocyanate (TRITC, Sigma-Aldrich, Milano, IT) for μCP: Collagen type I (Advanced BioMatrix, San Diego, CA) and Poly-L-lysine (PLL, Sigma-Aldrich, Milano, IT).

Collagen type I (~ 300 kDa), 3.1 mg/mL aqueous solution was used for μCP onto polystyrene (PS) ultra low attachment multiwell plates (Corning Incorporated, New York, USA). To visualize the transferred protein pattern with fluorescence microscopy, collagen was labeled with TRITC according to the protocol disclosed by Cross *et al.* [131]. Briefly, the collagen aqueous solution was lyophilized (LIO-5PDGT, 5Pascal, Milan, Italy) and then resuspended for 8 hours at 4 °C in 0.1 M sodium bicarbonate buffer (pH 9.0) at a final concentration of 20 mg/ml. The solution obtained was then mixed with 10 mg/ml TRITC solution in DMSO at a 3:1 molar ratio and stirred at 4 °C for 24 hours. The mixture was dialyzed for at least 72 hours at 4 °C in 0.1 % acetic acid using dialysis tubes with a molecular weight cut-off of 25 kDa.

Poly-L-lysine aqueous solution (70–150 kDa) was used at a concentration of 100 μg/mL. To visualize the transferred protein pattern, PLL was fluorescently labeled with TRITC according to the manufacturer's instructions. After incubation, the mixture was filtered through a 0.2 μm syringe. The labeled proteins were stored at 4 °C upon use. All procedures were performed in the dark.

3.1.3 Microcontact printing procedure

Stamps were inked by depositing the labeled protein solutions on their patterned side and by incubating in the dark for 20 and 30 minutes for collagen and PLL, respectively.

After incubation the inked stamp was dried under a mild nitrogen stream to remove excess ink and contacted with PS multiwell ultra low attachment substrates.

In the case of collagen, an accurate drying process was necessary to obtain a precise protein transfer. In particular, after incubation with labeled collage, excess ink was removed by a gentle N_2blow for 1 minute. PDMS was dried in vacuum desiccator for 10 minutes and, finally, contacted with the PS multiwell substrates for 30 seconds (figure 1 A – C).

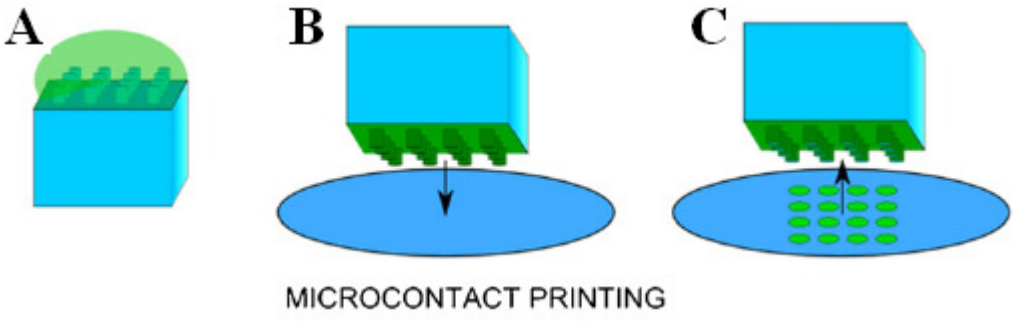

Figure 25: illustration of microcontact printing of PDMS replica onto a PS multiwell substrate (partially adapted from [132]).

In order to accurately control the amount of applied pressure, microcontact printing was performed using a customized jig mounted onto a tensile tester (model 3365, Instron, Norwood, MA) equipped with a 10N load cell. The setup was opportunely modified to house both the PDMS stamp and the PS multiwell substrate. The stamp was connected to the moving crosshead through a compliant rubber stub, which accommodated misalignments while allowing a better force resolution by lowering the stiffness of the system (figure 2).

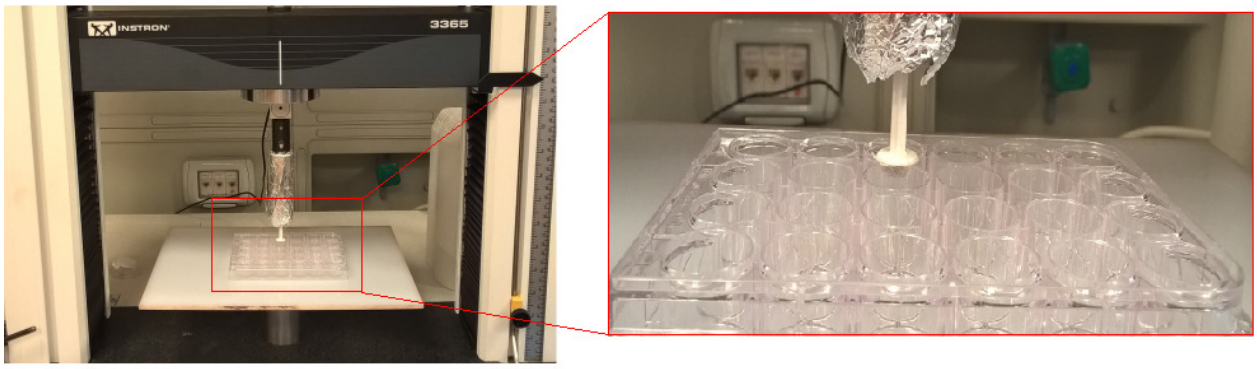

Figure 26: microcontactprinting system: a tensile tester was purposely modified to house the PDMS stamp and the PS multiwall substrate.

Protein transfer was performed by bringing the stamp into contact with the PS specimen surface at a constant crosshead speed. Depending upon the stamp contact area, a suitable loading force was applied to achieve the required as contact pressure. After contact time had elapsed, as the protein pattern was transferred to the substrate, the stamp was automatically retracted.

Prior to cell seeding, the multiwell with transferred protein pattern was sterilized under UV light for 10 minutes.

3.1.3.1 Immunofluorescence images

Images of μCP patterns were acquired with an epifluorescence microscope (Nikon, Tokyo, Japan) in order to optimize printing parameters (force, drying procedure and time of contact) and obtain an optimal transfer on the PS multiwell substrates.

3.1.4 Cells seeding

Two cells types were selected. Cell culture media and all supplements were provided by Life Techonologies (Life Techonologies, Milano, IT).

3.1.4.1 TSCs seeding

TSCs, previously described in § 2.2.5.1, were seeded at passage 1 on the patterned specimens at $2.5 \cdot 10^4$ cells per $cm^2$and cultured in αMEM supplemented with 10% (v/v) FBS, 1% (v/v) pen-strep and 1% L-glutamine under humidified atmosphere with 5% CO_2 at 37 °C. The experiments were conducted at different time points: 24, 72, 120 and 420 h (d1, d3, d5and d7) and the medium was changed twice a week. TSCs seeding were performed at the same density on tissue culture multiwell as a control (CTRL). Each experiment was done in triplicate and analyzed for morphometry, viability, proliferationand preservation of stemness with immunofluorescence staining.

3.1.4.1.1 Cell viability and proliferationanalysis

Live/Dead assay (Thermo Fisher Scientific, Monza, IT) was utilized to assess cellular morphology (d1) and cell viability (d3, d5 and d7), at predetermined time point, following manufacturer's protocol. Briefly, TSCs seeded onto microprinted surfaces were washed 3 times with PBS and staining with calcein and ethidium homodimer solutions at 2 μM and 4 μM concentration respectively. The cells were incubated at 37 °C for 45 min. Live cells retains calcein solution (green, λex/em ~495 nm/~515 nm) and exclude the ethidium that can only enter in dead cells (red, λex/em 495 nm/~635 nm). Cells were viewed under an inverted epifluorescence microscope (Nikon Ti-E) and counted using NIS Elements AR software. Viability was expressed as % viable cells.

Cell proliferation was assessed at time point d1, d3, and d5, by counting the number of cells (identified by their nuclei, DAPI stain) on each pad. Cells viability and proliferation were evaluated in three independent experiments.

3.1.4.1.2 Focal adhesion analysis

In order to study TSCs response towards microprinted pattern surfaces, focal adhesion contacts of cells were analyzed using immunofluorescence staining. In particular, α2β1 integrin mediate mainly cell adhesion to the collagen type I of ECM and contribute to activate intracellular pathway for regulation of gene expression and stem cell fate [133-136]. After 5 days of culture, TSCs were fixed in 4% w/v PFA solution for 3 minutes and washed in PBS three times. Then, BSA at 2% w/v in PBS was added for blocking nonspecific sites for 45 minutes at room temperature. Rabbit anti-human antibody against the α2β1 integrin (1:100, Abcam, Milan. IT) was added to the fixed cells for 1 h at 37°C. After washing in PBS the samples were incubated for 45 minutes with the specific secondary antibodies AlexaFluor 488 (1:500 green). Cells were then permeabilized with 0.1% v/v of Triton-X 100 solution in PBS for 10 minutes and stained for TRITC–conjugated Phalloidin (1:500, red). DAPI was used as a nuclear counterstain at 2 µg/mL concentration.
Images at d5 time points of three independent experiments were acquired (Nikon, Tokyo, Japan).

3.1.4.1.3 Stem cell preservation

In order to quantify the stem cells preservation, TSCs seeded on micropatterned PS substrates and on CTRL, were stained for STRO-1 antigen, a cell surface antigen expressed by stromal cell precursors [137-139]. After 3 and 5 days of culture, TSCs were fixed, washed and permeabilized as previously described (§ 3.2.4.1.2) and then stained with mouse anti-human antibody (Thermo Fisher Scientific, Monza IT) diluted 1:100 in PBS against STRO-1 antigen for 1h at 37 °C. After washing the anti-rabbit fluorescent secondary antibody diluted 1:500 in PBS (far-red, Thermo Fisher Scientific, Monza IT) was added for 45 min in the dark. DAPI was used as a nuclear counterstain. Fluorescence intensity was analyzed by NIS Elements AR software (Nikon, Tokyo, Japan) at d3 and d5 time points. For each image, background was subtracted to avoid overestimation of the measurements.

3.1.4.2 hMSC seeding

Human bone-marrow-derived mesenchymal stromal cells at passage 5 (hMSCs, Lonza, Basel, CH) were seeded with a density of $2 \cdot 10^4$ cells/cm^2 and cultured with the same complete medium in the same incubation condition.

3.1.4.2.1 Cell morphology and focal adhesion analysis on hard substrates

hMSC were seeded on PLL-patterned PS multiwell ultra low attachment substrates. Pattern consisted in an array of 25 μm circles with a pitch of 50 μm in both x and y directions. Morphology and focal adhesion contacts of hMSC were analyzed after 1 and 3 days.

Cells morphology was evaluated by phase contrast images, and focal adhesion were analyzed using immunofluorescence staining of vinculin. It is a protein that linking the membrane integrin connected with focal adhesion to actin cytoskeleton filaments [140-142]. After 3 days of culture, hMSCs were fixed in 4% w/v PFA solution for 3 minutes and washed in PBS three times. The cells were permeabilized with 0.1% v/v of Triton-X 100 solution in PBS for 10 minutes, added with BSA at 2% w/v in PBS for blocking nonspecific sites for 45 minutes at room temperature and stained for vinculin with mouse anti-human antibody (1:200, Abcam, Milan. IT)for 1 h at 37°C.After washing in PBS the samples were incubated for 45 minutes with the specific secondary antibodies AlexaFluor 488 (1:500 green, Thermo Fisher Scientific, Monza, IT). DAPI was used as a nuclear counterstain.

All images were acquired with inverted microscope (Eclipse Ti-E, Nikon, Japan).

3.1.5 Statistical analysis

Experimental data were analyzed using GraphPad Prism® 5 (GraphPad Software, USA). Conditions of normality were checked with Shapiro–Wilk test. Normally distributed data were analyzed for significance by *T*-Student test and ANOVA (one- or two-way), followed by Tukey's multiple comparison post hoc test (Tukey). Statistical significance was accepted at $p < 0.05$. Data are presented as mean value ± standard deviation.

3.2 Results and discussion

3.2.1 PDMS FE-SEM analysis

Figure 3 reports a macroscopic image of the SU-8 silicon master utilized for PDMS replica molding [107].

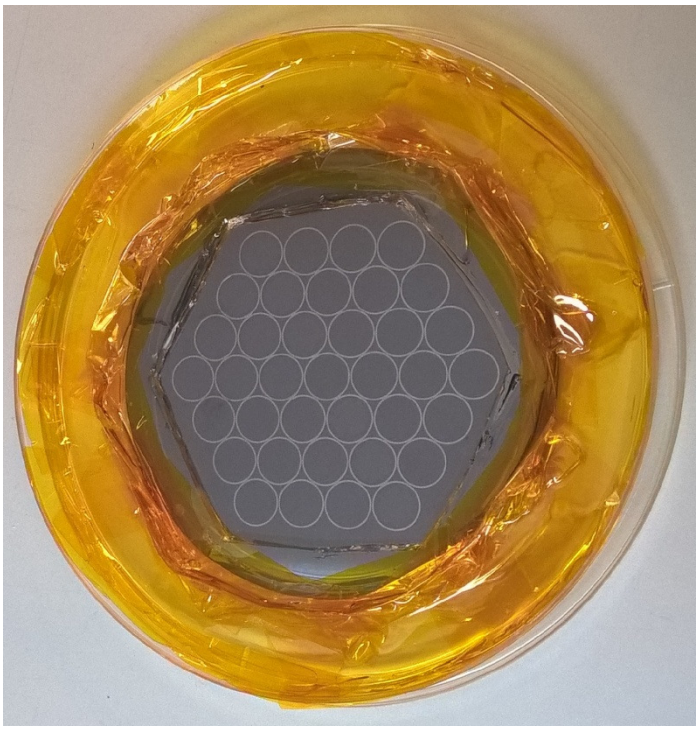

Figure 27: silicon master templates realized with soft lithography.

PDMS substrates obtained by replica molding were analyzed by FE-SEM microscopy. Micrographs reported in figure 4 showed the PDMS substrates for TSs culture. In particular it is evident high conformity between 10:1 w/w PDMS replica (Young's modulus 2.61 ± 0.021 MPa [107]) and Si master in terms of characteristic dimensions: diameters (25, 50, 75 and 100 μm), depth (20 μm) and pitch (200 μm) of circle base pillar (fig. 4 A – D). Furthermore, detail of each typology of PDMS stamps (figure 4 E – H) and representative micrograph of depth (figure 4 I) were reported.

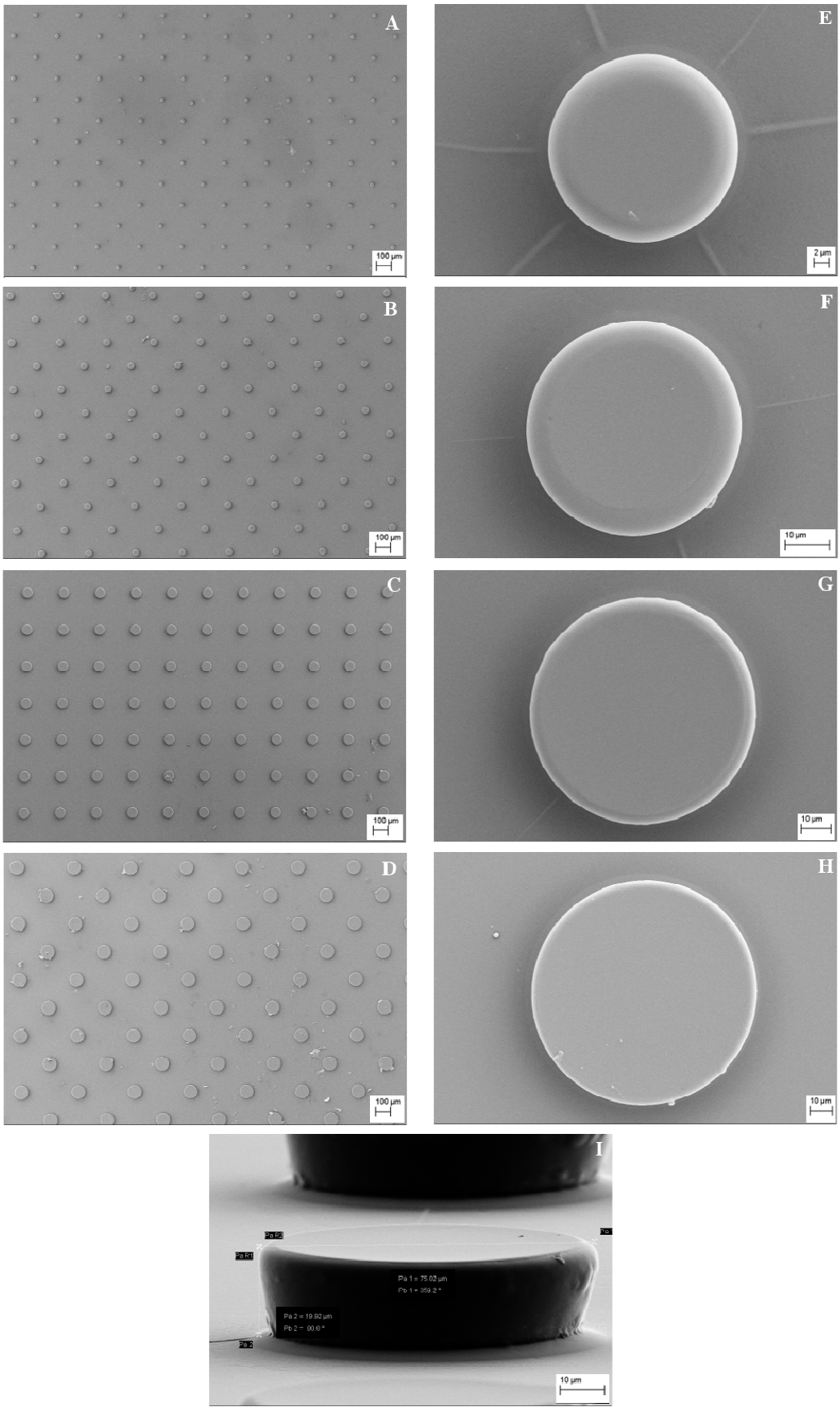

Figure 28: PDMS replica of circle base pillar of different diameters: 25 (A), 50 (B), 75 (C) and 100 µm (D) ; scale bar 100 µm. Detail of each stamps (E - H); scale bar 10 µm. Detail of depth of 20 µm; scale bar 10 µm

The surface morphology and fidelity of the PDMS patterns with Ø 25 µm and pitch 50 µm, for hMSC culture, were examined by FE-SEM. Representative micrograph of PDMS replica have been reported in figure 5. As shown, the pillars were about 25 µm with no defects.

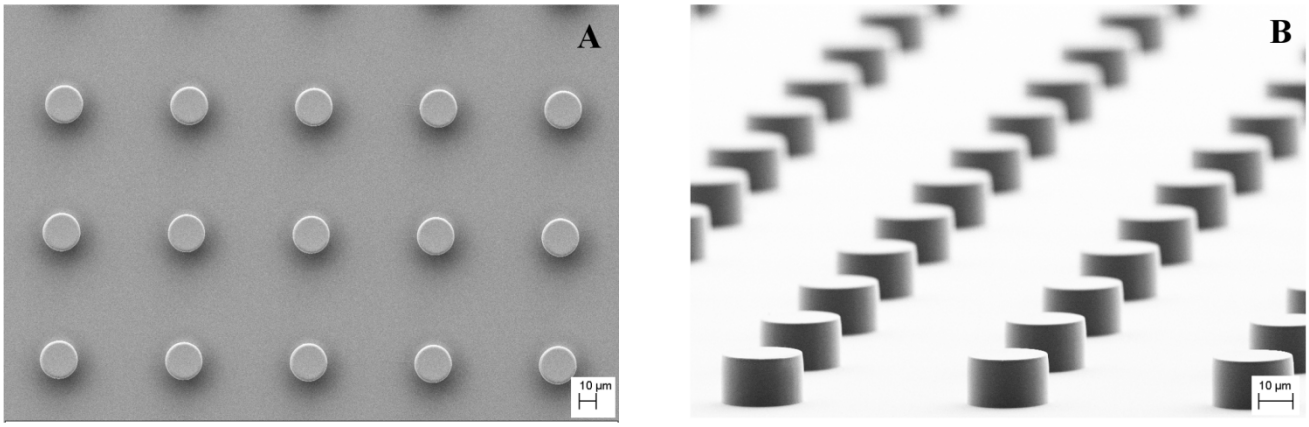

Figure 29: FEG-SEM micrograph of PDMS pillars obtained by replica molding Ø 25 µm spaced 50 µm. Magnification 1k (A) and 2 k (B). Scale bar 10 µm.

3.2.2 Immunofluorescence images

Figure 6 shows representative images of TRITC-labeled collagen transfers onto PS multiwell substrates. In particular, changing drying time before labeled protein deposition leads to light transfers of collagen (figure 6 A and C), while an increase of the loading force leads to a collapsing of the structure (figure 6 B and D).

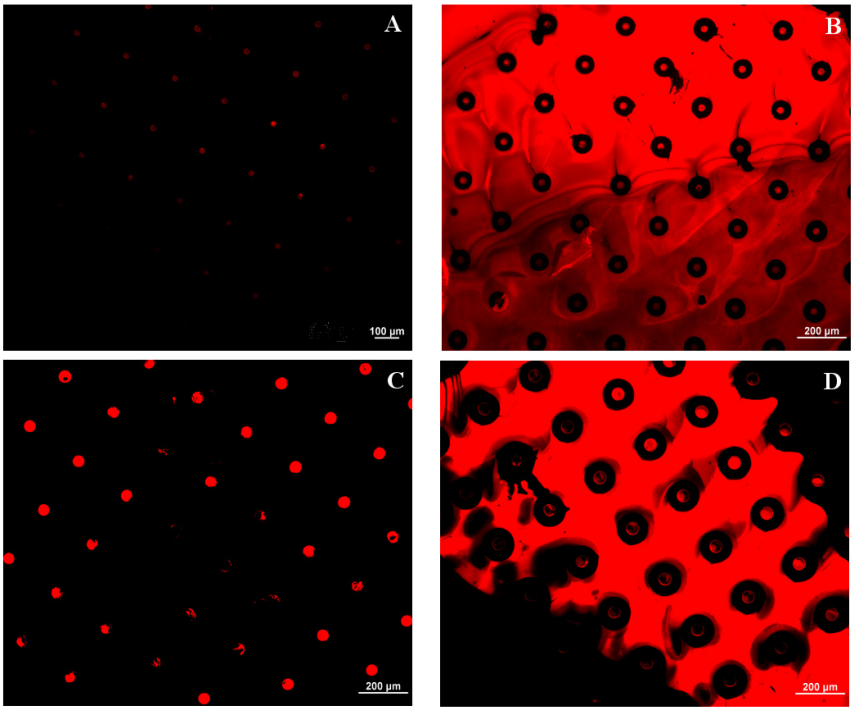

Figure 30: representative images Ø 25 (A, B) and 50 µm (C, D) of the inhomogeneous transfer of TRIC-labeled collagen by microcontact printing.

Optimization of process parameters was performed by iterative testing, evaluating the transfer efficiency with applied pressure values in the 170–350 kPa range and contact times between 20 and 60 sec. Uniformity of fluorescence intensity and number of incomplete/defective substrates (for a fixed number of replicas) were taken into account as discriminating factors. An applied pressure of 230 kPa and a contact time of 30 sec were chosen as the most suitable processing parameters for further investigations. Table 3 reported final force applied on PDMS replicas to obtain highest of the collagen island microprinted deposition on PS multiwell.

	Ø = 25 µm	Ø = 50 µm	Ø = 75 µm	Ø = 100 µm
Force (N)	0.19	0.38	0.56	0.75

Table 2: applied force is proportional to the contact area of labeled collagen microcontact printing.

In figure 7, results of µCP printing with optimized parameters are reported for different pad geometries.

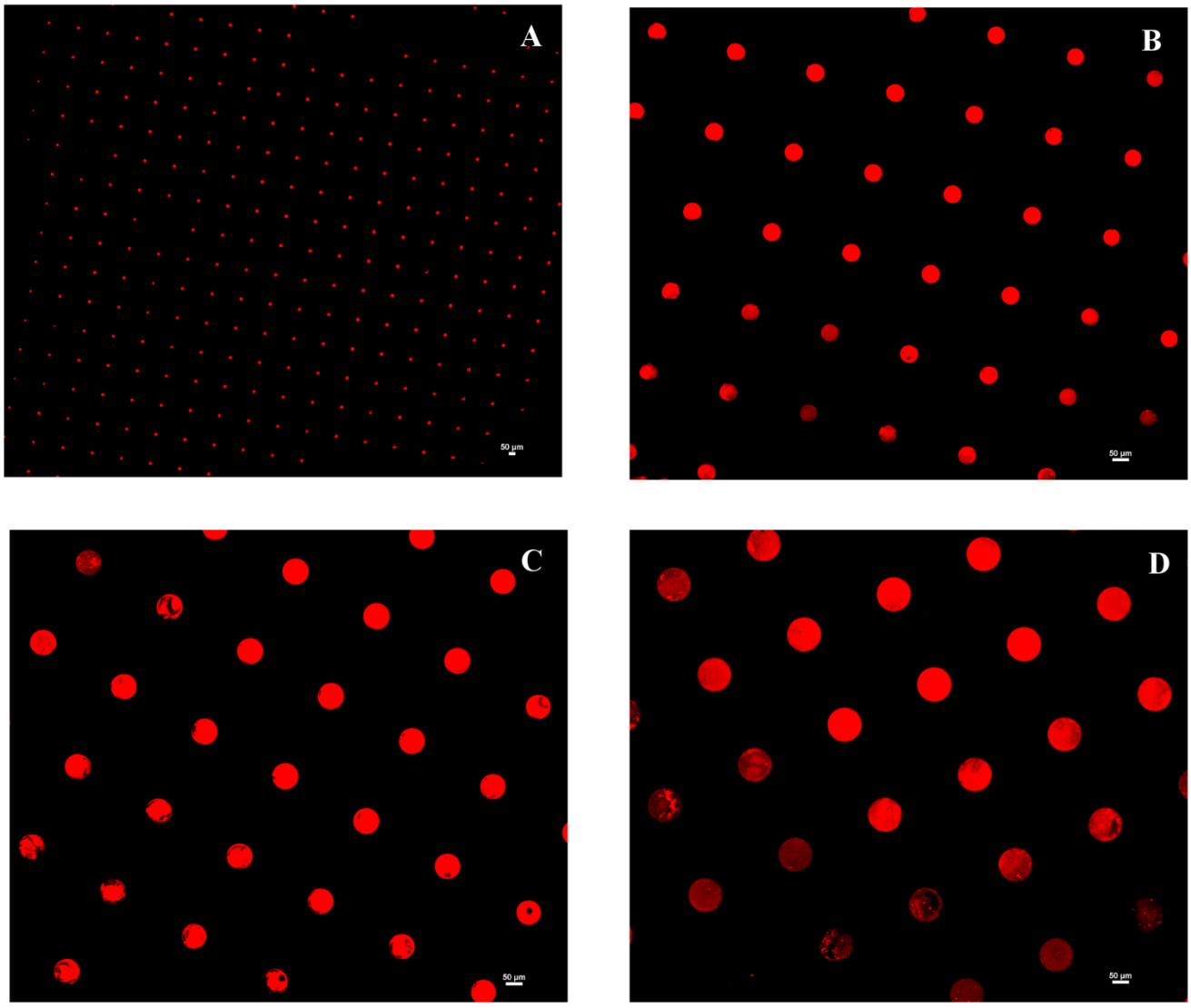

Figure 7: TRITC-labeled collagen transferred on PS substrates of different diameters: 25 (A), 50 (B), 75 (C) and 100 µm (D). Scale bar 50 µm (10X).

3.2.3 TSCs culture

Cell culture analysis

Cell morphology, viability and proliferation of TSCs cultured onto PS substrates with collagen islands microprinted were analyzed.

Live/dead assay was utilized at any time point (3, 5 and 7 days)to assess cell morphology and cell viability of each sample.

The morphology of cells cultured on PS substrates microprinted was reported in figure 8. TSCs do not spread on collagen, but prefer to be arranged in cell agglomerates increasing the number of cells per island. This morphology prevents any type of fluorescence intensity quantification of cells viability.

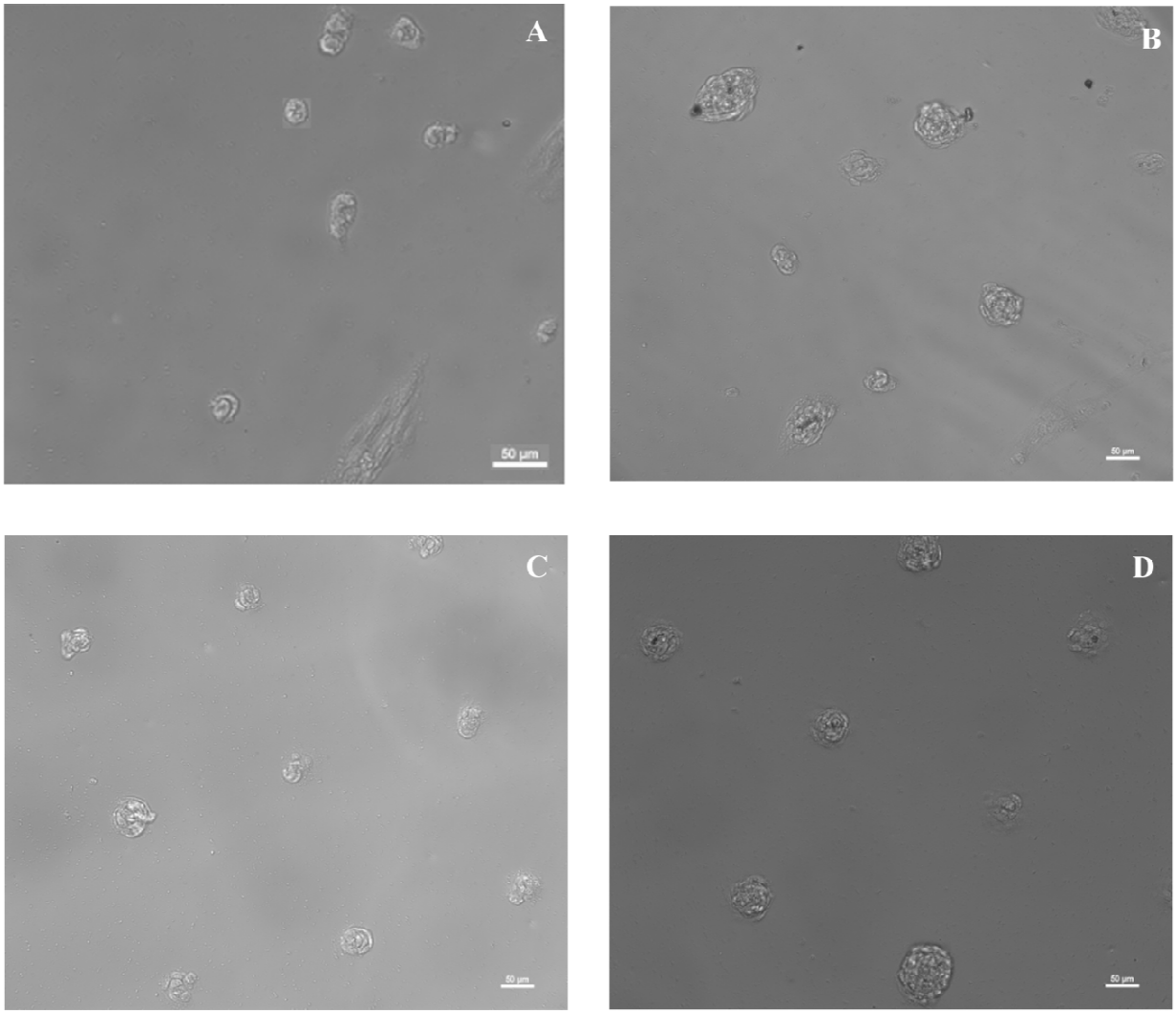

Figure 31: phase contrast of TSCs cultured onto Ø 25 (A), 50 (B), 75 (C) and 100 (D) µm of collagen islandsmicroprinted. Magnification 20X. Scale bar 50 µm.

Live/dead assay in figure 9 shows the viability of the TSCs cultured onto microprinted collagen pads. Cells are well spread on pads with more than 50 µm of diameter, while on patterns of Ø 25 µm, only few cells are capable of attachment. This is perhaps due to the lower quantity of collagen available for cell attachment. Furthermore, the images show that only TSCs cultured on pads with 75 and 100 µm diameter have a good viability at 5 day while, at 7 days, high mortality was observed in all type of simples.

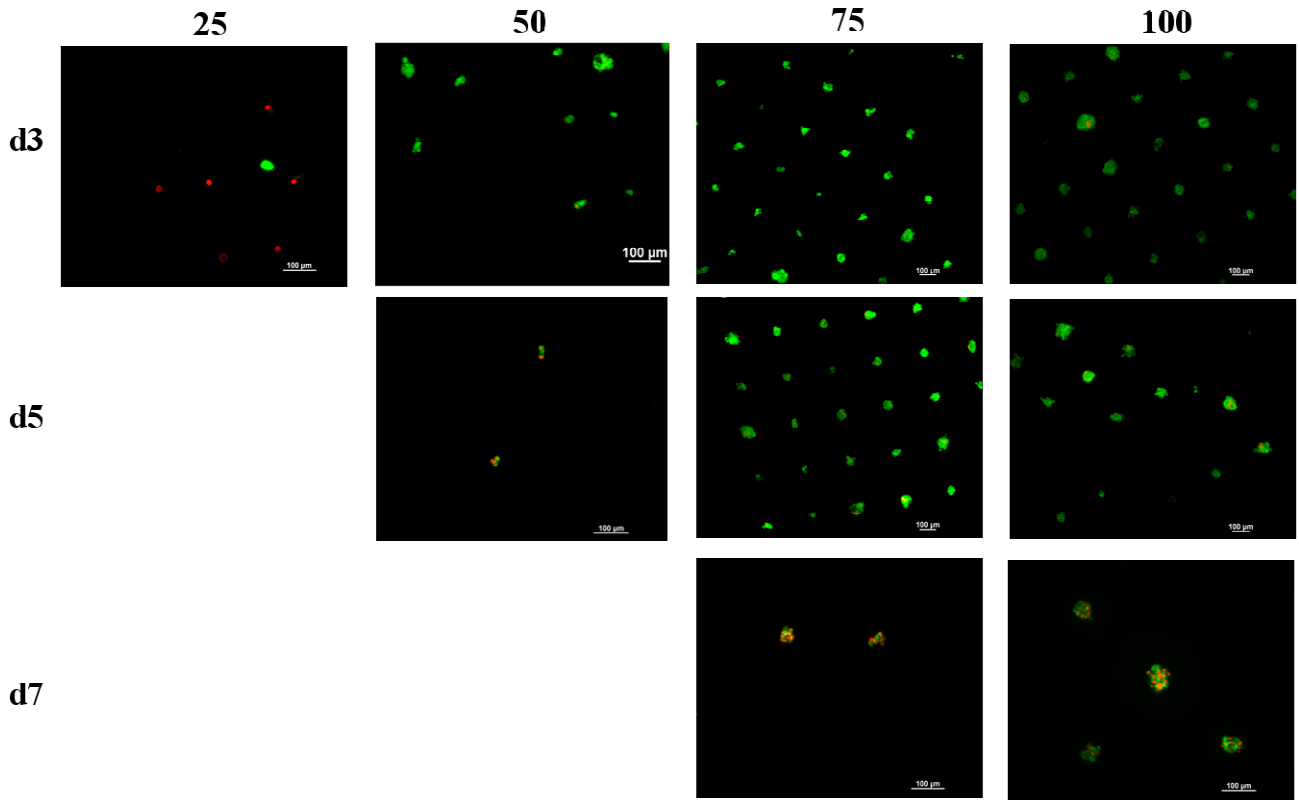

Figure 32: live/dead assay of TSCs cultured on collagen pattern microprinted.

Cell proliferation was evaluated by counting DAPI stained cell nuclei as previously described (§ 3.2.4.1.1). In order to quantify cellular density, the number of counted nuclei was normalized to the area of the collagen-coated circular pad and the data analyzed using a Two-Way ANOVA. As demonstrated by the bar chart in figure10, all islands microprinted allow cell proliferation regardless of the diameter size. In particular, excluding collagen island with Ø 75 µm, all specimens revealed a significant proliferation ($p< 0.05$) between d1 and d3 for Ø 25 µm pads or between d1 and d5 for Ø 50 and 100 µm.

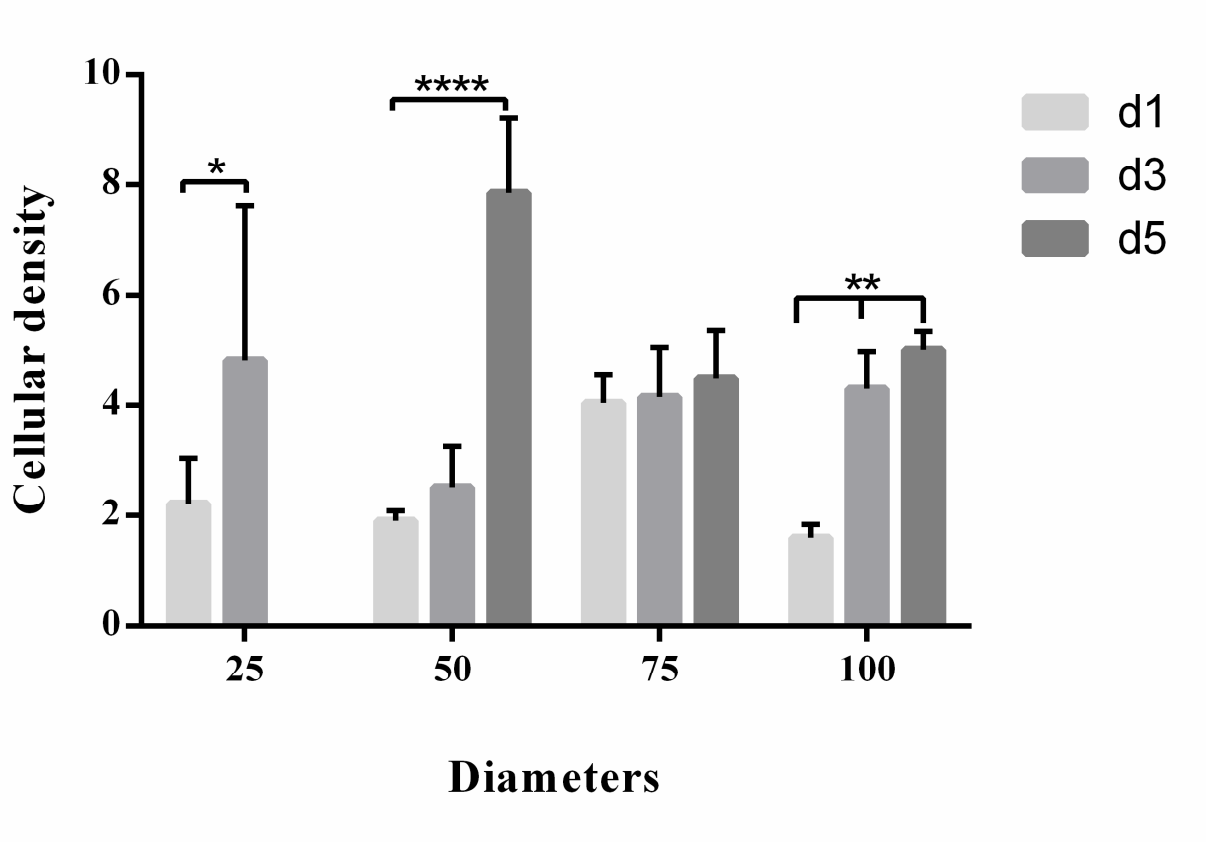

Figure 33: cellular density of TSCs cultured on collagen microprinted evaluated with nuclear count.

Focal adhesion analysis

Several studies suggest the implication of integrin-mediated focal adhesion (FA) in the topological sensing by adherent cells [67, 143]. In this study, formation of α2β1 integrin-mediated focal adhesion related to collagen islands microprinted was evaluated by immunofluorescence staining after 3 (Ø 25 μm) and 5 days (Ø 50, 75 and 100 μm) of TSCs culture. Figure 11 reports a representative image of focal adhesion (green) and nuclear (blue) staining of all simples.

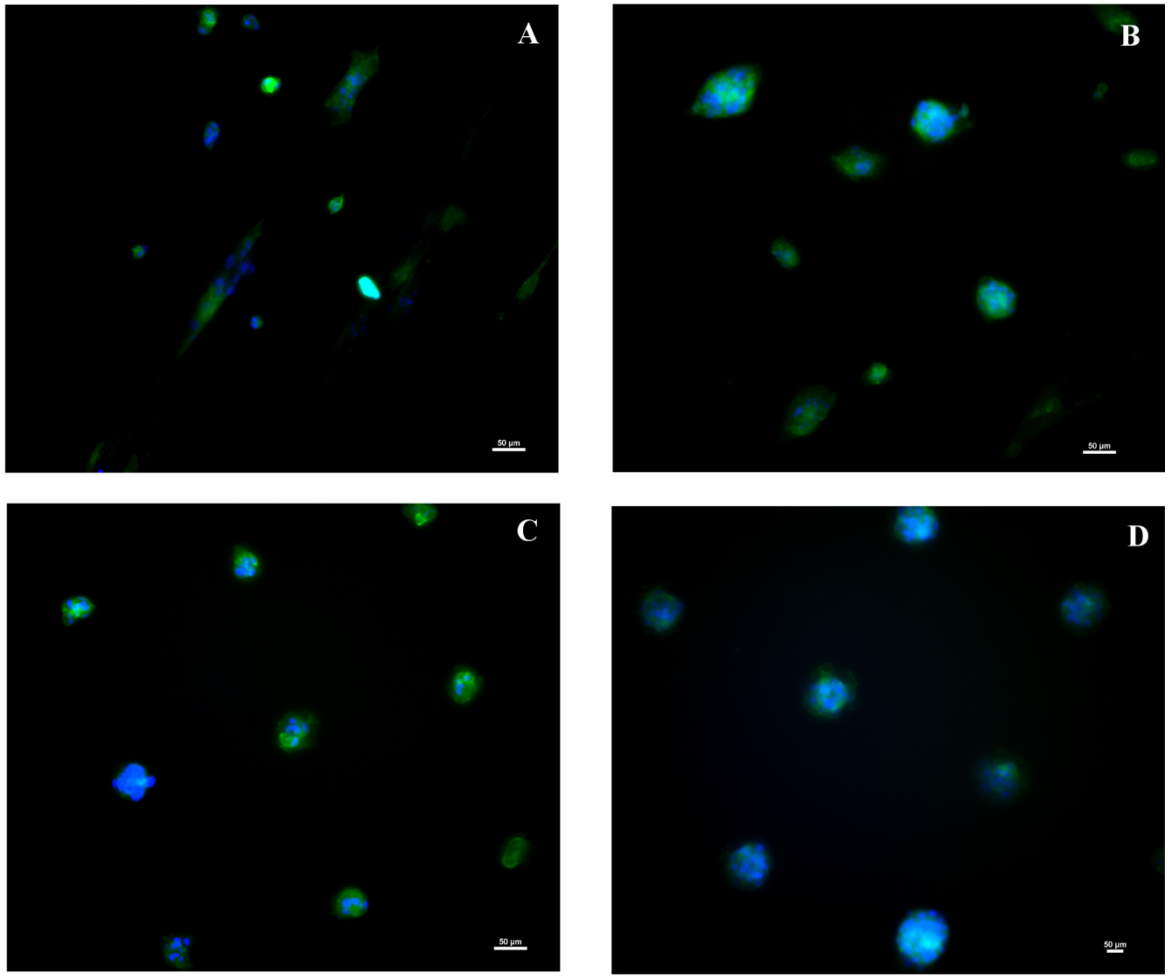

Figure 34: representative immunofluorescence images of α2β1 integrin (green) and nuclear staining (blue). Magnification 20X. Scale bar 50 µm

Stem cell preservation

In order to analyze stem cells preservation, TSCs cultured on the samples were stained for STRO-1 membrane antigen (far-red) and nuclei (blue) after 3 and 5 days (figure 12). Although at day 3 TSCs cultured on lower diameter pads (Ø 50 µm) showed a higher expression of membrane antigen STRO-1 compared to other groups, this value significantly decreased ($p < 0.05$) at d5. On the other hand, in the samples with higher diameter sizes (Ø 75 and 100 µm), no significant reduction of the STRO-1 expression between 3 and 5 days is observed. STRO-1 trend in the CTRL is in contrast to the other samples. In fact, although the data are not significant ($p > 0.05$), a decrease trend of STRO-1 expression is revealed in CTRL.

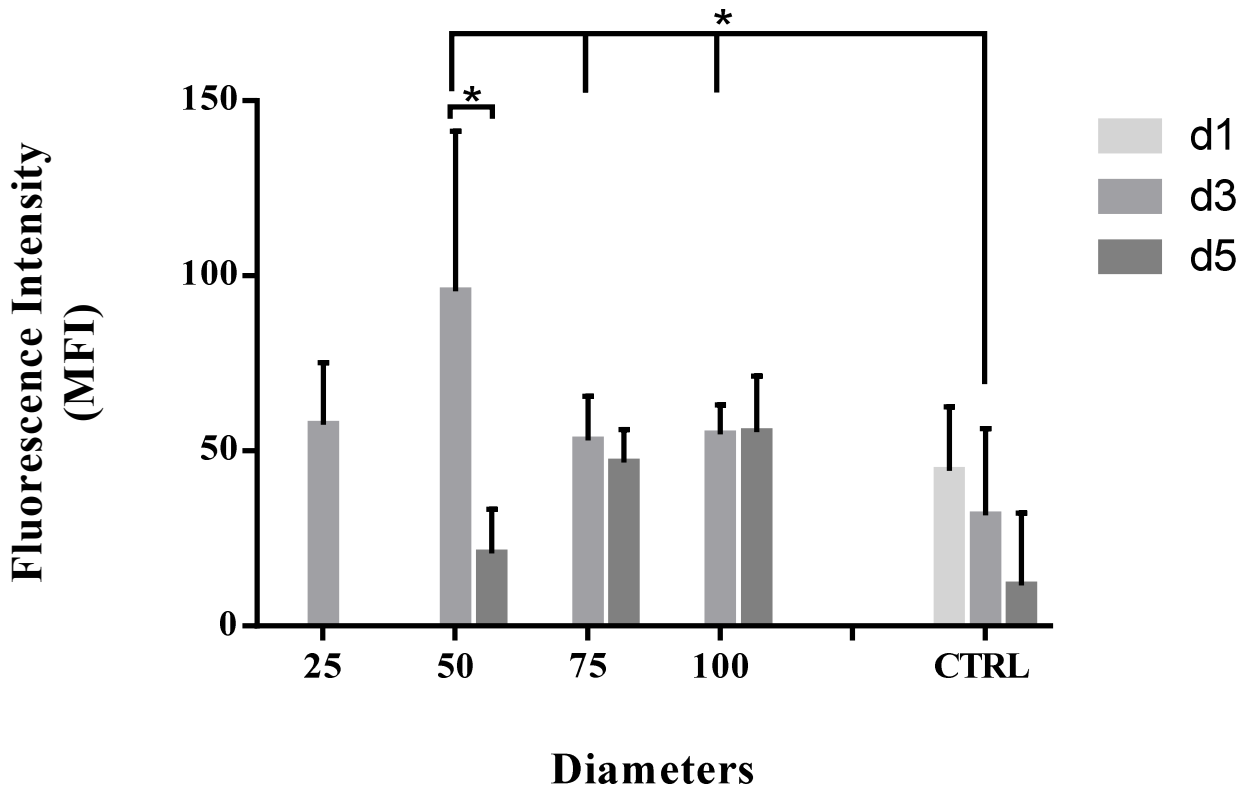

Figure 35: fluorescence intensity of STRO-1 antigen expressed by TSCs after 3 and 5 days of culture onto μCP collagen pads.

Figure 13 shows representative immunofluorescence images of STRO-1 membrane antigen (far-red) and nuclei (blue) expressed after 3 or 5 days of TSCs culture. 20x objective. Scale bar 50 µm.

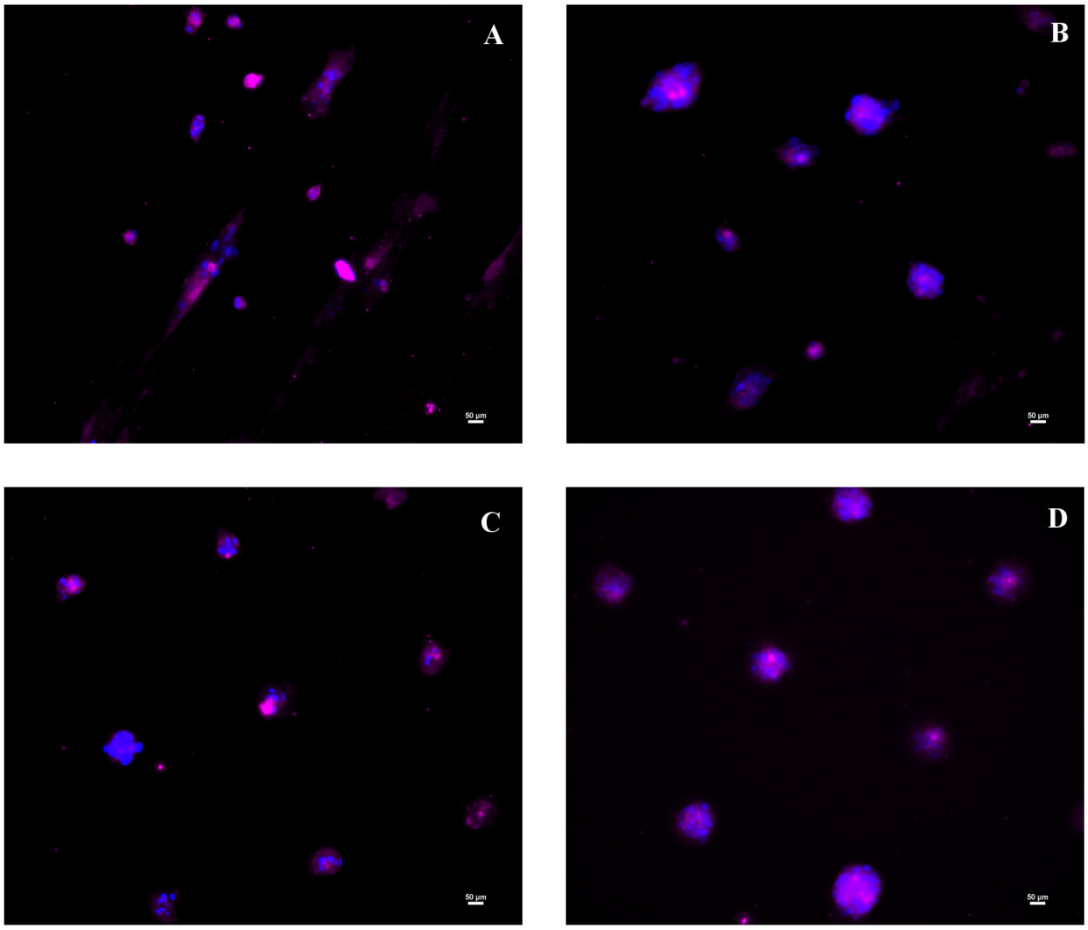

Figure 36: Immunofluorescence images of STRO-1 membrane antigen (far-red) and nuclei (blue) expressed by TSCs cultured after d3 for Ø 25 (A,) and d5 for Ø 50 (B), 75 (C) and 100 (D) µm onto collagen islands microprinted. Magnification 20X. Scale bar 50 µm.

3.3 hMSCs culture

hMSC morphology and focal adhesion analysis

Cell morphology of hMSCs cultured onto PS substrates with PLL pads is reported in figure 14. hMSCs were arranged cell agglomerates and formed bridges between two or more different PLL pads.

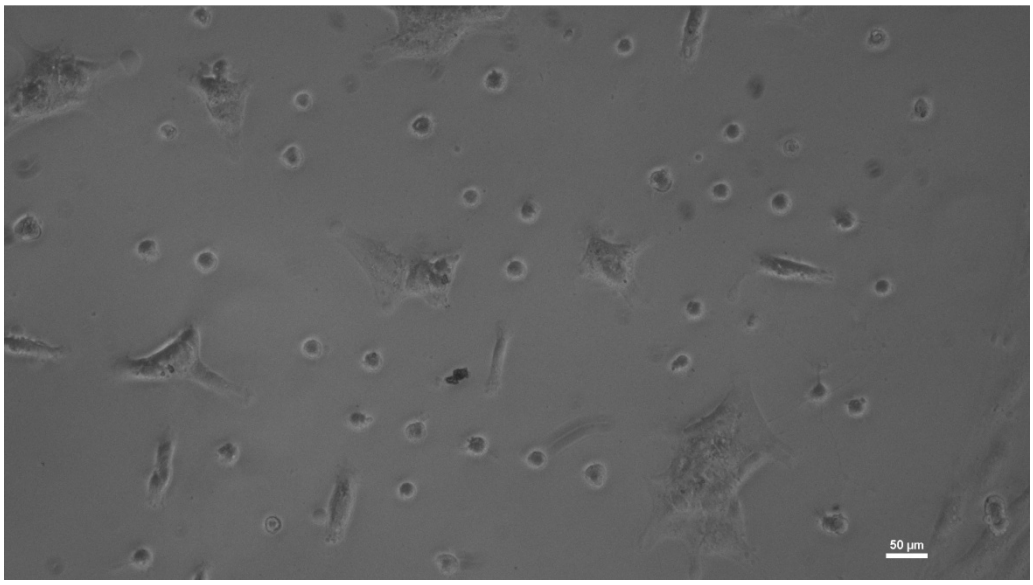

Figure 37: phase contrast of hMSCs cultured on 25 µm of diameters of PLL islands microprinted on PS low attachment multiwell. Magnification 10X. Scale bar 50 µm

Several studies suggest the implication of integrin-mediated focal adhesion (FA) in the chemical patterning by adherent cells [67, 143]. In this study vinculin was evaluated by immunofluorescence staining after 3 days of hMSCs culture. Figure 15 reports a representative image of focal adhesion (green) and nuclear (blue) staining of all simples at different magnifications.

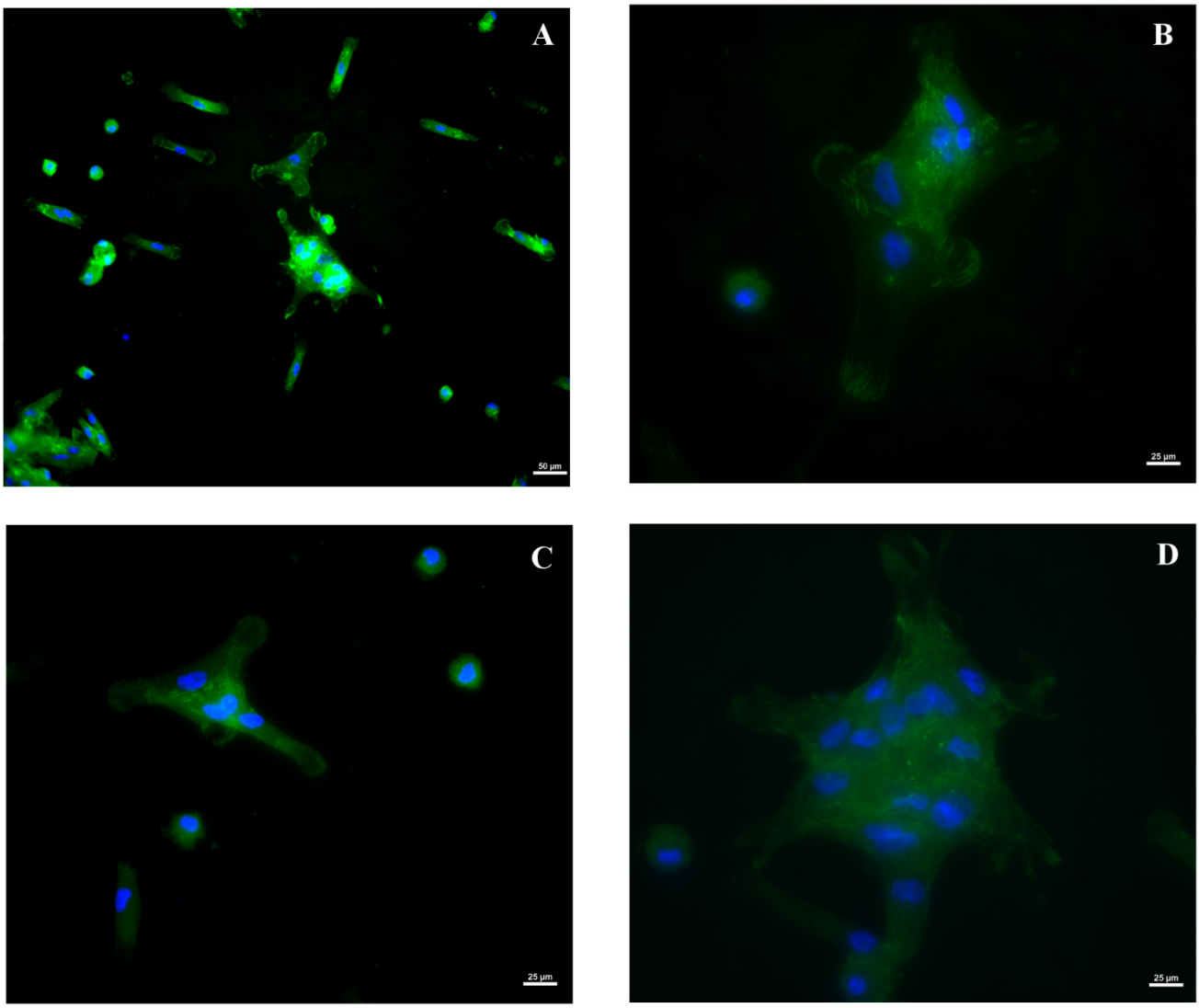

Figure 38: representative immunofluorescence images of vinculin (green) and nuclear staining (blue). Box A represents magnification 20X. Scale bar 50 µm; boxes B, C and D show a particular of box A at magnification of 60X and scale bar 25 µm.

3.3.1 Conclusions

In this study the results demonstrate that the proposed approach can be successfully pursued for precise transfer of different protein micropatterns with high precision and reproducibility. After multiple tests to optimize the parameters of μCP, a good printing resolution was achieved with a minimum feature size (~25 μm), which is comparable with other techniques for soft surface patterning [144].The results demonstrate that the focal adhesions of cells are localized only on the μCP protein-coated pads. Cell culture on features with Ø of 75 and 100 μm showed best stem cell preservation and viability with respect lower diameters.

Although a consolidated success has been achieved in the patterning of smooth surfaces, μCP application to soft and/or textured matrices has been mostly limited to the generation of spatially defined micro-architectures[145-146]. A future perspective of this work is to extend this study in order to obtain defined protein micropatterns with different resolutions onto soft electrospinning matrices by μCP.

CHAPTER 4: µCP on soft substrates

Introduction

Surface functionalization of biomaterials represents a promising strategy to obtain biologically instructive substrates for cell culture. In particular, advances in micro- and nanofabrication technologies were allowed the deposition of precise and highly reproducible patterns on biomaterials surfaces [1]. Although a consolidated success was achieved in the patterning of smooth surfaces, µCP application to soft and/or textured matrices was mostly limited to the generation of spatially defined micro-architectures [145-146]. Substrate sagging and difficulties in stamp removal are considered the principal causes of non-conformances in protein patterns transferred by conventional µCP on these surfaces. A possible solution was recently proposed by Yu et al. by the development of a novel trans-print technique to extend µCP to tacky and/or complex substrates such as polydimethylsiloxane or polyacrylamide gels [147].

However, while most studies were evaluated cell/material interactions on two-dimensional patterned surfaces, [131-132, 148] in physiological conditions, cells are surrounded by extra-cellular matrix and sense similar cues in a 3D environment. Consequently, an emerging field of research in this area concerns the development of spatially controlled deposition of biological cues onto porous media (i.e. scaffolds). Electrospun (ES) matrice was widely used as tissue engineering (TE) scaffolds owing to their dimensional similarity to native extra-cellular matrix [149-152].

In this work polymeric ES substrates were chosen as the target material for the patterning of proteins to provide external chemical cues for cellular organization.

The aim of this study is to use a custom-builtµCP apparatus to transfer protein patterns onto 3D ES substrates for soft TE applications. This represents the first attempt to obtain defined protein micropatterns with different resolutions onto soft ES matrices by µCP. The proposed approach was demonstrated for transfer of poly-L-lysine (PLL) patterns from PDMS stamps onto sub-micron-sized poly(ε-caprolactone) (PCL) ES fibers. Human bone-marrow-derived mesenchymal stromal cells (hMSCs) and tendon derived stem cells were seeded on protein micropatterns, and cell adhesion, spreading ,and spatial distribution were investigated.

4.1 Materials and Methods

4.1.1 Stamp fabrication

4.1.1.1 SU-8 Master molds fabrication

Master molds were fabricated on a silicon wafer with SU-8 negative photoresist (SU8-2010, Microchem, Newton, MA) as previously described in § 3.2.1.

4.1.1.2 Replica molding and washing of PDMS

Polydimethylsiloxane stamps at the weight ratio of 10:1 PDMS and its curing agent were mixed thoroughly, poured and cured as previously described in § 3.2.1.1.
In order to test the proposed method, patterns consisting of differently sized circles and lines were produced. The relief patterns contained arrays of variously spaced circles with diameters ranging from100 to 25 μm (C_100 and C_25) and a set of 25 μm wide parallel lines (L_25). Microstructure of the obtained PDMS replicas was evaluated by field emission gun scanning electron microscopy (Supra 1535; LEO Electron Microscopy, UK).
Obtained stamps were cleaned by 5min sonication in ethanol, ethanol/water, and distilled water, followed by drying under a nitrogen stream before use.

4.1.2 Scaffold fabrication

Poly(ε-caprolactone) (PCL) non-woven scaffolds were obtained by electrospinning (ES). Electrospinning is an electro-hydrodynamic technique that permits to process polymeric solutions into fibrous structures at the micro/nano scale by simply controlling few process parameters.
In this work an 8% w/v solution of PCL (MW 80kDa, Sigma-Aldrich, Milano, IT) in 70:30 v/v dichloromethane/methanol (Sigma-Aldrich, Milano, IT) was mixed. The solution was fed through a 23G needle with a feed rate of 0.5 $mL \cdot h^{-1}$ and ES onto an earthed collector placed at a distance of 15 cm, using a voltage of 15kV. Microstructure of the obtained PCL membranes was evaluated by field emission gun scanning electron microscopy (Supra 1535; LEO Electron Microscopy, UK).

4.1.3 Soft substrates fabrication

PCL non-woven scaffolds were obtained by electrospinning (ES). Electrospinning is an electro-hydrodynamic technique that permits to process polymeric solutions into fibrous structures at the micro/nano scale by simply controlling few process parameters.

In this work an 8% w/v solution of PCL (MW 80kDa, Sigma-Aldrich, Milano, IT) in 70:30 v/v dichloromethane/methanol (Sigma-Aldrich, Milano, IT) was mixed. The solution was fed through a 23G needle with a feed rate of 0.5 mL · h^{-1} and ES onto an earthed collector placed at a distance of 15 cm, using a voltage of 15kV. Microstructure of the obtained PCL membranes was evaluated by field emission gun scanning electron microscopy (Supra 1535; LEO Electron Microscopy, UK).

4.1.4 Microcontact printing procedure

TRITC labeled Poly-L-lysine solution was chosen as ink for microcontact printing procedure.

Stamp was inked by depositing the protein solution on its patterned side and incubated for 30 min in the dark. The inked stamp was dried under a mild nitrogen stream to remove excess ink and contacted with electrospun substrate (figure1).

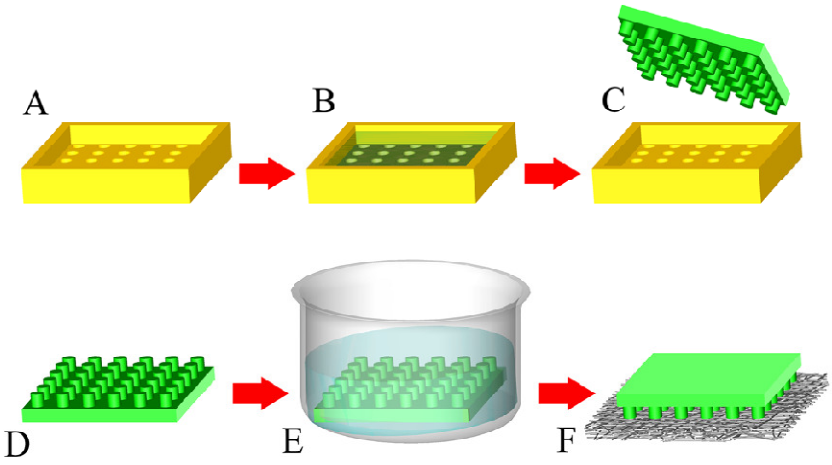

Figure 39: schematic outline of stamp fabrication (A–C) andmicrocontact printing procedure to transfer protein patternsonto electrospun substrates (D–F)[153].

To avoid deformation of the substrate during stamp removal, scaffolds were mounted and hold in place onto Cell Crown inserts (Scaffdex, Tampere, Finland), without introducing significant strain. A controlled pressure was mechanically applied using a customized jig mounted onto a tensile tester

(model 3365, Instron, Norwood, MA) equipped with a 10N load cell. The setup was opportunely designed to house both the stamp and the ES substrate (figure 2).

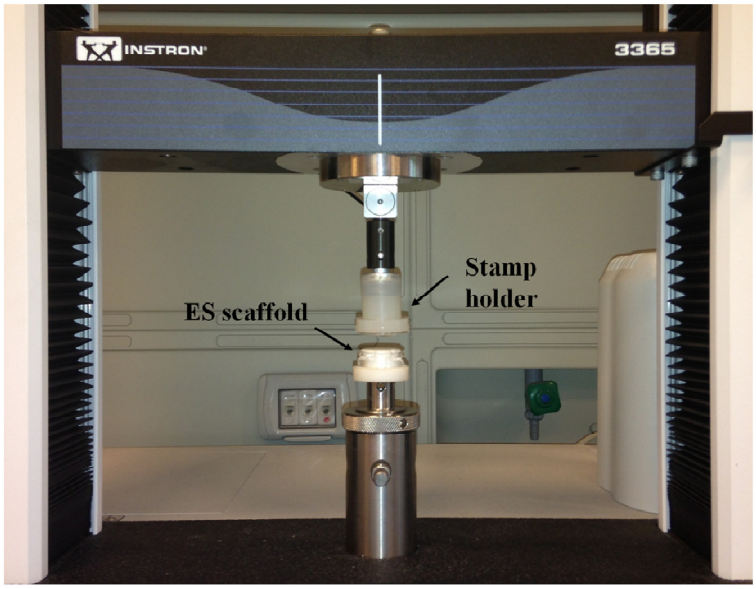

Figure 40: schematic of the custom-designed μCP device. A tensile tester was purposely modified to house the polydimethylsiloxane stamp and the electrospun substrate.

The stamp was connected to the moving crosshead through a compliant rubber stub, which accommodated misalignments while allowing a better force resolution by lowering the stiffness of the system. Protein transfer was performed by bringing the stamp into contact with the ES specimen surface at a constant crosshead speed. Depending upon the stamp contact area, a suitable loading force was applied to achieve the required contact pressure. After contact time had elapsed, as the protein pattern was transferred to the substrate, the stamp was automatically retracted.

Quality of transferred pattern and fate of inked protein were semi-quantitatively assessed by fluorescence microscopy observations (Nikon Ti-E). Optimization of process parameters was performed by iterative testing, evaluating the transfer efficiency with applied pressure values in the 100–320 kPa range and contact times between 1 and 7min. Uniformity of fluorescence intensity and number of incomplete/defective substrates(for a fixed number of replicas) were taken into account as discriminating factors.

An applied pressure of 320 kPa and a contact time of3min were chosen as the most suitable processing parameters for further investigations. For each sample, a square region of interest was selected and characteristic parameters of the transferred PLL features were quantified by ImageJ software (National Institute of Health, Bethesda, MA). Each region of interest was further divided

into several sub-regions, and a fluorescence intensity algorithm was applied to indirectly determine the uniformity of protein distribution.

The possibility to re-use the PDMS stamps over ten times after a routine cleaning procedure without loss of printing performance was also verified.

Patterned ES scaffolds were sterilized by ultraviolet irradiation for 20 min before cells seeding.

4.1.5 Cell culture experiments

Patterned ES scaffolds were sterilized by ultraviolet irradiation for 20 min and seeded with hMSCs (passage5, Lonza, Basel, CH) at a density of $2 \cdot 10^4$ cells/cm^2.

4.1.5.1 Cell morphology analysis on soft substrates

In order to avoid a specific deposition of serum proteins onto the substrate, a serum-free Minimum Essential Medium-Alpha (Lonza, Basel, CH) supplemented with 1%penicillin/streptomycin (Lonza, Basel, CH) was used for cells seeding. After 24 h, serum-free medium was replaced by complete medium supplemented with 10% fetal bovine serum. At the selected time point (3 days), specimens were fixed in 4% PFA solution for 15min and processed for fluorescence microscopy without sectioning. Briefly, constructs were repeatedly washed in PBS and permeabilized with 0.1% TritonX-100 for 5min. Constructs were then stained for F-Actin with Fluorescein Isothiocyanate (FITC)-labeled phalloidin (Sigma-Aldrich, Milano,IT), using DAPI (Life Technologies) as a nuclear counterstain and observed under an inverted fluorescence microscope (Nikon Ti-E).

4.1.6 Statistical analysis

Experimental data were analyzed using GraphPad Prism® 5 (GraphPad Software, USA). Conditions of normality were checked with Shapiro–Wilk test. Normally distributed data were analyzed for significance by *T*-Student and test two-way ANOVA followed by Tukey's multiple comparison post hoc test (Tukey). Statistical significance was accepted at $p < 0.05$. Data are presented as mean value ± standard deviation.

4.2 RESULTS AND DISCUSSION

4.2.1 FE-SEM analysis and optimization of protein transfer

A proof of concept implementation of μCP in combination with biocompatible ES scaffolds was pursued in view of possible Tissue Engineering applications. Although μCP has for long represented the gold standard for surface patterning, to date, it is considered almost inappropriate to transfer protein patterns on complex-shaped and soft substrates. Many groups have addressed this problem proposing modifications to the conventional μCP [147] or alternative solutions for soft surface patterning [127, 154]. However, up to now, a reliable and versatile method to microcontact print patterns of proteins on ES substrates has never been proposed.

Poly(ε-caprolactone) substrates obtained by electrospinning consisted in non-woven mats of finely intertwined fibers, with an average diameter of374 ± 56nm (figure 3). Such a low standard deviation value testifies the high reproducibility of the process.

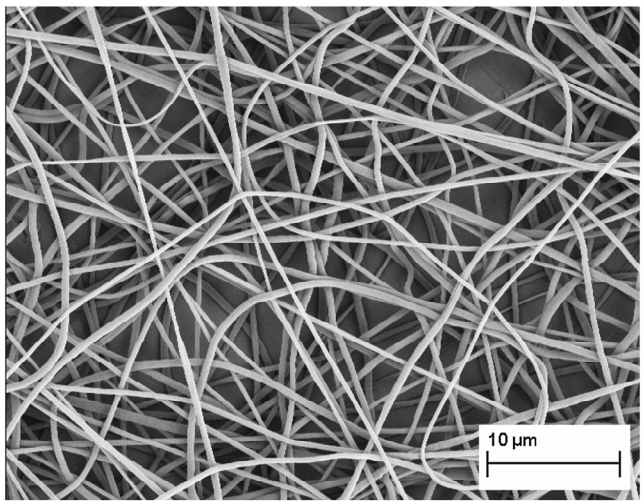

Figure 41: FE-SEM micrograph of poly(ε-caprolactone) electrospun scaffolds.

In the present study, a custom-built µCP apparatus was used to transfer PLL protein patterns from PDMS stamps onto these ES substrates. Printing parameters were chosen in light of an optimization process, which results are summarized in Table 1. A pressure of 320 kPa and a contact time of 3 min were selected for the fabrication of PLL patterns.

	Pressure (kPa)			
Time (min)	100	200	260	320
1	x	x	x	x
3	x	x	x	✓
5	x	x	✓	✓
7	x	x	✓	E

x, incomplete/defective protein transfer.
✓, efficient protein transfer.
E, excessive protein transfer.

Table 3: efficiency of protein transfer for different applied pressures and contact times.

Figure 4 shows a representative images of microcontact printing on PCL scaffold with extremes x and E values. In particular figure 4 A shows an incomplete protein transfer, while in figure 4 B is displayed an excessive protein deposition on scaffold.

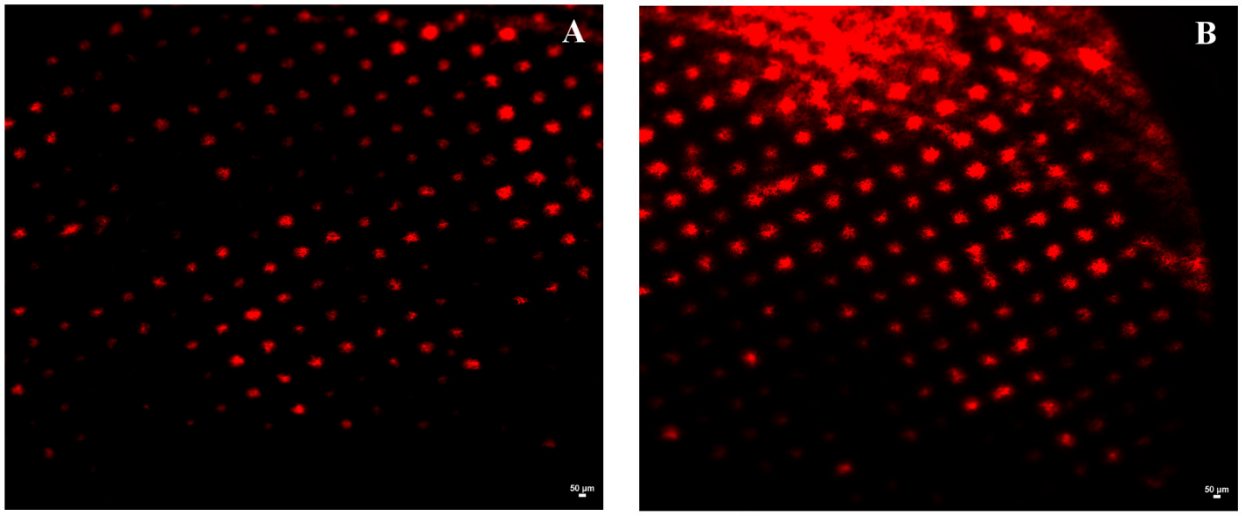

Figure 42: representative images of labeled collagen deposition on PCL scaffold with x and E extreme value.

Quality of the transferred protein pattern and efficiency of the printing process were assessed by optical fluorescence microscopy. Figure 5 shows a series of fluorescently labeled PLL patterns generated by µCP using this optimized set of parameters. In particular, fig. 15 A and B show

patternC_100: array of 100 µm diameter islands with a pitch of 200 µm in the X and Y directions at different magnifications; figure 15 C and D show pattern C_25: array of 25 µm diameter islands, pitch 75 µm. Figure 15 E and F show pattern L_25: equally spaced strips with width25µm and pitch 50µm.In all the cases, feature edges at the micron-scale level were perfectly smooth with clearly identified boundaries between patterned and non-patterned areas.

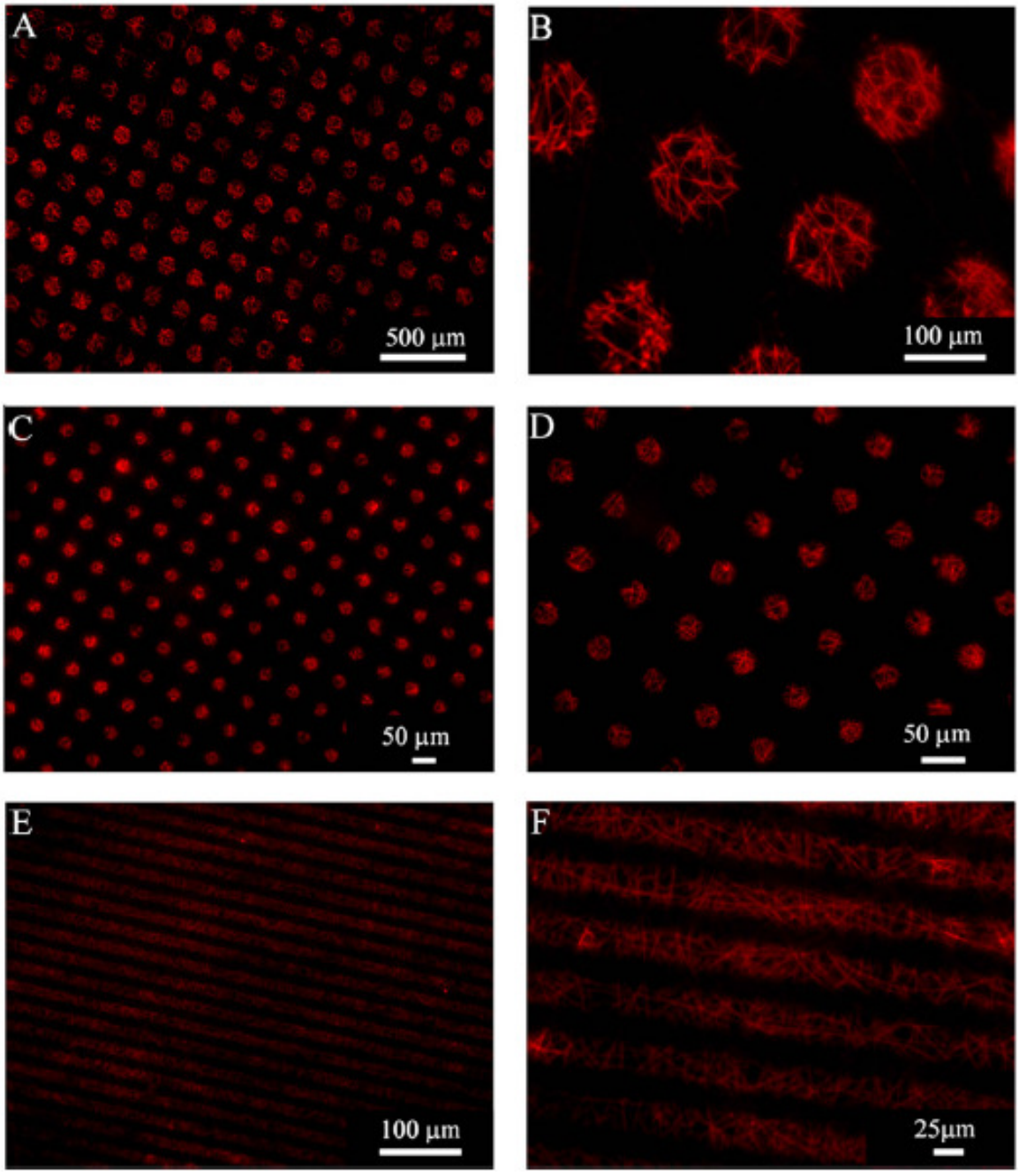

Figure 43: Optical fluorescence micrographs showing different poly-L-lysine patterns transferred onto electrospun poly(ε-caprolactone) membranes.

Dimensional features of the transferred patterns were extracted by image analysis and compared with target values (table 2). No significant differences were found, confirming the high-dimensional fidelity guaranteed by the process.

Furthermore, the uniform distribution of fluorescence intensity across the surface indirectly testified the good printing efficiency achievable by the proposed method. Indeed, a maximum 8% deviation from the mean fluorescence intensity value was registered.

Additionally, no alterations in the scaffold microfibrillar structure were assessed after μCP process.

Pattern	Target dimension (μm)	Target circularity†	Actual dimension (μm)	Actual circularity
C_100	100 (diameter)	1	103.07 ± 1.72	0.993 ± 0.015
C_25	25 (diameter)	1	26.06 ± 0.87	0.997 ± 0.026
L_25	25 (width)	N/A	25.7 ± 1.03	N/A

†Circularity is defined as: $4\pi \times A/p^2$, where p is the perimeter and A is the surface of the given feature. A circularity value of 1 indicates a perfect circle.

Table 4: measurements of characteristic feature sizes for different patterns. Values are expressed as mean value ± SD (n>10).

4.2.2 Effects of protein patterns on cell organization

Patterned scaffolds were tested in combination with hMSCs at passage 5. Figure 6 shows fluorescence micrographs of hMSCs seeded on ES scaffolds in which protein patterns (red), cytoskeletal F-actin (green) and cell nuclei (blue) were recorded simultaneously. Although cells adhered also on the uncoated areas of the scaffold, a more effective spreading can be detected in hMSCs adhered onto PLL patterns. In particular, cells cultured over protein islands tend to spread toward neighboring adhesive pads (figure6 A), while cells grown on parallel stripes tend to form cellular chords aligned with protein pattern (figure6 B).

The reported partial non-specificity in terms of cell adhesion can be partially explained by the fact that ES PCL provides per se a good substrate for cell adhesion, leading to weak confinement potential. Depending on the adhesion-promoting biomolecules and on the inertness of the chosen substrate, the inclusion of non-fouling agents to block non-specific protein adsorption can be critical in order to guide cell attachment on microcontact printed areas.

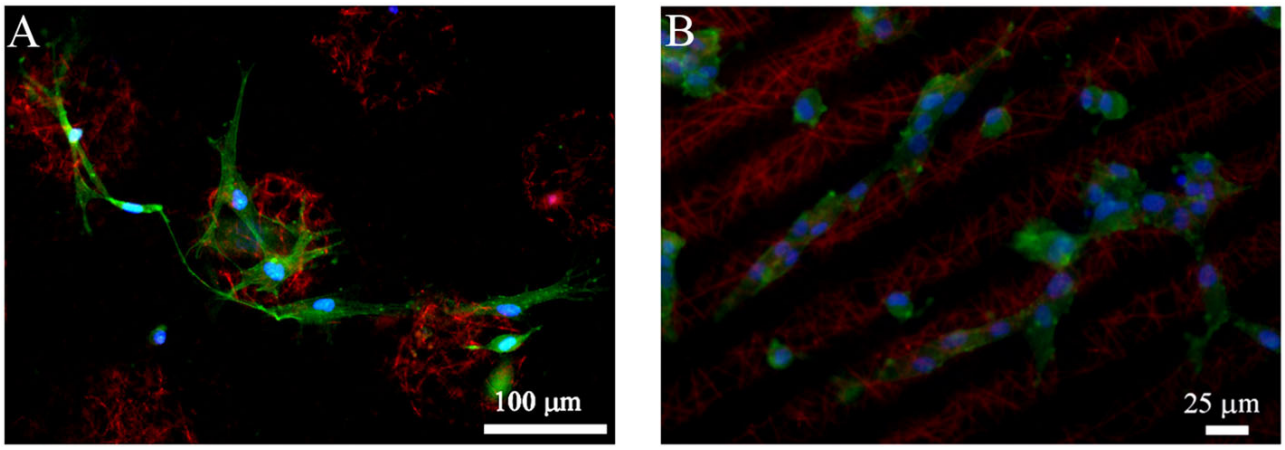

Figure 44: optical fluorescence micrographs of hMSCs seeded on poly-L-lysine patterned scaffolds for 3 days:(A) hMSCs seeded on C_100 scaffolds and (B) on L_25 scaffolds.

4.3 Conclusions

Several literature studies demonstrated the capability to control cell position taking advantage from protein patterning surface [155-158]. In this work the results demonstrate that the approach studied can be successfully utilized for gentle transfer of different protein micropatterns on soft substrate obtaining high precision and reproducibility. Indeed, the use of our custom designed apparatus, assuring precise movements and uniformly applied loads, avoided deformation of stamp features and uneven stamp removal which are at the base of non-conformities in pattern transfer. Althout the substrates utilized are not uniform and plain, shape and fluorescence intensity of protein patterns transferred on ES scaffolds show high conformity with respect to the PDMS stamps. Moreover no alterations in the scaffold microfibrillar structure were assessed after μCP process.

Furtheremore, although protein adhesion was sufficiently strong to maintain the printed pattern upon prolonged immersion in aqueous solution, the chemical grafting of the deposited biomolecules to the substrate should be pursued to further enhance cell response.

To this aim, further work will address polymer surface activation to specifically interact with inked proteins and back-filling of non-stamped regions to reduce non-specific cell adhesion.

CHAPTER 5:

Conclusion

This thesis aimed at studying the influence of differently engineered substrates obtained through two well-established soft-lithographic techniques (Replica Molding and Micro-Contact Printing) on cell behaviour.

Hereinafter anoutlook to the obtained resultsand future works is reported.

- MicropatternedPDMS substrateswith lines and base squared pillarsfeatures at different half-pitch were fabricatedin order to mimic tendon ECM native condition. These substrateswereused for TSCs and tenocytes culturewithout any additional physical or mechanical external stimuli. The obtained results demonstrate the stronglyinfluence of surface features withregard to spreading, morphology and cell orientation. Extensive studies on the tenocytes ECM deposition and migration were addressed. In particular, the lack of significant differences in nuclear elongation of tenocytes cultured on lines and pillar patterns, demonstrates that, independently of the featurestype, an ECM deposition is present: However,only the lower lines half-pitch are able to promote the production of type I collagen like native tendon ECM.

Regarding tenocytes migration, the results demonstrate that there are preferential directions of the migration of both cells cultured on the linear features although there aren't significant differences in terms of velocity. Only lower topographical features (L1 and P1) highlight a greater motility from their starting point probably due to their small features.

Overall this work suggests a potential 2D surface texture to integrate in the synthesis of TE scaffolds with the aim to guide specific in vitro cell response.

-Protein islands pattern with different featural parameters were obtained through Micro-Contact Printingon hard substrates. The results demonstrate that the proposed approach can be successfully pursued for precise transfer of different protein micropatterns with high precision and reproducibility. Focal adhesions of cells are localized only on the microprinted protein islands, and the best viability and preservation of cell stemness were obtained on features of 75 and 100 μm diameters with respect lower values.

-As a natural advancement of previous reported results, the same technique has been appliedto the patterning of a more biomimetic substrate. 3D polymeric ES scaffolds were chosen as the target material to provide external chemical cues for cellular organization. This represents the first attempt to obtain defined protein micropatterns with different resolutions onto soft ES matrices by μCP. The proposed approach was demonstrated for transfer of poly-L-lysine patterns from PDMS stamps onto

sub-micron-sizedES fibers. The results demonstrate that the proposed approach can be successfully utilized for gentle transfer of different protein micropatternson soft substrate obtaining high precision and reproducibility. Indeed, the use of our custom designed apparatus, assuring precise movements and uniformly applied loads, avoided deformation of stamp features and uneven stamp removalwhich are at the base of non-conformities in pattern transfer.Although the chosen substrates are not uniform and plain, shape and fluorescence intensity of protein patterns transferred on ES scaffolds show high conformity with respect to the PDMS stamps. Moreover no alterations in the scaffoldmicrofibrillar structure were assessed after μCP process.

Taken together all these results confirm the significant effect of substrate topography and chemistry on the control of cell behavior andhighlightthe potential ofsubstrate engineering to program cell response without the addition of other external factors.

Future outlook

5.1 Biomimetic micro-fibrous PLLA substrates for tendon regeneration: a preliminary in vitro study

Management of tendon lesions accompanied by big loss of substance represents a serious issue in orthopaedic surgery. Such lesions, which cannot be repaired with an end-to-end suture, demand for tendon augmentation procedures. It is known that tendon niche comprises primarily parallel collagen fibers, and plays an important role in regulating their function and differentiation.

In light of the results obtained on PDMS patterned substrates, the aim of this study is the synthesis of a biomimetic micro-fibrous PLLA scaffold with aligned fibers to be used in combination with tenocytes and tendon stem cells, to produce a construct for tendon augmentation. Preliminary in vitro results were obtained with tenocytes.

Aligned fibers were synthesized by electrospinning adopting a spinning disk configuration, starting from a poly-L-lactide (inherent viscosity 0.9-1.2 dL/g) 13 wt% solution in a 10:1 v/v dichloromethane/methanol mixture. The solution was then fed into a 5mL glass syringe, which was controlled by a syringe pump with a rate of 2.5 ml/h. A high voltage (15 kV) was applied to the needle tip, placed 15 cm above the collector. The disk rotating speed was set at 6000 rpm. Scanning electron microscopy (SEM) was adopted to evaluate samples morphology.

Two different human cell populations were isolated for the study and seeded on the scaffolds: tenocytes from intact tendons (TI) and from ruptured tendons (TR).

Scaffolds were investigated in terms of cell viability and proliferation. Quantization andtyping (type I and III) of synthesized collagen was performed after 1 and 3 weeks of *invitro* culturing.

SEM analysis confirmed that we were able to obtain fibrous PLLA scaffolds with a high degree of fibres alignment. Constructs revealed good engraftment, with cell in-growth and proliferation within the scaffolds, and a specific organization following the direction of PLLA microfibers orientation (figure 1).

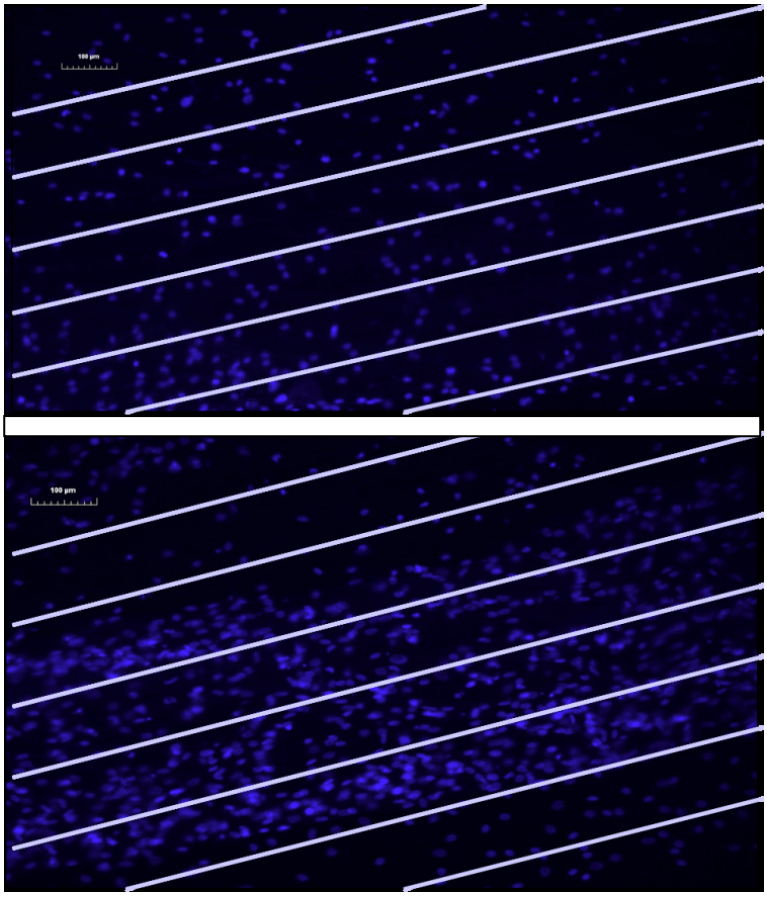

Figure 45: cell alignment on PLLA electrospun fibers~~,~~ after 7 and 21 days

TI and TR showed comparable results in terms of total collagen production. In particular, TIs showed the expression of Collagen I, while Collagen III was not expressed; at the same time point, TRs showed a shift in collagen expression from Type III to Type I.

In conclusion, PLLA electrospun scaffolds with aligned fibres, demonstrated compatibility with both tenocytes isolated from ruptured and intact tendons. Scaffolds promoted the aligned orientation of cells, and induced type I collagen production of tenocytes. As type I collagen is normally expressed in intact and healthy tendons, while type III collagen isexpressed in ruptured or

tendinopathic tendons, we think that such results candidate this scaffold as promising for tendon augmentation strategies.

Main future purpose will be to determine the effects of aligned scaffold topography on the differentiation of human tendon stem cells (hTSCs). The multi-differentiation potential of hTSCs toward osteogenesis, adipogenesis, and chondrogenesis is well established. To evaluate the effect of this biomimetic niche toward tendon-lineage differentiation, the expression of specific markers at the mRNA level will be examined by means of real time PCR.

5.2 Chemical grafting of protein islands on biomimetic micro-fibrous PCL scaffolds

Chemical grafting of the microprinted biomolecules to soft substrates should be pursued to further enhance cell confinement.

This preliminary work addresses polymer surface activation to specifically interact with inked proteins and back-filling non-stamped regions to reduce non-specific cell adhesion.

PCL scaffold obtained as previously described was treated in order to increase the surface concentration of carboxyl groups and permit a chemical grafting of deposited protein. The functionalization was performed following Sun *et al* method described in [159]. Briefly, the scaffolds were immersed in 0.1 M NaOH solution for alkali-catalyzed hydrolysis and reacted for 90 min at 37 °C, in order to hydrolyze ester groups (leading to free –COO– surface groups). Afterwards, scaffolds were protonated with 0.01 M HCl solution for 30 min to give polymer surfaces bearing carboxylic groups. After extensive washing in PBS, activated samples, were immersed in a catalyst solution containing 1-ethyl-3-(3-dimethylaminopropyl) carbodiimide hydrochloride (EDC) and N-hydroxysuccinimide (NHS),0.4 M and 0.1 M respectively, in MES buffer 0.1 M (pH=6.20) for 1 h. Finally, after washing with MES buffer and water, samples were dried in dessicator overnight. At this point the scaffolds are ready to form covalent bonds between carboxylic acid groups and the amine groups of the protein.

A schematic representation of the developed protocol is shown in figure 2.

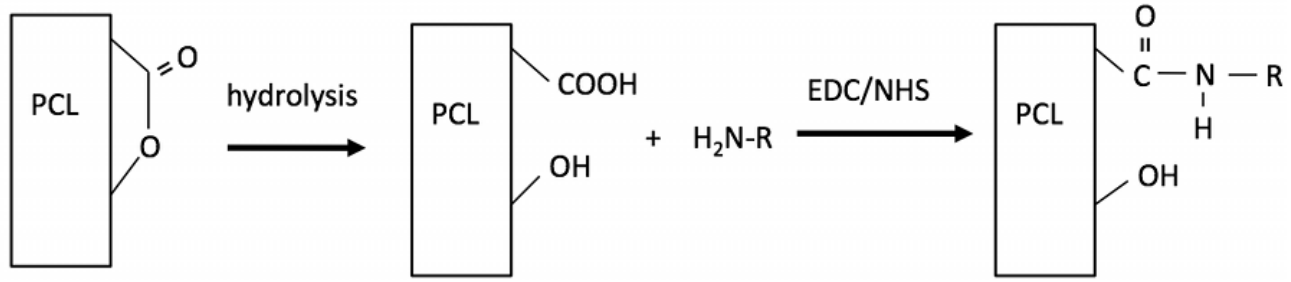

Figure 46: scheme of the grafting protocol: "R" indicates the generic protein (i.e. collagen type I).

Collagen type I aqueous solution was used as ink stamp for μCP on PCL scaffolds. PDMS mold with diameter of 25 μm, depth 20 μm and pitch 50 μm was chosen to coat with labeled-collagen solution. Apparatus and parameters utilized in this study for μCP were the same as previously described. Due to the hydrophilic nature of the functionalized PCL scaffold the enlargement of the collagen islands was measured to monitor protein dispersion and avoid an unconfined cell seeding.

At the same time, in order to preliminarily evaluate the effect of passivation on cell adhesion, non-printed scaffolds were grafted with Polyethylene glycol monoamine (mPEG, Sigma-Aldrich, Milano,IT) widely used as biologically inert interfaces [155, 160-162]. Scaffolds covalent passivation with mPEG (10 kDa) was carried out according to Jain *et al.* protocol [162]. Briefly, a 23 mM solution of mPEG in freshly prepared sodium bicarbonate buffer (10 mM sodium bicarbonate, pH 8.5) was mixed. This solution was then added in a single drop into the center of the functionalized scaffold for 3 h in the dark in humidified environment at room temperature. After incubation the scaffolds were repeatedly washed in water, dried with nitrogen gas and store at +4 °C in the dark.

TSCs (passage 1) at density of 5000 cells · cm^2 were seeded on the whole surface of two sample: passivated scaffold and functionalized but non-passivated scaffold as a control and cultured for 1 day. Cells nuclei were then stained with DAPI and a large image acquisition was performed (Nikon, Tokyo, Japan) to evaluate the yield of the passivation process in terms of cell adhesion. The fluorescence intensity of 18 selected ROIs was evaluated.

Figure 3 reports images of circle base pillar with 100 μm of diameters that was monitored to control the eventual dispersion of collagen. The images show a good preservation of protein edges from the first instant of μCP (A) to 1 day (B), 2 days (C) and 6 days after the microcontact process.

TSCs seeded on passivated scaffold show a significant decrease of nuclear fluorescence intensity ($p < 0.05$) with respect to cell cultured on only functionalized scaffold (figure 4).

The next challenge will be to integrate protein printing and substrate passivation to obtain cells confinement only on protein pattern.

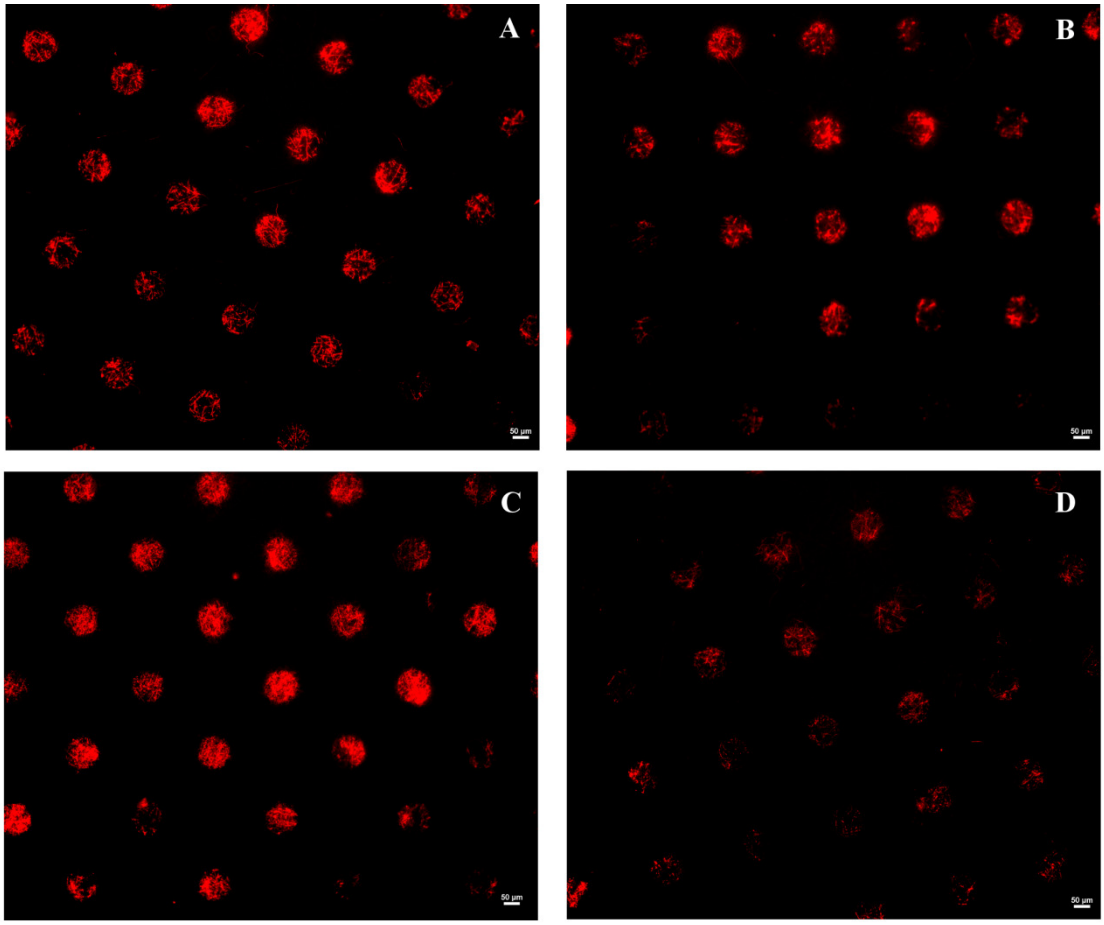

Figure 47: immunofluorescence images of dispersion of collagen circle base pillar with Ø 100 µm. Magnification 10X. Scale bar 50 µm.

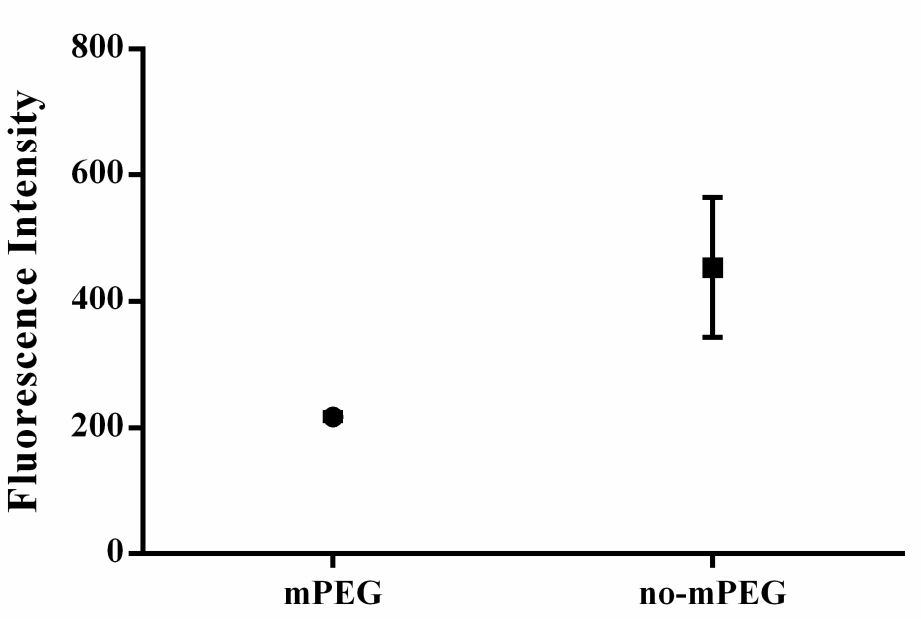

Figure 48: nuclear staining of TSCs cultured on passivated scaffold and on functionalized non-passivated scaffold.

To obtain selective cell confinement on μCP protein islands, as successfully demonstrated for 2D hard substrates, a covalent mPEG passivation was performed. Despite high hydrophilicity of the substrate, shape and fluorescence intensity of protein patterns transferred on ES functionalized scaffolds show high conformity with respect to the PDMS stamps. At the same time, the result of the passivation process demonstrates a significant decrease of cells seeding in the passivated area with respect to the non-passivated one.

Main future purpose will be to confine the cells on the biomolecules micro-printed on soft substrates.

References

1. Qin, D., Y. Xia, and G.M. Whitesides, *Soft lithography for micro-and nanoscale patterning.* Nature protocols, 2010. **5**(3): p. 491-502.
2. Kane, R.S., et al., *Patterning proteins and cells using soft lithography.* Biomaterials, 1999. **20**(23): p. 2363-2376.
3. Whitesides, G.M., et al., *Soft lithography in biology and biochemistry.* Annual review of biomedical engineering, 2001. **3**(1): p. 335-373.
4. Kim, P., et al., *Soft lithography for microfluidics: a review.* 2008.
5. Zhao, X.-M., Y. Xia, and G.M. Whitesides, *Soft lithographic methods for nano-fabrication.* J. Mater. Chem., 1997. **7**(7): p. 1069-1074.
6. Gates, B.D., et al., *New approaches to nanofabrication: molding, printing, and other techniques.* Chemical reviews, 2005. **105**(4): p. 1171-1196.
7. Tan, J.L., et al., *Cells lying on a bed of microneedles: an approach to isolate mechanical force.* Proceedings of the National Academy of Sciences, 2003. **100**(4): p. 1484-1489.
8. Chen, C.S., et al., *Geometric control of cell life and death.* Science, 1997. **276**(5317): p. 1425-1428.
9. Kumar, A. and G.M. Whitesides, *Features of gold having micrometer to centimeter dimensions can be formed through a combination of stamping with an elastomeric stamp and an alkanethiol ''ink''followed by chemical etching.* Applied Physics Letters, 1993. **63**(14): p. 2002-2004.
10. Xia, Y., et al., *Replica molding using polymeric materials: A practical step toward nanomanufacturing.* Advanced Materials, 1997. **9**(2): p. 147-149.
11. Zhao, X.M., Y. Xia, and G.M. Whitesides, *Fabrication of three-dimensional micro-structures: Microtransfer molding.* Advanced Materials, 1996. **8**(10): p. 837-840.
12. Prebiotic, R., *Polymer microstructures formed by moulding in capillaries.* Nature, 1995. **376**: p. 581-584.
13. King, E., et al., *Solvent-assisted microcontact molding: A convenient method for fabricating three-dimensional structures on surfaces of polymers.* Advanced Materials, 1997. **9**(8): p. 651-654.
14. Rogers, J.A., et al., *Using an elastomeric phase mask for sub-100 nm photolithography in the optical near field.* Applied Physics Letters, 1997. **70**(20): p. 2658-2660.
15. Jeon, S., et al., *Three-Dimensional Nanofabrication with Rubber Stamps and Conformable Photomasks.* Advanced Materials, 2004. **16**(15): p. 1369-1373.
16. Xia, Y., et al., *Non-photolithographic methods for fabrication of elastomeric stamps for use in microcontact printing.* Langmuir, 1996. **12**(16): p. 4033-4038.
17. Prabhakaran, M.P., et al., *Methods for Nano/Micropatterning of Substrates: Toward Stem Cells Differentiation.* International Journal of Polymeric Materials and Polymeric Biomaterials, 2015. **64**(7): p. 338-353.
18. Burek, M.J. and J.R. Greer, *Fabrication and microstructure control of nanoscale mechanical testing specimens via electron beam lithography and electroplating.* Nano letters, 2009. **10**(1): p. 69-76.
19. Clarson, S.J. and J.A. Semlyen, *Siloxane polymers*. 1993: Prentice Hall.
20. Palchesko, R.N., et al., *Development of polydimethylsiloxane substrates with tunable elastic modulus to study cell mechanobiology in muscle and nerve.* PloS one, 2012. **7**(12): p. e51499.
21. Leclerc, E., Y. Sakai, and T. Fujii, *Microfluidic PDMS (polydimethylsiloxane) bioreactor for large-scale culture of hepatocytes.* Biotechnology progress, 2004. **20**(3): p. 750-755.
22. Baudoin, R., et al., *Development of a renal microchip for in vitro distal tubule models.* Biotechnology progress, 2007. **23**(5): p. 1245-1253.
23. O'Neill, A.T., N.A. Monteiro-Riviere, and G.M. Walker, *Characterization of microfluidic human epidermal keratinocyte culture.* Cytotechnology, 2008. **56**(3): p. 197-207.
24. Jang, K., et al., *Development of an osteoblast-based 3D continuous-perfusion microfluidic system for drug screening.* Analytical and bioanalytical chemistry, 2008. **390**(3): p. 825-832.
25. Leclerc, E., et al., *Study of osteoblastic cells in a microfluidic environment.* Biomaterials, 2006. **27**(4): p. 586-595.

26. Chao, P.G., et al., *Dynamic osmotic loading of chondrocytes using a novel microfluidic device.* Journal of biomechanics, 2005. **38**(6): p. 1273-1281.
27. Huh, D., G.A. Hamilton, and D.E. Ingber, *From 3D cell culture to organs-on-chips.* Trends in cell biology, 2011. **21**(12): p. 745-754.
28. D'Amico Oblak, T., P. Root, and D.M. Spence, *Fluorescence monitoring of ATP-stimulated, endothelium-derived nitric oxide production in channels of a poly (dimethylsiloxane)-based microfluidic device.* Analytical chemistry, 2006. **78**(9): p. 3193-3197.
29. Tkachenko, E., et al., *An easy to assemble microfluidic perfusion device with a magnetic clamp.* Lab on a Chip, 2009. **9**(8): p. 1085-1095.
30. Mammoto, T., et al., *Mechanochemical control of mesenchymal condensation and embryonic tooth organ formation.* Developmental cell, 2011. **21**(4): p. 758-769.
31. Chung, K., et al., *A microfluidic array for large-scale ordering and orientation of embryos.* Nature methods, 2011. **8**(2): p. 171-176.
32. Cousin, H.S., et al., *Design and Analysis of Fluid Flows through PIV and CFD Modeling.* 2015.
33. Singhvi, R., et al., *Engineering cell shape and function.* Science, 1994. **264**(5159): p. 696-698.
34. Dike, L.E., et al., *Geometric control of switching between growth, apoptosis, and differentiation during angiogenesis using micropatterned substrates.* In Vitro Cellular & Developmental Biology-Animal, 1999. **35**(8): p. 441-448.
35. Polte, T.R., et al., *Extracellular matrix controls myosin light chain phosphorylation and cell contractility through modulation of cell shape and cytoskeletal prestress.* American Journal of Physiology-Cell Physiology, 2004. **286**(3): p. C518-C528.
36. Feinberg, A.W., et al., *Muscular thin films for building actuators and powering devices.* Science, 2007. **317**(5843): p. 1366-1370.
37. Alford, P.W., et al., *Biohybrid thin films for measuring contractility in engineered cardiovascular muscle.* Biomaterials, 2010. **31**(13): p. 3613-3621.
38. Gates, B.D. and G.M. Whitesides, *Replication of vertical features smaller than 2 nm by soft lithography.* Journal of the American Chemical Society, 2003. **125**(49): p. 14986-14987.
39. Xia, Y., et al., *Complex optical surfaces formed by replica molding against elastomeric masters.* Science, 1996. **273**(5273): p. 347-349.
40. Chou, S.Y., P.R. Krauss, and P.J. Renstrom, *Imprint lithography with 25-nanometer resolution.* Science, 1996. **272**(5258): p. 85.
41. Takayama, S., et al., *Subcellular positioning of small molecules.* Nature, 2001. **411**(6841): p. 1016.
42. Jeon, N.L., et al., *Neutrophil chemotaxis in linear and complex gradients of interleukin-8 formed in a microfabricated device.* Nature biotechnology, 2002. **20**(8): p. 826-830.
43. Selimović, S.e., et al., *Generating nonlinear concentration gradients in microfluidic devices for cell studies.* Analytical chemistry, 2011. **83**(6): p. 2020-2028.
44. Jun, Y., et al., *Microfluidic spinning of micro-and nano-scale fibers for tissue engineering.* Lab on a Chip, 2014. **14**(13): p. 2145-2160.
45. Kim, S., et al., *Hydrodynamic fabrication of polymeric barcoded strips as components for parallel bio-analysis and programmable microactuation.* Lab on a Chip, 2005. **5**(10): p. 1168-1172.
46. Kang, E., et al., *Digitally tunable physicochemical coding of material composition and topography in continuous microfibres.* Nature materials, 2011. **10**(11): p. 877-883.
47. Kang, E., et al., *Microfluidic spinning of flat alginate fibers with grooves for cell-aligning scaffolds.* Advanced Materials, 2012. **24**(31): p. 4271-4277.
48. Leng, L., et al., *Mosaic Hydrogels: One-Step Formation of Multiscale Soft Materials.* Advanced Materials, 2012. **24**(27): p. 3650-3658.
49. Bhatia, S.N. and D.E. Ingber, *Microfluidic organs-on-chips.* Nature biotechnology, 2014. **32**(8): p. 760-772.
50. Tormen, M., et al., *3D patterning by means of nanoimprinting, X-ray and two-photon lithography.* Microelectronic Engineering, 2004. **73**: p. 535-541.
51. Esch, M., T. King, and M. Shuler, *The role of body-on-a-chip devices in drug and toxicity studies.* Annual review of biomedical engineering, 2011. **13**: p. 55-72.

52. Sin, A., et al., *The design and fabrication of three-chamber microscale cell culture analog devices with integrated dissolved oxygen sensors.* Biotechnology progress, 2004. **20**(1): p. 338-345.
53. Viravaidya, K., A. Sin, and M.L. Shuler, *Development of a microscale cell culture analog to probe naphthalene toxicity.* Biotechnology progress, 2004. **20**(1): p. 316-323.
54. Sung, J.H., C. Kam, and M.L. Shuler, *A microfluidic device for a pharmacokinetic–pharmacodynamic (PK–PD) model on a chip.* Lab on a Chip, 2010. **10**(4): p. 446-455.
55. Sung, J.H. and M.L. Shuler, *A micro cell culture analog (μCCA) with 3-D hydrogel culture of multiple cell lines to assess metabolism-dependent cytotoxicity of anti-cancer drugs.* Lab on a Chip, 2009. **9**(10): p. 1385-1394.
56. Viravaidya, K. and M.L. Shuler, *Incorporation of 3T3-L1 cells to mimic bioaccumulation in a microscale cell culture analog device for toxicity studies.* Biotechnology progress, 2004. **20**(2): p. 590-597.
57. Imura, Y., K. Sato, and E. Yoshimura, *Micro total bioassay system for ingested substances: assessment of intestinal absorption, hepatic metabolism, and bioactivity.* Analytical chemistry, 2010. **82**(24): p. 9983-9988.
58. Lutolf, M.P. and H.M. Blau, *Artificial stem cell niches.* Adv Mater, 2009. **21**(32-33): p. 3255-68.
59. Wirtz, D., K. Konstantopoulos, and P.C. Searson, *The physics of cancer: the role of physical interactions and mechanical forces in metastasis.* Nat Rev Cancer, 2011. **11**(7): p. 512-22.
60. Spanoudes, K., et al., *The biophysical, biochemical, and biological toolbox for tenogenic phenotype maintenance in vitro.* Trends in biotechnology, 2014. **32**(9): p. 474-482.
61. Wood, M., *Colloidal lithography and current fabrication techniques producing in-plane nanotopography for biological applications.* Journal of the Royal Society Interface, 2007. **4**(12): p. 1-17.
62. Kim, D.-H., et al., *Matrix nanotopography as a regulator of cell function.* The Journal of cell biology, 2012. **197**(3): p. 351-360.
63. Li, Y., et al., *Engineering cell alignment in vitro.* Biotechnology advances, 2014. **32**(2): p. 347-365.
64. Lee, P., et al., *Microfluidic alignment of collagen fibers for in vitro cell culture.* Biomed Microdevices, 2006. **8**(1): p. 35-41.
65. Qin, D., Y. Xia, and G.M. Whitesides, *Soft lithography for micro- and nanoscale patterning.* Nat Protoc, 2010. **5**(3): p. 491-502.
66. WEISS, P. and H.B. HISCOE, *Experiments on the mechanism of nerve growth.* J Exp Zool, 1948. **107**(3): p. 315-95.
67. Chen, W., et al., *Nanotopography influences adhesion, spreading, and self-renewal of human embryonic stem cells.* ACS nano, 2012. **6**(5): p. 4094-4103.
68. Khademhosseini, A., et al., *Co-culture of human embryonic stem cells with murine embryonic fibroblasts on microwell-patterned substrates.* Biomaterials, 2006. **27**(36): p. 5968-5977.
69. Ingber, D.E., *Cellular mechanotransduction: putting all the pieces together again.* FASEB J, 2006. **20**(7): p. 811-27.
70. Prager-Khoutorsky, M., et al., *Fibroblast polarization is a matrix-rigidity-dependent process controlled by focal adhesion mechanosensing.* Nat Cell Biol, 2011. **13**(12): p. 1457-65.
71. Verhulsel, M., et al., *A review of microfabrication and hydrogel engineering for micro-organs on chips.* Biomaterials, 2014. **35**(6): p. 1816-32.
72. Holst, J., et al., *Substrate elasticity provides mechanical signals for the expansion of hemopoietic stem and progenitor cells.* Nat Biotechnol, 2010. **28**(10): p. 1123-8.
73. Gilbert, P.M., et al., *Substrate elasticity regulates skeletal muscle stem cell self-renewal in culture.* Science, 2010. **329**(5995): p. 1078-81.
74. Gerberich, B.G. and S.K. Bhatia, *Tissue scaffold surface patterning for clinical applications.* Biotechnology journal, 2013. **8**(1): p. 73-84.
75. Higuchi, A., et al., *Physical cues of biomaterials guide stem cell differentiation fate.* Chemical reviews, 2013. **113**(5): p. 3297-3328.
76. Pittenger, M.F., et al., *Multilineage potential of adult human mesenchymal stem cells.* Science, 1999. **284**(5411): p. 143-147.

77. Alberti, K., et al., *Functional immobilization of signaling proteins enables control of stem cell fate.* Nature methods, 2008. **5**(7): p. 645-650.
78. Liao, S., C.K. Chan, and S. Ramakrishna, *Stem cells and biomimetic materials strategies for tissue engineering.* Materials Science and Engineering: C, 2008. **28**(8): p. 1189-1202.
79. Park, J., et al., *Control of stem cell fate and function by engineering physical microenvironments.* Integrative Biology, 2012. **4**(9): p. 1008-1018.
80. Evans, N.D., et al., *Substrate stiffness affects early differentiation events in embryonic stem cells.* Eur Cell Mater, 2009. **18**(1): p. e13.
81. Balakrishnan, B. and R. Banerjee, *Biopolymer-based hydrogels for cartilage tissue engineering.* Chemical reviews, 2011. **111**(8): p. 4453-4474.
82. Saha, K., et al., *Substrate modulus directs neural stem cell behavior.* Biophysical journal, 2008. **95**(9): p. 4426-4438.
83. Kapoor, A., et al., *Microtopographically patterned surfaces promote the alignment of tenocytes and extracellular collagen.* Acta biomaterialia, 2010. **6**(7): p. 2580-2589.
84. English, A., et al., *Substrate topography: A valuable in vitro tool, but a clinical red herring for in vivo tenogenesis.* Acta biomaterialia, 2015. **27**: p. 3-12.
85. Zhou, Q., et al., *Directional nanotopographic gradients: a high-throughput screening platform for cell contact guidance.* Scientific reports, 2015. **5**.
86. Kong, Y.P., et al., *Expression of Oct4 in human embryonic stem cells is dependent on nanotopographical configuration.* Acta biomaterialia, 2013. **9**(5): p. 6369-6380.
87. Yang, K., et al., *Nanotopographical manipulation of focal adhesion formation for enhanced differentiation of human neural stem cells.* ACS applied materials & interfaces, 2013. **5**(21): p. 10529-10540.
88. Yang, K., et al., *Multiscale, hierarchically patterned topography for directing human neural stem cells into functional neurons.* ACS nano, 2014. **8**(8): p. 7809-7822.
89. Yang, K., et al., *Biodegradable nanotopography combined with neurotrophic signals enhances contact guidance and neuronal differentiation of human neural stem cells.* Macromolecular bioscience, 2015. **15**(10): p. 1348-1356.
90. Lee, E.A., S.G. Im, and N.S. Hwang, *Efficient myogenic commitment of human mesenchymal stem cells on biomimetic materials replicating myoblast topography.* Biotechnology journal, 2014. **9**(12): p. 1604-1612.
91. Ahn, E.H., et al., *Spatial control of adult stem cell fate using nanotopographic cues.* Biomaterials, 2014. **35**(8): p. 2401-2410.
92. Harris, G.M., M.E. Piroli, and E. Jabbarzadeh, *Deconstructing the effects of matrix elasticity and geometry in mesenchymal stem cell lineage commitment.* Advanced functional materials, 2014. **24**(16): p. 2396-2403.
93. Kim, J., et al., *Multiscale patterned transplantable stem cell patches for bone tissue regeneration.* Biomaterials, 2014. **35**(33): p. 9058-9067.
94. Nemeth, C.L., et al., *Enhanced chondrogenic differentiation of dental pulp stem cells using nanopatterned PEG-GelMA-HA hydrogels.* Tissue Engineering Part A, 2014. **20**(21-22): p. 2817-2829.
95. Matsuda, A., et al., *Immobilization of laminin peptide in molecularly aligned chitosan by covalent bonding.* Biomaterials, 2005. **26**(15): p. 2273-2279.
96. Curtis, A. and C. Wilkinson, *Topographical control of cells.* Biomaterials, 1997. **18**(24): p. 1573-1583.
97. Kuo, C.K., J.E. Marturano, and R.S. Tuan, *Novel strategies in tendon and ligament tissue engineering: advanced biomaterials and regeneration motifs.* BMC Sports Science, Medicine and Rehabilitation, 2010. **2**(1): p. 1.
98. Amiel, D., et al., *Tendons and ligaments: a morphological and biochemical comparison.* Journal of Orthopaedic Research, 1983. **1**(3): p. 257-265.
99. Birk, D.E., et al., *Collagen fibrillogenesis in vitro: interaction of types I and V collagen regulates fibril diameter.* Journal of cell science, 1990. **95**(4): p. 649-657.
100. Canty, E.G., et al., *Coalignment of plasma membrane channels and protrusions (fibripositors) specifies the parallelism of tendon.* The Journal of cell biology, 2004. **165**(4): p. 553-563.

101. Dickinson, R.B., S. Guido, and R.T. Tranquillo, *Biased cell migration of fibroblasts exhibiting contact guidance in oriented collagen gels.* Annals of biomedical engineering, 1994. **22**(4): p. 342-356.
102. Wang, W., et al., *Single cell behavior in metastatic primary mammary tumors correlated with gene expression patterns revealed by molecular profiling.* Cancer research, 2002. **62**(21): p. 6278-6288.
103. Meshel, A.S., et al., *Basic mechanism of three-dimensional collagen fibre transport by fibroblasts.* Nature Cell Biology, 2005. **7**(2): p. 157-164.
104. Provenzano, P.P., et al., *Contact guidance mediated three-dimensional cell migration is regulated by Rho/ROCK-dependent matrix reorganization.* Biophysical journal, 2008. **95**(11): p. 5374-5384.
105. Perentes, J.Y., et al., *In vivo imaging of extracellular matrix remodeling by tumor-associated fibroblasts.* Nature methods, 2009. **6**(2): p. 143.
106. Funk, L., *Tendon Healing Mechanobiology*. 2007, WWW-dokumentti.
107. Wang, Z., A.A. Volinsky, and N.D. Gallant, *Crosslinking effect on polydimethylsiloxane elastic modulus measured by custom-built compression instrument.* Journal of Applied Polymer Science, 2014. **131**(22).
108. Lee, J.B., et al., *Photo-crosslinkable, thermo-sensitive and biodegradable Pluronic hydrogels for sustained release of protein.* Journal of Biomaterials Science, Polymer Edition, 2004. **15**(12): p. 1571-1583.
109. Con, C. and B. Cui, *Effect of mold treatment by solvent on PDMS molding into nanoholes.* Nanoscale research letters, 2013. **8**(1): p. 1-6.
110. Graham, D.J., D.D. Price, and B.D. Ratner, *Solution assembled and microcontact printed monolayers of dodecanethiol on gold: a multivariate exploration of chemistry and contamination.* Langmuir, 2002. **18**(5): p. 1518-1527.
111. Kaufmann, T. and B.J. Ravoo, *Stamps, inks and substrates: polymers in microcontact printing.* Polymer Chemistry, 2010. **1**(4): p. 371-387.
112. Ruzzini, L., et al., *Characterization of age-related changes of tendon stem cells from adult human tendons.* Knee surgery, sports traumatology, arthroscopy, 2014. **22**(11): p. 2856-2866.
113. Riley, G., et al., *Tendon degeneration and chronic shoulder pain: changes in the collagen composition of the human rotator cuff tendons in rotator cuff tendinitis.* Annals of the rheumatic diseases, 1994. **53**(6): p. 359-366.
114. Estévez, M., et al., *Adhesion and migration of cells responding to microtopography.* Journal of Biomedical Materials Research Part A, 2015. **103**(5): p. 1659-1668.
115. Sahai, E., *Illuminating the metastatic process.* Nature Reviews Cancer, 2007. **7**(10): p. 737-749.
116. Petrie, R.J., A.D. Doyle, and K.M. Yamada, *Random versus directionally persistent cell migration.* Nature reviews Molecular cell biology, 2009. **10**(8): p. 538-549.
117. Friedl, P. and K. Wolf, *Tube travel: the role of proteases in individual and collective cancer cell invasion.* Cancer research, 2008. **68**(18): p. 7247-7249.
118. Aubin, H., et al., *Directed 3D cell alignment and elongation in microengineered hydrogels.* Biomaterials, 2010. **31**(27): p. 6941-6951.
119. Khademhosseini, A., et al., *Microfluidic patterning for fabrication of contractile cardiac organoids.* Biomedical microdevices, 2007. **9**(2): p. 149-157.
120. Manbachi, A., et al., *Microcirculation within grooved substrates regulates cell positioning and cell docking inside microfluidic channels.* Lab on a Chip, 2008. **8**(5): p. 747-754.
121. Hwang, C., et al., *Controlled cellular orientation on PLGA microfibers with defined diameters.* Biomedical microdevices, 2009. **11**(4): p. 739-746.
122. Hasirci, V. and H. Kenar, *Novel surface patterning approaches for tissue engineering and their effect on cell behavior.* 2006.
123. Lim, J.Y. and H.J. Donahue, *Cell sensing and response to micro-and nanostructured surfaces produced by chemical and topographic patterning.* Tissue engineering, 2007. **13**(8): p. 1879-1891.
124. Murugan, R., et al., *Biomaterial surface patterning of self-assembled monolayers for controlling neuronal cell behaviour.* International journal of biomedical engineering and technology, 2009. **2**(2): p. 104-134.

125. Wu, C.C., et al., *Strategies for Patterning Biomolecules with Dip-Pen Nanolithography.* Small, 2011. **7**(8): p. 989-1002.
126. Sekula, S., et al., *Multiplexed Lipid Dip-Pen Nanolithography on Subcellular Scales for the Templating of Functional Proteins and Cell Culture.* Small, 2008. **4**(10): p. 1785-1793.
127. Khan, M.S., et al., *Biosurface engineering through ink jet printing.* Colloids and Surfaces B: Biointerfaces, 2010. **75**(2): p. 441-447.
128. Pan, C.-J., et al., *Control of osteoblast cells adhesion and spreading by microcontact printing of extracellular matrix protein patterns.* Colloids and Surfaces B: Biointerfaces, 2013. **104**: p. 18-26.
129. Bernard, A., et al., *Microcontact printing of proteins.* Advanced Materials, 2000. **12**(14): p. 1067-1070.
130. Corum, L.E., et al., *Using microcontact printing of fibrinogen to control surface-induced platelet adhesion and activation.* Langmuir, 2011. **27**(13): p. 8316-8322.
131. Pan, C.-J. and Y.-D. Nie, *Microcontact printing of BMP-2 and its effect on human chondrocytes behavior.* Applied Surface Science, 2010. **256**(6): p. 1878-1882.
132. Ricoult, S.G., et al., *Generation of microisland cultures using microcontact printing to pattern protein substrates.* Journal of neuroscience methods, 2012. **208**(1): p. 10-17.
133. Boisvert, M., et al., *Alpha2beta1 integrin is the major collagen-binding integrin expressed on human Th17 cells.* European journal of immunology, 2010. **40**(10): p. 2710-2719.
134. Vandenberg, P., et al., *Characterization of a type IV collagen major cell binding site with affinity to the alpha 1 beta 1 and the alpha 2 beta 1 integrins.* The Journal of cell biology, 1991. **113**(6): p. 1475-1483.
135. Gullberg, D., et al., *Analysis of alpha 1 beta 1, alpha 2 beta 1 and alpha 3 beta 1 integrins in cell--collagen interactions: identification of conformation dependent alpha 1 beta 1 binding sites in collagen type I.* The EMBO Journal, 1992. **11**(11): p. 3865.
136. KERN, A., et al., *Interaction of type IV collagen with the isolated integrins α1β1 and α2β1.* European Journal of Biochemistry, 1993. **215**(1): p. 151-159.
137. Simmons, P.J. and B. Torok-Storb, *Identification of stromal cell precursors in human bone marrow by a novel monoclonal antibody, STRO-1.* Blood, 1991. **78**(1): p. 55-62.
138. Tamayo, E., et al., *A quantitative assay that evaluates the capacity of human stromal cells to support granulomonopoiesis in situ.* Stem Cells, 1994. **12**(3): p. 304-315.
139. Dennis, J.E., et al., *The STRO-1+ marrow cell population is multipotential.* Cells Tissues Organs, 2001. **170**(2-3): p. 73-82.
140. Dumbauld, D.W., et al., *How vinculin regulates force transmission.* Proceedings of the National Academy of Sciences, 2013. **110**(24): p. 9788-9793.
141. Chen, H., et al., *Spatial distribution and functional significance of activated vinculin in living cells.* The Journal of cell biology, 2005. **169**(3): p. 459-470.
142. Ohmori, T., et al., *Vinculin activates inside-out signaling of integrin αIIbβ3 in Chinese hamster ovary cells.* Biochemical and biophysical research communications, 2010. **400**(3): p. 323-328.
143. Vogel, V. and M. Sheetz, *Local force and geometry sensing regulate cell functions.* Nature reviews Molecular cell biology, 2006. **7**(4): p. 265-275.
144. Delgado-Rivera, R., et al., *Microscale plasma-initiated patterning of electrospun polymer scaffolds.* Colloids and Surfaces B: Biointerfaces, 2011. **84**(2): p. 591-596.
145. Liu, J., et al., *Parametric optimization of micro-contact printing based thermal transfer of electrospun nanofibers.* Microelectronic Engineering, 2010. **87**(12): p. 2513-2517.
146. Shi, J., L. Wang, and Y. Chen, *Microcontact printing and lithographic patterning of electrospun nanofibers.* Langmuir, 2009. **25**(11): p. 6015-6018.
147. Yu, H., et al., *Insights into the role of focal adhesion modulation in myogenic differentiation of human mesenchymal stem cells.* Stem cells and development, 2012. **22**(1): p. 136-147.
148. Lagunas, A., et al., *Continuous bone morphogenetic protein-2 gradients for concentration effect studies on C2C12 osteogenic fate.* Nanomedicine: Nanotechnology, Biology and Medicine, 2013. **9**(5): p. 694-701.

149. Kim, G.-M., et al., *Electrospinning of PCL/PVP blends for tissue engineering scaffolds.* Journal of Materials Science: Materials in Medicine, 2013. **24**(6): p. 1425-1442.
150. Rainer, A., et al., *Electrospun hydroxyapatite-functionalized PLLA scaffold: potential applications in sternal bone healing.* Annals of biomedical engineering, 2011. **39**(7): p. 1882-1890.
151. Spadaccio, C., et al., *AG-CSF functionalized scaffold for stem cells seeding: a differentiating device for cardiac purposes.* Journal of cellular and molecular medicine, 2011. **15**(5): p. 1096-1108.
152. Rainer, A., et al., *Load-adaptive scaffold architecturing: a bioinspired approach to the design of porous additively manufactured scaffolds with optimized mechanical properties.* Annals of biomedical engineering, 2012. **40**(4): p. 966-975.
153. Giannitelli, S.M., et al., *Surface decoration of electrospun scaffolds by microcontact printing.* Asia-Pacific Journal of Chemical Engineering, 2014. **9**(3): p. 401-406.
154. Eichinger, C.D., T.W. Hsiao, and V. Hlady, *Multiprotein microcontact printing with micrometer resolution.* Langmuir, 2012. **28**(4): p. 2238-2243.
155. Arnold, M., et al., *Activation of integrin function by nanopatterned adhesive interfaces.* ChemPhysChem, 2004. **5**(3): p. 383-388.
156. Blau, H.M. and D. Baltimore, *Differentiation requires continuous regulation.* J Cell Biol, 1991. **112**(5): p. 781-783.
157. Critchley, D.R., *Focal adhesions–the cytoskeletal connection.* Current opinion in cell biology, 2000. **12**(1): p. 133-139.
158. Zamir, E. and B. Geiger, *Molecular complexity and dynamics of cell-matrix adhesions.* Journal of cell science, 2001. **114**(20): p. 3583-3590.
159. Sun, W., et al., *Computer-aided tissue engineering: overview, scope and challenges.* Biotechnology and applied biochemistry, 2004. **39**(1): p. 29-47.
160. Elbert, D.L. and J.A. Hubbell, *Conjugate addition reactions combined with free-radical cross-linking for the design of materials for tissue engineering.* Biomacromolecules, 2001. **2**(2): p. 430-441.
161. Koo, L.Y., et al., *Co-regulation of cell adhesion by nanoscale RGD organization and mechanical stimulus.* Journal of cell science, 2002. **115**(7): p. 1423-1433.
162. Jain, A., et al., *Single-molecule pull-down for studying protein interactions.* Nature protocols, 2012. **7**(3): p. 445-452.